

**Photoelectron spectroscopy studies  
of  
carbon based  
fusion reactor materials**

**Inauguraldissertation**

zur

Erlangung der Würde eines Doktors der Philosophie

vorgelegt der

Philosophisch-Naturwissenschaftlichen Fakultät

der Universität Basel

von

Matthias Töwe

aus Hamburg, Deutschland

Basel, 2003

Genehmigt von der Philosophisch-Naturwissenschaftlichen Fakultät  
auf Antrag von

Prof. Dr. Peter C. Oelhafen  
Prof. Dr. Ernst Meyer

Basel, den 18.09.2001

Dekan Prof. Dr. Andreas D. Zuberbühler

Damp from the press is born the current book,

But manuscripts wear a more reverent look.

[...]

The book which, dyed with printers' ink, is thrust

On Shelves abandoned to the moths and dust

[...]

*John Donne*

Well?

*M.T.*



---

<b>Contents</b> .....	<b>I</b>
<b>Abstract</b> .....	<b>III</b>
<b>Kurzfassung (German)</b> .....	<b>IV</b>
<b>Einleitung (German)</b> .....	<b>V</b>
<b>1 Introduction</b> .....	<b>1</b>
<b>2 Background: fusion reactors</b> .....	<b>3</b>
2.1 <i>Conditions for fusion reactions</i> .....	3
2.2 <i>The role of wall materials</i> .....	4
<b>3 Materials</b> .....	<b>7</b>
3.1 <i>Carbon: graphite</i> .....	7
3.2 <i>Amorphous carbon (a-C)</i> .....	8
3.3 <i>Alkali metals: lithium and sodium</i> .....	10
3.4 <i>Carbon host and alkali-metal guest</i> .....	11
<b>4 Photoelectron spectroscopy (PES)</b> .....	<b>13</b>
4.1 <i>Principle</i> .....	13
4.2 <i>Experimental aspects of PES</i> .....	15
4.3 <i>Information from PES</i> .....	16
<b>5 Experimental</b> .....	<b>19</b>
5.1 <i>Ultrahigh-vacuum system</i> .....	19
5.2 <i>In situ sample preparation</i> .....	19
5.3 <i>Ex situ samples</i> .....	22
5.4 <i>Analysis with PES</i> .....	22
5.5 <i>Determination of work functions by UPS</i> .....	23
<b>6 Results: metal-carbon interaction in a-C:Na</b> .....	<b>25</b>
6.1 <i>Deposition</i> .....	25
6.2 <i>Comparison of pristine carbons</i> .....	25
6.2.1 <i>Binding energies</i> .....	26
6.2.2 <i>Full widths at half maximum (FWHM)</i> .....	27
6.2.3 <i>Valence bands in UPS</i> .....	28
6.3 <i>Carbon structure probed with sodium atoms</i> .....	
6.3.1 <i>a-C:Na - valence bands</i> .....	29
6.3.2 <i>Core level spectra</i> .....	34
6.4 <i>Carbon and metal: interpretation</i> .....	39

---

<b>7 Reactivity of lithium containing amorphous carbon .....</b>	<b>43</b>
7.1 <i>Chemical reaction with molecular oxygen .....</i>	
7.1.1 Elemental distributions in the films.....	48
7.1.2 Model for the oxidation driven segregation .....	52
7.1.3 Exposure to air .....	54
7.1.4 Oxidation and annealing - UPS .....	56
7.1.5 EELS measurements - electron irradiation .....	57
7.2 <i>Irradiation with oxygen ions.....</i>	62
7.2.1 Amorphisation of graphite .....	63
7.2.2 Irradiation of oxidized a-C:Li .....	64
7.2.3 Oxygen ion irradiation after hydrogen ion treatment .....	68
7.3 <i>Reactivity and implications for fusion .....</i>	69
<b>8 Electronic effects.....</b>	<b>71</b>
<b>9 Samples from the TCV first wall.....</b>	<b>77</b>
9.1 <i>Graphite wall tiles .....</i>	77
9.2 <i>Aim of the investigation.....</i>	78
9.3 <i>Samples .....</i>	79
9.4 <i>Procedure .....</i>	80
9.5 <i>Results .....</i>	80
9.6 <i>Summary of the TCV results.....</i>	85
<b>10 Summary .....</b>	<b>87</b>
<b>11 Zusammenfassung (German).....</b>	<b>89</b>
<b>12 References.....</b>	<b>91</b>

## Abstract

In this work the deposition and in-situ analysis of alkali-metal (Li, Na) containing amorphous carbon (a-C) films by photoelectron spectroscopy under ultrahigh vacuum (UHV) conditions are reported. Ultraviolet and X-ray photoelectron spectroscopy (UPS/XPS) were applied and complemented by electron energy loss spectroscopy (EELS).

The background of this study is the search for suitable carbon based oxygen gettering materials which are compatible with the operating conditions inside a thermonuclear fusion reactor and could be installed in the first wall of such a reactor's vacuum vessel. Therefore, the reactivity of the prepared carbon materials was tested by exposure to reactive species such as molecular oxygen, oxygen ions, hydrogen ions and air. Each single step was monitored by subsequent electron spectroscopic analysis with respect to elemental composition, chemical bonding and electronic properties. Results include the formation of a metal oxide overlayer through reaction driven segregation of lithium from the carbon bulk when oxygen in any form is present. This process is accompanied by a strong decrease in electron work functions.

In addition, results of ex-situ post-operation analysis of boronized graphite samples from the first wall of the fusion research facility TCV (tokamak à configuration variable) at the Centre de Recherches en Physique des Plasmas (CRPP) in Lausanne are presented.

## Kurzfassung

Diese Arbeit befasst sich mit der Abscheidung und in-situ Analyse von alkalimetallhaltigen (Li, Na) amorphen Kohlenstofffilmen (a-C) mit Hilfe der Photoelektronenspektroskopie unter Ultrahochvakuum (UHV)-Bedingungen. Es wurden Ultraviolett- und Röntgenphotoelektronenspektroskopie eingesetzt und durch Elektronenenergieverlustspektroskopie (EELS) ergänzt.

Im Hintergrund dieser Untersuchung steht die Suche nach geeigneten kohlenstoffbasierten sauerstoffbindenden Materialien, die mit den Betriebsbedingungen in einem thermonuklearen Fusionsreaktor kompatibel sind und darum in der „ersten Wand“ (first wall) des Vakuumgefäßes eines solchen Reaktors installiert werden könnten. Aus diesem Grunde wurde die Reaktivität der hergestellten Kohlenstoffmaterialien durch die Exposition gegenüber reaktiven Spezies wie molekularem Sauerstoff, Sauerstoffionen, Wasserstoffionen und Luft getestet. Jedem Einzelschritt folgte eine elektronenspektroskopische Analyse im Hinblick auf elementare Zusammensetzung, chemische Bindungszustände und elektronische Eigenschaften. Zu den Resultaten gehören die Bildung einer Metalloxidschicht durch Segregation von Lithium aus dem Kohlenstoffmaterial in der Gegenwart von Sauerstoff. Sie geht einher mit einer starken Absenkung der Elektronenaustrittsarbeit des Materials.

Ergänzend werden die Ergebnisse von ex-situ Analysen an boronisierten Graphitproben vorgestellt, die während des Betriebs in der ersten Wand des Fusionsforschungsreaktors TCV (tokamak à configuration variable) am Centre de Recherches en Physique des Plasmas (CRPP) in Lausanne installiert waren.



## Einleitung

Die hier vorgestellten Ergebnisse wurden im Rahmen eines Forschungsprojektes mit dem Titel "Surface studies related to fusion reactor materials" erarbeitet. In der Tat sind materialwissenschaftliche Gesichtspunkte von zentraler Bedeutung für die Realisierung einer kontrollierten thermonuklearen Fusionsreaktion. Dies betrifft insbesondere die dem Plasma ausgesetzte Innenwand des Vakuumgefässes. Die Wahl von Materialien zur Verkleidung der sogenannten "ersten Wand" (first wall) eines Reaktors beeinflusst die Qualität des Vakuums, die Eigenschaften des Plasmas und sogar die Menge aktivierten Abfalls. Eine ausführlichere Darstellung hierzu findet sich in Kapitel 2.2.

Gegenstand dieser Arbeit sind Eigenschaften von Materialien für die erste Wand, die dem Fusionsplasma ausgesetzt ist. In den bisherigen Reaktorkonzepten sind die Limiter und/oder der Divertor die am stärksten belasteten Bereiche. Hintergrund der Untersuchungen ist das Ziel, die günstigen Eigenschaften des Kohlenstoffs für die Verwendung in der Wandbeschichtung zu kombinieren mit der Fähigkeit eines reaktiven Bestandteils, Sauerstoff und sauerstoffhaltige Moleküle aus dem Restgas zu binden. Dadurch können Energieverluste vermindert und das Plasmaverhalten verbessert werden [1]. Zum grösseren Teil beschäftigt sich die Arbeit mit Laborexperimenten, in denen in einer Ultrahochvakuumanlage dünne Schichten von amorphem Kohlenstoff (a-C) unter Zugabe von Lithiumatomen abgeschieden und anschliessend ohne Aufhebung des Vakuums mit Hilfe der Photoelektronenspektroskopie charakterisiert wurden. Diese Charakterisierung betraf vor allem die Reaktivität der erhaltenen Schichten gegenüber Sauerstoffmolekülen und -ionen verschiedener Energie. In der Folge wurden Veränderungen der chemischen Zusammensetzung und der Schichtstruktur analysiert. Zu einem kleineren Teil umfasst die Arbeit die Analyse von bor- und kohlenstoffhaltigen Schichten, die zur Konditionierung eines Fusions-Versuchsreaktors abgeschieden wurden (Tokamak à configuration variable, TCV an der EPFLausanne) sowie mit Proben aus den in dieser Anlage als Wandverkleidung eingesetzten Graphitziegeln.

Weiteres Augenmerk richtete sich auf die elektronischen Eigenschaften. Hier wurden auffallend niedrige Elektronenaustrittsarbeiten beobachtet, die für einige technische Anwendungen von grossem Interesse sind. In letzter Zeit war es vor allem die Suche nach effizienten Materialien für die Verwendung als Emitter in Feldemissionsdisplays, die grosse Aufmerksamkeit auf so unterschiedliche Materialien wie Diamant [2] und Nanotubes [3] gelenkt hat.

Der Einbau von Lithiumatomen in Kohlenstoffmatrices spielt zudem in anderen Bereichen der Energieforschung eine wichtige Rolle: Bei der Entwicklung wiederaufladbarer Lithiumbatterien sind als Elektroden Materialien gefragt, deren Struktur die reversible Aufnahme einer möglichst grossen Anzahl von Lithiumatomen erlaubt. Neben polymeren Werkstoffen zeigen ungeordnete Kohlenstoffe hier bisher die grössten Kapazitäten [4, 5]. Für den Einsatz von Brennstoffzellen wiederum sind wasserstoffspeichernde Medien gefragt. Auch hier werden lithiumhaltige Kohlenstoffe untersucht [6].



# 1 Introduction

The results presented in this work have been obtained within a project on "Surface studies related to fusion reactor materials". Materials-related issues are of paramount importance for the realisation of a controlled thermonuclear fusion reaction. This holds true particularly for those components of the vacuum vessel which are in contact with the fusion plasma itself. The choice of the appropriate materials for covering a reactor's "first wall" decisively influences plasma performance and even the amount of highly activated waste produced during operation. A more detailed account of this is given in chapter 2.2.

This study is dealing with first wall materials under two different aspects based on the common principle of combining the favourable properties of carbon for use in first wall materials with the ability of a more reactive element (B, Be, Si, Li...) to getter oxygen and oxygen-containing molecules from the residual gas in the vacuum vessel. By such measures, energy losses from the plasma are reduced and overall plasma performance during operation can be improved [1]. The major part of this work deals with small scale laboratory experiments performed under ultrahigh vacuum (UHV) conditions. Thin films of amorphous carbon (a-C) were deposited with the addition of lithium atoms and characterized by photoelectron spectroscopy (PES) and electron energy loss spectroscopy (EELS) without intermediate exposure to air. This in situ procedure allowed subsequent controlled experiments regarding the films' reactivity towards oxygen. Both molecules and ions of various energies were employed in this study. On the other hand, films consisting of boron- and carbon were investigated which were deposited during wall conditioning procedures in a fusion research facility (Tokamak à configuration variable, TCV, at EPFLausanne). Samples from graphite tiles mounted on the first wall of the TCV were likewise analysed. These materials and procedures are well introduced and our data mainly supported operations at TCV.

Further attention focused on the electronic properties of materials produced in the laboratory experiments. In particular, strikingly low electron work functions were observed, which are of great technological and therefore commercial interest for a number of applications. Recently, mainly the search for efficiently field emitting media for electronic display purposes has attracted much interest in and scientific effort on materials as diverse as diamond [2] and nanotubes [3].

The incorporation of lithium atoms into carbon matrices plays an important role in other fields of energy research: in the development of rechargeable lithium ion batteries there is a need for electrodes whose structure allows the reversible uptake of as much lithium atoms as possible. Along with polymer materials, various forms of amorphous carbon have so far shown the highest capacities for the incorporation of lithium atoms [4, 5]. For the application of fuel cells, hydrogen storing materials are required. Again, lithium containing carbons are investigated for this purpose [6].

Together with the closer background of this work, the combination of different approaches to the same class of materials made their investigation such an interesting task.



## 2 Background: fusion reactors

As one of the possible power sources for the 21st century, controlled thermonuclear fusion is investigated and developed in worldwide collaborations. Nuclear fusion appears as a very promising option because of the vast stocks of non-radioactive raw material for the production of its fuels. Tritium as one of the fuel species is radioactive, but is produced only inside the reactor by a nuclear reaction between neutrons and lithium (chapter 3.3) in comparatively small quantities which are consumed immediately. The Helium isotope which is obtained as the final product of the nuclear reaction is not radioactive. From the point of view of safety, a fusion reactor is favoured in comparison to a fission reactor because an uncontrolled chain reaction is physically impossible. The fusion plasma breaks down when any important part of the process or its controls fails because the plasma can only be maintained in a rather narrow window of parameters. The nuclear activation of reactor vessel walls and of other structural materials in a fusion reactor is supposed to be smaller than the one in today's conventional light water fission reactors by orders of magnitude [7].

The facts which have been considered as advantages above at the same time prove to be responsible for some disadvantages of the process: as a self-sustained fusion reaction can only take place under extreme conditions, a complex technology is required to achieve this. The necessary development has already taken decades and will take more. Although the level of nuclear activation is much lower, the mere quantity of activated waste from walls and structures of a fusion reactor at the end of its lifetime will be comparable to the one from today's light water fission reactors.

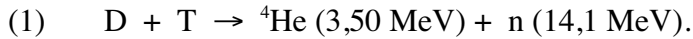
In this respect, materials research can contribute at least at two points: on the one hand, it can find materials which suffer only low activation and on the other hand it can help to choose materials which support the complex processes of plasma control wherever possible. The minimum requirement, of course, is that no material inside of the vessel has an avoidable detrimental influence on plasma performance. Both low activation and support of plasma performance are required for plasma-facing materials on the inner vessel wall ("first wall"). These materials will be in the focus of the following discussion.

### 2.1 Conditions for fusion reactions

For the realisation of nuclear fusion, different reactor concepts are pursued. They differ mainly in the way the plasma confinement is achieved. While the principle of inertial confinement is a special case, the concepts of stellarator and tokamak<sup>1</sup> differ in the technical realisation of magnetic confinement [8]. If not explicitly mentioned, the following statements are usually restricted to reactors of the tokamak type which is the one developed the farthest. The basic fusion reaction between a deuterium and a tritium nucleus is in the focus of the development of the next large international project "ITER-FEAT" (International Thermonuclear Experimental Reactor - Fusion Energy Advanced Tokamak) [9]. The reaction yields a helium nucleus and a neutron (1):

---

<sup>1</sup> short for Russian: "toroidalnaya kamera magnitnaya" (about: "toroidal magnetic chamber")



While the energy of the helium nuclei directly serves for heating the plasma, the neutrons leave the plasma. They carry the utilizable thermal energy and deposit it in the lithium cooling blanket of the reactor. From there it is extracted through heat exchangers and used for conventional generation of electricity. At the same time, the neutrons participate in the breeding of new tritium fuel by a nuclear reaction with lithium in the blanket (cf. chapter 3.3). However, in an even longer term perspective, the desirable fusion reaction should be the one of two deuterium nuclei which is still more difficult to ignite, but avoids the risks of tritium handling and allows higher energy yields.

As already implied by the classification of reactor types according to the confinement concept, the confinement of the fusion plasma is of paramount importance for any attempt to realize nuclear fusion by technical means. This aim requires much higher temperatures than those prevailing in the sun itself which appears most familiar to us and is of course the most important fusion "reactor" in present and future. The enormous gravity and therefore density inside the sun facilitate the maintenance of nuclear fusion already at much lower temperatures. Such conditions cannot be achieved on earth.

Fusion of deuterium and tritium nuclei can occur above  $4 \cdot 10^7 \text{K}$ , but the necessary reaction rates are not achieved below  $10^8 \text{K}$ . For the process to be self sustaining, single reactions must take place with sufficient frequency. This requires a certain particle density inside the reactor. The so called fusion or plasma product  $P_p$  (2) is defined as one parameter accounting for the quality of fusion plasmas:

$$(2) \quad P_p = T_i \cdot n_i \cdot \tau_E.$$

- $T_i$ : ion energy inside the plasma [eV] (typical:  $1\text{-}2 \cdot 10^4 \text{ eV}$ )
- $n_i$ : ion density inside the plasma [ $\text{m}^{-3}$ ] (typical:  $2,5 \cdot 10^{20} \text{ m}^{-3}$ )
- $\tau_E$ : energy confinement time [s] (typical: 1-2 s).

The values in parentheses are the ones required for a D-T-Plasma to be ignited [10]. The energy confinement time denotes the time during which the system cools down when all external heat sources are turned off. Thus it characterizes the velocity of energy loss through heat conduction, particle transport and radiation. Accordingly, one aim of the development must be to minimize energy loss processes and still ensure the transport of fusion products from the plasma. This has to be taken into account already in reactor design and has led to concepts which aim at the control of heat and particle fluxes. The choice of appropriate materials contributes significantly to the minimization of radiative energy loss from the plasma centre [1].

## 2.2 *The role of wall materials*

Depending on the construction and the operation mode envisaged for the respective reactor, more or less extended areas of the inner wall of the vacuum vessel are covered with materials other than the ones employed in its structural parts. Such material can be mounted permanently in the form of

solid tiles or blocks. In an alternative or complementary approach, coatings can be deposited in an in situ conditioning procedure. Usually, the latter effect is achieved by performing gas discharges with appropriate working gases within the vacuum chamber prior to fusion plasma operation or by evaporation [11, 12].

Reactor walls must withstand high thermal loads already in optimal operation ( $10 \text{ MW}\cdot\text{m}^{-2}$  on the divertor in the original ITER layout [13]). In the case of uncontrolled events such as plasma disruptions, locally and momentarily even higher power loads occur. If it was possible to avoid disruptions by a so called "thermal quench" power loads of  $120 \text{ GW}\cdot\text{m}^{-2}$  were calculated for the original ITER design (cited in [14]). Therefore, apart from the problems of absorbing the according forces in the machine's structure the materials to be applied must possess high melting points and good heat conductivity. In addition, they should suffer minimal chemical and physical erosion because eroded material dilutes the plasma fuel and is detrimental to plasma performance. From these criteria alone, refractive metals like tungsten and molybdenum seem to be the materials of choice. From the point of view of plasma confinement, however, they have been regarded with some caution for some time due to their high atomic numbers. If atoms of such "high-Z" elements reach the plasma core, they cause high radiative energy loss and the plasma cools down. The atomic number is of such importance in this context because the radiative loss is proportional to  $Z^\alpha$  ( $\alpha=3$  to 4) [1].

For these reasons, solid graphite tiles or bricks have been installed for wall protection in several fusion research facilities around the world (e.g. JET, Culham; TCV, Lausanne; ASDEX-Upgrade, Garching; TEXTOR, Jülich...). In spite of its considerable chemical erosion under certain conditions [15] and its large hydrogen uptake leading to unforeseen releases, graphite meets most of the requirements for a first wall material. Even more, it is easily and cheaply supplied and processed. Carbon has a low atomic number, but still transport of carbon atoms into the plasma core must be avoided. Any atoms different from the hydrogen fuel species dilute the fusion fuel and can cause plasma instabilities. An important issue related to any erosion process within the reactor is the question of where eroded material is redeposited and which components are formed during redeposition. Currently, analysis of graphite samples from the TCV at CRPP (Centre de recherches en physique des plasmas) in Lausanne is aiming at this question with respect to certain impurities. They should be complemented by laboratory experiments in the future. In the meantime, the view on high-Z metals and carbides has changed. Due to improved plasma control and better knowledge of the (short!) trajectories of eroded high-Z atoms prior to redeposition, it seems possible to master the risk of their transport into the plasma core [16]. Therefore, the ITER project is planned to make use of high-Z materials for large surface areas while in the present designs carbon based materials are still chosen for certain regions of this device depending on specific requirements [17].

In TCV as well as in other tokamaks, regular deposition of thin films on the walls is performed as a wall conditioning procedure, in the case of TCV on the graphite tiles which cover 90 % of its inner surface. For the given reasons, light elements are used, e.g. boron, beryllium or in some cases silicon. In this work the results of boronisation procedures in the vacuum vessel TCV were monitored. Test substrates were introduced into the torus during boronisation and removed for analysis afterwards (see chapter 9). The light elements complement the positive passive properties of graphite by their reactivity towards oxygen. Oxygen is the main contaminant in the residual gas

of the vacuum system. Therefore, it is desirable to remove most of it from the gas and make it bind to the wall material. Quite naturally, interest grew in introducing lithium as an even more reactive and lighter element. In promising experiments mainly on the facility TFTR (Princeton), lithium was added to the burning fusion plasma in the form of pellets [18, 19]. Depending on the details of the procedure in different fusion research devices, the results of experiments with lithium yielded sometimes even contrary results [20, 21]. Although by now some of these differences are more or less understood, there remains a number of questions regarding the interaction of carbon and lithium and of the interaction of the carbon-lithium system with species of the plasma. Even reactor concepts with a liquid lithium containing divertor surface are under investigation [22]. The divertor is one construction feature introduced in order to control the transport of helium and vacuum impurities out of the reactor. It is the region with the highest heat load and the largest particle influx.

In front of this background, our group already investigated amorphous hydrogenated carbon films (a-C:H) with lithium [23, 24] and boroncarbide [25, 26]. The use of a-C in this study reduces the parameters of the system by the absence of hydrogen in the matrix. Furthermore, a-C approximates the state of graphite which is becoming amorphous at its surface through ion bombardment as it occurs in fusion devices. In combination with lithium as a reactive species, amorphous carbons are in the focus of the in situ experiments of the work presented here.

Apart from the possible application in nuclear fusion, these materials provide interesting links with other fields of application. E.g. their electronic properties called for an investigation with respect to field emission and the storage of lithium atoms into carbon materials is of high importance for the development of rechargeable lithium batteries for use in mobile electronic devices (e.g. [27, 28]). Research in the latter field in particular provided valuable connections with this work. Carbon based materials both with and without lithium guest atoms are also studied as hydrogen storage materials in connection with fuel cell operation [6, 29]. Actually, it is this capability of hydrogen absorption which causes some of the problems with the use of carbon in fusion devices which are based on the use of hydrogen reactants. Hydrogen release from this reservoir [30] changes the conditions for proper plasma operation and must not happen without control. Furthermore, the accumulation of tritium in the walls is to be prevented. In this study directly hydrogen related issues play a minor role as in photoelectron spectroscopy any data on hydrogen must be gathered indirectly from the other elements' signals. Hydrogen itself cannot be detected in photoemission experiments.



## 3 Materials

This section presents basic characteristics of the investigated materials, including graphite and amorphous carbon (a-C), the alkali-metals lithium and sodium and combinations of these components such as a-C:Li.

### 3.1 Carbon: graphite

Carbon is the very basis of life as we know it [31]. This fact alone makes it stand out of the elements known to us. In addition, it forms - not only with beneficial consequences - the main part of today's most important sources of energy. Mankind has made it a very well investigated element and has added millions of compounds of carbon with other elements to those present in nature. This paramount importance of the element makes it such a surprising fact that the wealth of allotropes of elemental carbon itself known to us has grown so considerably only during recent years with the discovery of fullerenes [32], nanotubes [33], carbon onions [34], nanocones [35], nanohorns [36].....? Even in the description of the most unusual of these molecules (because that is, strikingly, what they are), authors quite naturally refer to planar sheets of carbon to illustrate the formation of these structures through curling of graphene layers. With respect to the technical application in question here, graphite must stand at the beginning of the discussion, as well.

Graphite is the thermodynamically stable carbon modification under normal conditions [37]. It consists of graphene sheets of six-membered rings which are formed by carbon atoms in  $sp^2$ -hybridisation. In this state, three equivalent  $sp^2$ -orbitals define a plane with  $120^\circ$  between each orbital while the non-hybridised  $p_z$ -orbital points along the normal of the plane. Within the sheets, electrons are delocalised in an extended  $\pi$ -electron system which results in a considerable electric conductivity along the sheets. The stacking of the graphene sheets is only effected by van-der-Waals bonding between them. Only a small overlap of localised electronic states exists and therefore limits electric conductivity normal to the graphene sheets to low values. The weakness of this intralayer bond is also the reason for the ease with which the graphene sheets can be separated mechanically. Due to the latter property, graphite has been used as a lubricant for special purposes. For other applications including the one in fusion reactors the good machinability of the soft graphite in polycrystalline form is an important advantage. In this kind of polycrystalline material, the layered structure is less obvious than in, e.g, synthetically produced highly oriented pyrolytic graphite (HOPG), which readily decomposes into single sheets under mechanical force in spite of its polycrystallinity. Finally, there exist naturally grown graphite single crystals which differ from all the synthetic materials in their long range regular stacking of graphene layers.

Graphite as a layered material with only weak interplanar binding forces can serve as a host material for the incorporation of guest atoms into these spacings (fig. 3.1). Graphite intercalation compounds (GICs) have been produced with a number of species of varying character including donor species such as all alkali-metals or acceptors like metal-chlorides or halogens (e.g.  $FeCl_3$ ,

Br<sub>2</sub>) [38, 39]. Ternary compounds are also known. Data on GICs has been valuable reference material throughout the work presented here.

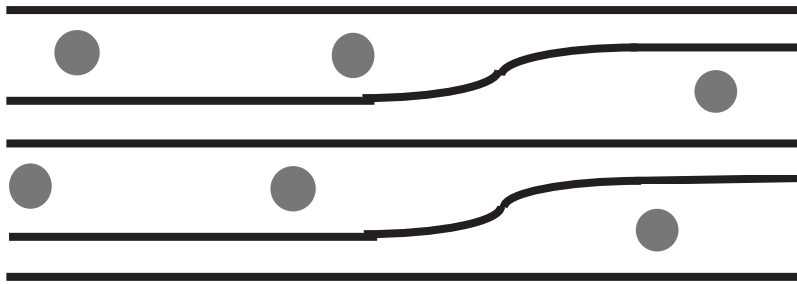


*fig. 3.1: schematic of a graphite intercalation compound according to the model of Daumas and Hérold as cited in [39]. Intercalant atoms are organized in domains rather than in continuous interlayers between graphene sheets.*

Being the thermodynamically stable modification, graphite preserves its structural integrity at temperatures up to its sublimation at 4000°C [40]. It is thus a suitable material for the application on the first wall of fusion devices where high heat loads have to be endured. The quality and purity of the material is very important in this respect and analysis of material which was to be mounted in TCV was carried out with this perspective. The aim is not only to avoid high-Z contamination of the plasma, but also to minimize the risk of sudden evaporation of wall material ("carbon bloom") [41] when the sublimation temperature is reached. The seriousness of this kind of event is one reason for the search for alternative wall materials. In addition, despite of its inertness in many ways, graphite suffers considerable erosion through physical and chemical sputtering. The experimental determination of erosion and redeposition [42], its theoretical understanding [43] and the study of the transport of eroded material in the vessel [44] are still among the most pressing concerns in fusion research and in the field of plasma-wall interactions in particular .

The impact of ions from a plasma leads to a superficial amorphisation of graphite with the destruction of its two dimensionally ordered structure. In our experiments this process is taken into account by the use of various forms of amorphous carbon.

### **3.2 Amorphous carbon (a-C)**

In contrast to graphite, amorphous carbon materials are the product of deposition processes which are carried out far from the conditions of thermodynamic equilibrium. The choice of the actual conditions determines the properties of the respective material. Amorphous carbon can be viewed as "frozen" in a state of structural disorder with not even medium range order [45]. Its atoms could not obtain the most favourable arrangement as they do in graphite, but depending on deposition conditions amorphous carbons can already exhibit some characteristics of graphite while others are not yet developed. The most important common property is the sp<sup>2</sup>-hybridisation of the carbon atoms. In perfect graphite, this is the hybridisation of all the carbon atoms. In amorphous carbon, sp<sup>2</sup>-hybridised atoms are the dominating species. Both calculations [46] and experiments ((e,2e) spectroscopy [47]) yielded fractions of 85-100 % sp<sup>2</sup> in evaporated a-C the rest being formed by sp<sup>3</sup>-carbon. Under normal conditions virtually no sp<sup>1</sup>-carbon was found. The figures depend on the deposition method (for ion sputtered material the range is 75-100 %) and on the measurement method (e.g. down to 70 % from photoemission [48] or 60 % from NEXAFS/EXAFS [49]). For completeness one should note that using special preparation methods also materials designated as

ta-C (tetrahedral amorphous carbon) can be produced which contain an  $sp^3$ -fraction of in excess of 90 at% [50]. They are not to be mixed up with the amorphous carbons of this study. As indicated by the term "amorphous", the most important difference between the materials is the degree of long- and medium-range order of the atoms within the material. In ideal graphite, the periodicity of both the atoms in each sheet and of the stacking of the sheets upon each other are maintained over long distances. The network of amorphous carbon lacks this kind of long range order and a considerable number of atoms has not been able to obtain enough binding partners to saturate its valences. As a consequence, there exists a number of so called dangling bonds which are potential binding sites for sufficiently mobile species. In spite of these features of disorder, planar sheets of  $sp^2$ -carbon exist and might even be stacked in a graphite-like manner within smaller regions of the material (fig. 3.2).

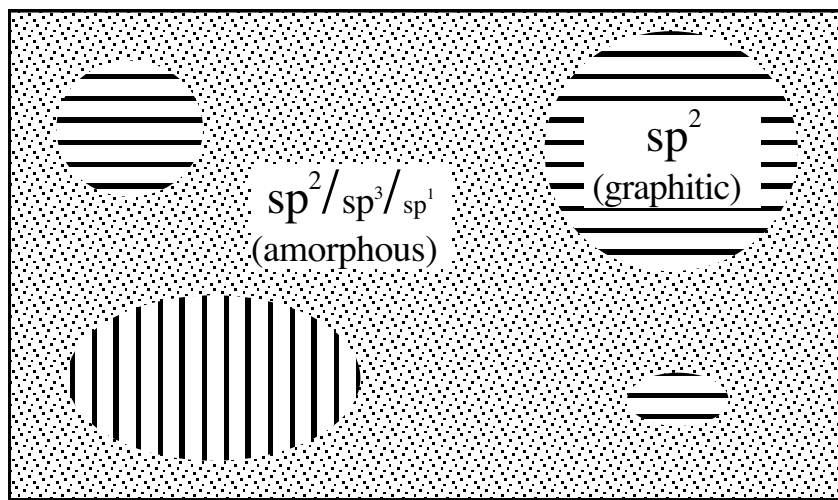


*fig. 3.2: model of an amorphous carbon material with the disordered, though  $sp^2$ -dominated matrix and the embedded graphite-like clusters. With increasing deposition temperature, the size of the latter increases [51].*

The extension of such regions depends mainly on the temperature during deposition of the respective material, i.e. on how far from equilibrium the formation takes place and how mobile carbon atoms are when they have reached the substrate. From earlier depositions with the same setup used for this work (see chapter 5), sizes of graphitic clusters have been determined. They range from 2 nm cross sections in room temperature deposited samples to 20 nm in samples deposited at 800°C [51]. The edges of these clusters themselves are supposed to play a vital role in the interaction of guest atoms with the clusters and in their attachment to them [52]. A schematic of clusters and their edges is shown in fig. 3.3. Binding sites equivalent to the dangling bonds already present after film growth can be created by bombardment with particles of sufficient energy for bond breaking (see chapter 7).

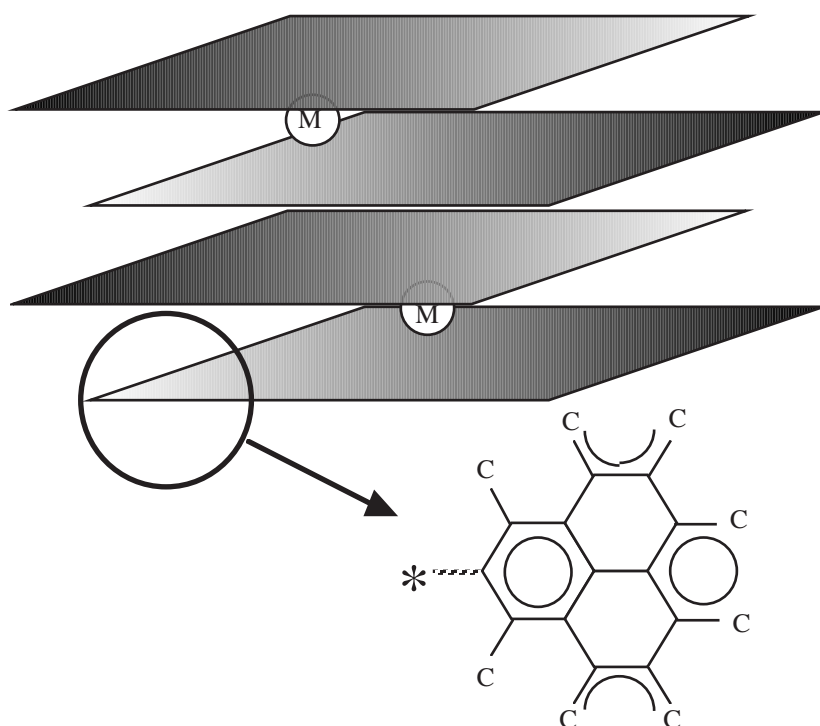
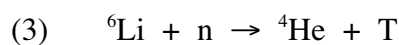


**fig. 3.3:** schematic of cluster edges. While intercalation is possible between graphene layers, at the cluster edges there are dangling bonds available as binding sites for guest species.

With one interest of this study being an investigation of the graphite-lithium interaction, it is tempting to simply use the most graphite-like phases and regard them as examples for imperfect graphite structures. However, as is known from earlier investigations on other forms of carbon, the damage of the graphite structure under particle impact is much more severe and better represented by room temperature deposited films. In most of our experiments, these layers were not generated by actual ion bombardment in order to separate the purely structural modification from complications through chemical effects and to avoid an inhomogeneous film structure. Especially with respect to the structural investigation of the carbon matrices, additional experiments were carried out using sodium atoms instead of lithium. This facilitated this kind of analysis because the sodium 1s electron has a photoionisation cross section which exceeds the one of the Li1s state by more than two orders of magnitude (cf. chapter 4.3). These experiments were extended over the whole temperature range from room temperature (r.t.) to 800°C, while most other measurements were performed on samples produced at either r.t. or 800 C or on graphite itself.

### 3.3 Alkali metals: lithium and sodium

Lithium plays a key role in the technical realisation of the fusion reaction between deuterium and tritium nuclei because it is the material from which tritium can be produced by the nuclear reaction with fast neutrons ("breeding"). This reaction is possible with both lithium isotopes:



However, in this way lithium is to be employed in the breeding blanket which surrounds the fusion vessel on the outside. This must not be confused with its role on the inner "first" wall of the reactor, which is the topic of this work. It is the combination of its low atomic number and its very high reactivity towards oxygen and oxygen containing species which made lithium attractive for this purpose [23]. At the same time, the high reactivity requires special care already in our laboratory experiments and of course even more so in possible large scale use.

### ***3.4 Carbon host and alkali-metal guest***

In the focus of this study is the interaction of lithium atoms with various carbon matrices. As already mentioned, there exists a whole class of composite materials of graphite with guest atoms which is known under the name of graphite intercalation compounds (GICs) [38, 39]. These are classified as donor or acceptor GICs, respectively, depending on the guest species' nature. Quantitatively, they are labelled by their "stage", which denominates the number of graphene layers between neighbouring guest layers. A stage-1 compound is the richest in guest atoms with alternating host and guest layers. As the well ordered structure of crystalline graphite is one prerequisite for the formation of such compounds, it is obvious that an amorphous host material should behave differently. It can be expected that the structural diversity is reflected in some way. Part of this work is thus dedicated to the investigation of the influence of carbon structure on the incorporation of alkali-metal atoms. Apart from lithium, sodium was used for this purpose, because some subtle effects can be observed much easier on its more intensive photoemission signals due to sodium's much larger photoionisation cross section (tab. 4.a). Interest in the combination of alkali-metals in carbon is by far not confined to the field of nuclear fusion. Solids with a high capacity for the reversibel uptake of lithium are of great technological and economic relevance in the development of rechargeable lithium batteries [28, 53, 54] and even for hydrogen storage for fuel cell technology [6]. Apart from these core fields of energy research, there are other specialised functional uses, just one example being sodium containing humidity sensors [55].

Where the application as a getter material was concerned in this work, lithium was used. From this point of view, the reactivity and stability of the metal-containing material under the influence of reactive species were in the centre of interest. In order to account at least for some of the relevant effects in a plasma device, different gaseous species were applied, mainly oxygen (molecular and ionic), hydrogen (molecular, atomic and ionic) and air.

Analysis of the elemental composition and the chemical properties was carried out with x-ray photoelectron spectroscopy (XPS/ESCA). For analysis of the electronic structure of the material, ultraviolet photoelectron spectroscopy (UPS) was used. For carbon in its different geometric structures, UPS or valence band (VB) spectroscopy is an even more valuable tool as carbon's electronic structure is closely linked to its atomic structure [56]. It is thus possible to draw conclusions regarding the structure of the carbon network from UPS.



## 4 Photoelectron spectroscopy (PES)

Photoelectron spectroscopy is a classical tool of non destructive surface analysis. While today it is mainly employed in investigations of solid surfaces, it is not limited to this field and can be applied to free molecules [57] as well as to e.g. liquid metals [58] when the experimental facilities are adapted to this.

### 4.1 Principle

The indirect observation of the photoelectronic effect [59] even before the discovery of the electron and its investigation [60] played an important role in the development and acceptance of the concept of the quantised nature of light [61] and thus of early quantum theory in general. Basically, the following is observed: When a solid is irradiated with light of a certain wavelength, it emits electrons with well defined kinetic energies. When the intensity of the light is increased, the energy of the emitted electrons remains the same and only their number increases proportionally. The latter observation does not agree with the classical concept of light waves and therefore called for an alternative explanation. The postulate of the existence of the photon as the quantum of light allowed the formulation of Einstein's equation:

$$(4) \quad E_{\text{kin}} = h \cdot \nu - E_{\text{b}} - \Phi_{\text{s}}$$

- $E_{\text{kin}}$ : kinetic energy of the escaped electron
- $h$ : Planck's constant
- $\nu$ : frequency of light
- $E_{\text{b}}$ : binding energy of the respective electron
- $\Phi_{\text{s}}$ : electronic work function of the sample.

In the experiment, the spectrometer is calibrated in order to account for the spectrometer work function  $\Phi_{\text{sp}}$  which is usually larger than the one of the sample. When leaving the sample, the electron loses the energy  $\Phi_{\text{s}}$ . The spectrometer's detector, however, is in contact with the sample and therefore, when hitting the detector, the electron is decelerated by the contact potential between sample and spectrometer which equals the difference  $\Phi_{\text{sp}} - \Phi_{\text{sample}}$  (cf. fig. 5.3). Thus, the sample's work function might not be relevant for the process as a whole as long as the measured kinetic energies are corrected for  $\Phi_{\text{sp}}$ .

A mechanistic model for the photoemission process is the three-step model which divides the process into three largely independent steps. Although it contains some oversimplifications, this model has been very successful. In the first step of optical excitation, a photon is absorbed and the respective electron is excited into an unoccupied state in a direct or indirect transition. Direct transitions with conservation of electron momentum are observed mainly at low temperatures and in crystalline material. In amorphous structures, the distinction between direct and indirect transitions is no longer applicable because the k-vector, which is depending on a crystal's symmetry is no longer defined. In this case excitations with a change of electron momentum due to the participation

of phonons dominate and the electronic density of states is reflected in UPS spectra. During the second step of transport to the surface part of the photoelectrons suffer energy losses through inelastic collisions with electrons or phonons or through the excitation of plasmons (collective electronic excitations). It is therefore a mixture of electrons with the full kinetic energy from the excitation and of inelastically scattered secondary electrons which finally can leave through the surface where they have to overcome the work function:

$$(5) \quad I(E, \omega) = I_p(E, \omega) + I_s(E, \omega) \quad [62].$$

$I(E, \omega)$ : distribution of all emitted electrons  
 $I_p(E, \omega)$ : distribution of primary electrons  
 $I_s(E, \omega)$ : distribution of secondary background electrons.

The influence of the steps on the electron distribution curve (EDC) of photoemitted primary electrons *without* energy loss is summarised by formula (6):

$$(6) \quad I_p(E, \omega) = P(E, \omega) \times T(E) \times D(E) \quad [62].$$

$P(E, \omega)$ : distribution of photoexcited electrons (first step)  
 $T(E)$ : transmission function (second step)  
 $D(E)$ : escape function (third step).

The great value of photoelectron spectroscopy in surface and interface analysis is to no small part due to its surface sensitivity which on the other hand naturally limits the applicability of the method. The reason for the surface sensitivity directly follows from the three-step model: The energy losses a photoelectron suffers on its way to the sample surface grow with the length of the electron's path. Therefore, most electrons which are excited in the bulk will not be able to reach the surface, but will be decelerated and stopped within the material. The inelastic mean free path  $\lambda$  is defined as the the mean distance traveled by an electron without energy loss. According to the formula:

$$(7) \quad I_d = I_\infty \cdot (1 - e^{-d/\lambda \cdot \sin \theta}) \quad [63]$$

$I_d$ : intensity from a layer of thickness  $d$  at the surface  
 $I_\infty$ : intensity from an infinitely thick layer  
 $d$ : layer thickness  
 $\lambda$ : inelastic mean free path  
 $\theta$ : take-off angle relative to sample surface

it follows that 63% of the intensity originate from within distance  $\lambda$  from the surface, 87% from within  $2 \cdot \lambda$  and 95% from within  $3 \cdot \lambda$ . While naturally no absolute cut-off can be given, it is a reasonable approximation that most of the photoelectrons are emitted from within a layer thickness of  $3 \cdot \lambda$ . This depth is considered as the "information depth" of the method. It depends on the kinetic energy of the respective electrons [64, 65]. One can make use of this fact by regarding different electronic states or, alternatively, by using excitation sources with different photon energies. In the first case, photoelectrons originating from these states carry information about different sample depths. In the latter case, excitation from the *same* electronic state yields photoemission at kinetic



energies which depend on the respective excitation energy. Under suitable conditions, this allows a non destructive profiling within a narrow surface layer. In the case of thin film deposition on a chemically different substrate, the development of the signal intensity ratio from overlayer and substrate, respectively, can even give evidence of the growth mode of the deposited material [66, 67].

In this work, carbon is usually the most abundant element in the samples. An electron in the carbon 1s (C1s) state has a binding energy of about 284 eV with variations depending on the chemical state of the atom. When excited by MgK $_{\alpha}$ -radiation (1253.6 eV), its kinetic energy in vacuum is approximately 970 eV. The inelastic mean free path or "escape depth"  $\lambda$  according to [64, 65] amounts to about 1.2 nm. For O1s electrons  $\lambda$  is about 0.9 nm and for Li1s electrons 2.2 nm.

## 4.2 Experimental aspects of PES

From the known theoretical principles, photoelectron spectroscopy was developed as a powerful analytical technique not until the 1960s. This was partly due to the previous lack of equipment for the maintenance of ultrahigh vacuum (UHV) conditions which are a prerequisite for reliable results. Only UHV conditions allow the preparation and preservation of clean sample surfaces for sufficiently long periods of time. At the same time, the emitted electrons should reach the analyser without changes in kinetic energy which could result from collisions with gas molecules if the mean free path was too short.

Disregarding a number of practical complications, formula (4) contains everything that is needed for the use of photoemission in chemical analysis at least of conducting samples. For example, a major problem is the determination of the spectrometer's work function independently of other parameters because this work function defines the zero point of the energy scale. To calibrate the energy scale for practical purposes, one refers all measurements to known samples whose binding energies are set to their appropriate values and adjusts all other parameters as required. Usually, the Fermi edge ( $E_b = 0$ ) of the system is identified with the onset of a spectrum of a well defined and clean metal sample, often gold. Its position should figure at  $h\nu - \Phi_{sp}$  which is equivalent to the highest kinetic energy emitted electrons can have. The most severe problem in the analysis of insulating materials is charging upon ionisation. The accumulated positive charge lowers the kinetic energy of the emitted electrons and a reliable interpretation is hardly possible. Various techniques exist to overcome this limitation, but the most universal approach is the production of appropriately thin films on conducting substrates. In this case, photoelectrons from the substrate enter into the insulating film and compensate its electron deficiency [68].

Typical laboratory light sources make use of x-ray radiation (XPS, mostly MgK $_{\alpha}$  = 1253.6 eV or AlK $_{\alpha}$  = 1486.6 eV) and of ultraviolet (UV) light from noble gas discharge lamps (UPS, usually He I = 21.22 eV and He II = 40.82 eV). The large differences in energy already indicate that these sources serve different purposes: X-ray excitation is used to excite core electrons which are bound closely to the nucleus while UV light is applied in the analysis of valence electrons whose binding energy is much lower. Even the small difference between the two helium lines yields additional information because for symmetry reasons these sources favour the excitation of different though

partly overlapping electronic states. For special purposes and higher resolution, synchrotron radiation with very small linewidth can be used. In general, monochromators can be used to decrease the linewidths of the other sources and to eliminate accompanying light of slightly deviating wavelengths ("satellite lines"). Unfortunately, this measure naturally decreases the overall intensity, too. Therefore, the appropriate source must be chosen in each case.

### 4.3 Information from PES

The primary information obtained from photoemission measurements is the binding energy of electrons in the irradiated atoms. As the electron binding energies are characteristic of the respective element, the chemical composition of samples can be determined. Therefore, XPS is often referred to as "electron spectroscopy for chemical analysis" or ESCA, a phrase coined by Nobel Laureate Kai Siegbahn. For quantitative results, the relative photoionisation cross sections of the respective initial electronic states and their population are important to assign the correct weight to peak areas. Cross sections vary by two and more orders of magnitude e.g. between Li1s and most other relevant core levels (tab. 4.a). For this study, cross sections are referred to the one of the C1s state set as 1. The values for the other states are those calculated by [69]. In this work, usually a Tougaard type background [70] was subtracted from photoemission signals for the purpose of area calculation. All spectra shown, however, are the originally measured ones without background subtraction or satellite correction.

core level	photoionisation cross section
C1s	1.00
O1s	2.85
Li1s	0.0593
Na1s	7.99
Si2p	0.865
Au4f <sub>7/2</sub>	9.79

*tab. 4.a: calculated atomic photoionisation cross sections for selected electronic states for excitation with 1253.6 eV MgK<sub>α</sub>-irradiation [69].*

In addition to the elemental composition, one can draw conclusions regarding the chemical bonding within the material from deviations of a signal's position with respect to the pure element's line. In a rather basic approach ("point charge model"), only the electronegativity enters into the consideration [71]. As the electron accepting species receives an electron surplus, the shielding of its nuclear charge is amplified and the energy levels of its binding electrons are shifted. Escaping electrons therefore appear at lower binding energy. At the same time, the electron donating species becomes electron deficient and an opposite effect of less effective shielding influences its electrons. The corresponding signal appears at higher binding energy. In more complex chemical systems, this principle can be obscured and even reversed by other effects which will be discussed later. The

assignment of chemical states is of course most reliably performed when there are only a few elements involved and when reference data is available for the compounds in question.

The kind of information which can be obtained from PES also depends on the energy of the photons used and on the crystallinity of the material under investigation. In the case of carbon, e.g., the XPS mode mainly excites electrons from states with s-symmetry [56, 72], whereas excitation with photons of lower energy favours electrons from states with p-symmetry. This is exploited in the recording of valence band spectra with ultraviolet light. As the covalent bonding in carbon materials is dominated by electronic states with p-symmetry, the resulting valence band spectra are strongly correlated with the geometric bonding structure of the respective carbon material and do not only reflect its electronic structure. Molecular carbon species such as fullerenes for example, yield spectra with sharp and narrow maxima which can be attributed to individual electronic states. For solids, an additional complication arises from variations in crystallinity within the materials as mentioned above. In crystalline graphite, for example, direct electronic transitions with conservation of the k-vector generate a sharp maximum in valence band spectra at about 13.8 eV [73, 74] cf. fig. 6.4). In amorphous material, the k-vector selection rule does not apply and the spectra become rather a representation of the electronic density of states in the material weighted by the photoionisation cross sections of the respective states [75]. The latter fact explains the different appearance of He I and He II excited spectra which can be observed throughout this work.



## 5 Experimental

### 5.1 Ultrahigh-vacuum system

In fig. 5.1 the layout of the vacuum device in which the experimental work was carried out is shown schematically. It consists of two UHV chambers which can be connected or separated via a valve. Base pressure was generally lower than  $10^{-10}$  mbar, for special purposes it was reduced by an order of magnitude by using a liquid nitrogen cooling trap. Samples are mounted on the head of a linear translator and can be moved from the preparation chamber (right) to the measurements position inside the spectrometer chamber (left). It is thus possible to avoid exposure to air between deposition and measurement and the inevitable contamination by adsorption can be minimized. Not shown is an additional high vacuum (HV, base pressure  $\leq 10^{-6}$  mbar) chamber which serves as a transfer lock to introduce samples into the preparation chamber from atmosphere without the necessity to vent the whole system. Such samples and their measurements are denoted as "ex situ" in the following.

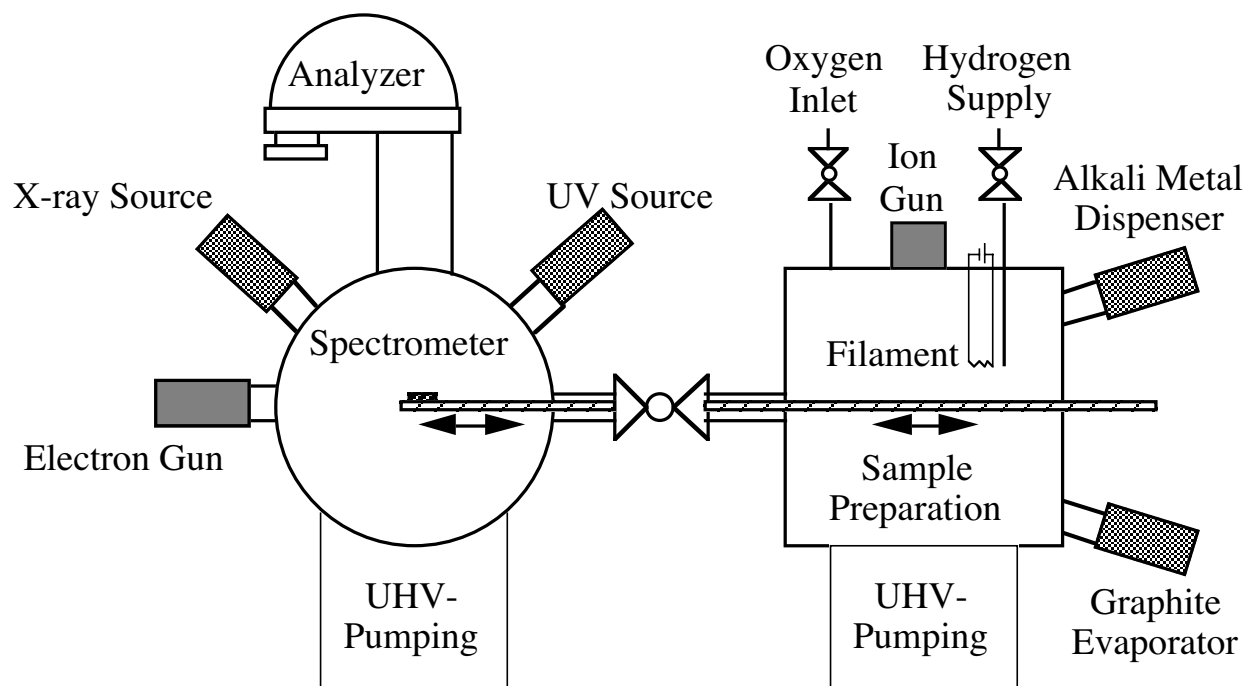


*fig. 5.1: the ultrahigh vacuum system with photoelectron spectrometer (left) and preparation chamber (right). In situ sample transfer is possible with the linear translator between the two chambers. The sample can be heated and or biased with respect to the spectrometer.*

### 5.2 In situ sample preparation

With respect to the requirement of very good vacuum conditions the value of preparation and analysis in separate chambers of the same UHV device is obvious. Thus, exposure to air is avoided and clean surfaces are preserved. On the very versatile preparation chamber a wide selection of

deposition devices can be mounted. For this work, apart from the usual equipment for the maintenance and control of vacuum conditions, the following facilities were used:

- electron beam evaporator (Leybold-Heraeus ESV 2 with power supply HV 2.2) for graphite (Ringsdorff purest, EK 50) used for the deposition of amorphous carbon;
- liquid nitrogen cooled alkali-metal source using commercial dispensers (SAES Getters Li/NF/1.25/25 FT10+10 and Na/NF/3/25 FT10+10) supplying alkali atoms from a thermally induced chemical reaction between alkali chromates ( $M_2CrO_4$ ) and a ZrAl-alloy (St101; 84% Zr, 16% Al);
- a Penning-type ion source which generates ions in an internal plasma discharge and was operated with oxygen, hydrogen, and argon, respectively; it was employed in the irradiation of the in situ deposited films and for sputtering the ex situ samples from TCV;
- a source for the thermal production of hydrogen atoms from hydrogen passing a hot tungsten filament;
- quartz crystal oscillator probes for monitoring deposition rates.

Carbon thin films were deposited on silicon (100) substrates which were mounted on a sample holder which was heatable and electrically insulated against the transfer rod and thus the spectrometer. Substrates were heated during sample deposition in order to achieve the desired structural properties in the deposited layer. The temperature was adjusted between room temperature (r.t.) and 800°C. The deposition of the carbon matrix was usually followed by steps of sample processing, including the incorporation of alkali-metal atoms and exposures to oxygen and oxygen ions or air and in a small number of cases to hydrogen, hydrogen atoms and ions. Some sequences of sample processing are schematically illustrated in fig. 5.2.

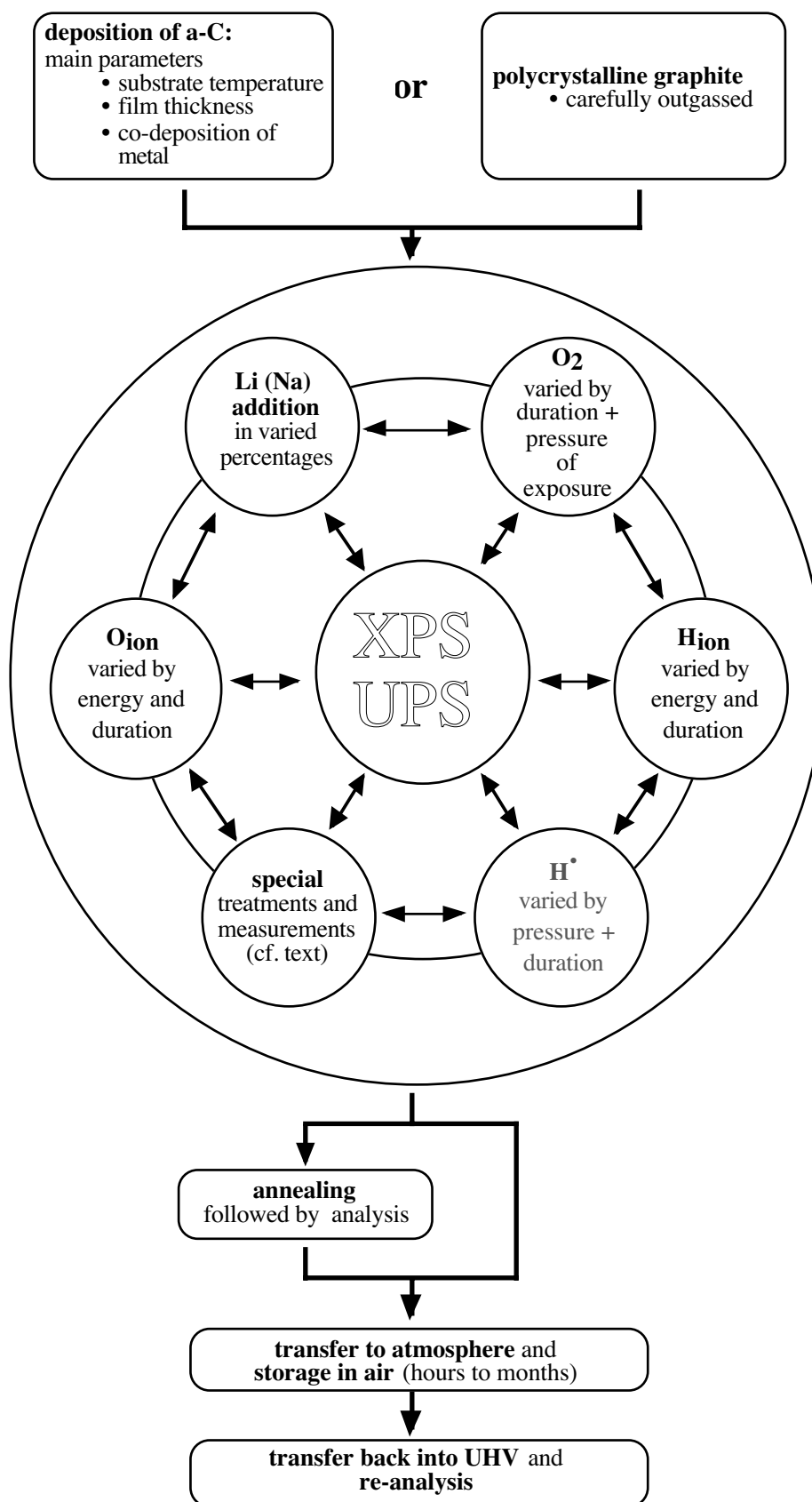


*fig. 5.2: scheme of typical sequence during experiments; the circle in the middle comprises a number of operations which were carried out in various combinations and in virtually every possible order; each individual step was followed by in situ XPS and UPS measurements. The measurements in connection with atomic hydrogen had preliminary character and are only mentioned very briefly.*

### 5.3 *Ex situ samples*

When test substrates or graphite first wall samples arrived from TCV in Lausanne, they were of course covered with a film of adsorbed hydrocarbons, carbon oxides, oxygen, water...as can be expected on any sample exposed to air. Before a reasonable analysis of the underlying solid becomes possible, such surfaces have to be cleaned. The TCV samples underwent a number of sputtering cycles with argon ions from the Penning source in order to remove adsorbates. However, one has to be aware that this can already influence both structure and composition of the film itself. As some elements are sputtered preferentially, there is a danger of depleting the film of one species so that the concentration determined afterwards will be lower than its actual value in the original material. Other mechanisms changing the composition include ion mixing, bond breaking in adsorbate species and subsequent ion induced incorporation into the film. Therefore some care must be taken when considering *absolute* concentrations. In particular by the comparison of samples which have been treated in the same way, very useful *relative* results can be obtained answering important questions arising - in this case - from the operation of the tokamak in Lausanne or from any other ex situ application.

### 5.4 *Analysis with PES*

After each step of processing the samples were transferred inside the UHV-system to a measurement position in the spectrometer chamber adjacent to the preparation part. Analysis was routinely performed at room temperature in  $\text{MgK}_\alpha$  (1253.6 eV) x-ray excited mode and in He I and He II modes (21.22 eV and 40.82 eV). Wide scans of the whole energy range were measured in XPS before the single core levels were studied in more detail. The spectrometer chamber also possessed a monochromatised  $\text{AlK}_\alpha$ -source (1486.6 eV) which was applied when its higher resolution outweighed the sometimes excessive measuring times required because of its strongly reduced intensity. The spectrometer chamber was also equipped with a scanning ion source for sputtering and with an electron gun for electron energy loss spectroscopy (EELS).

The spectrometer itself was a Leybold/SPECS EA 11/100 MCD (multichannelplate detection) which operates with a hemispherical analyser through which the electrons have to pass. XPS was always measured with constant pass energy which means that all the photoelectrons entering the analyser are retarded to the same velocity with which they pass through the analyser. Thus the transmission is scaling with the reciprocal of the kinetic energy. In the standard mode of a pass energy of 50.4 eV, the resolution was about 0.9 eV. In UPS, the constant retardation ratio (CRR) was usually favoured. In the CRR-mode, all the electrons are decelerated by the same factor of their velocity and thus pass through the analyser with different energies. Transmission in this case scales directly with the energy and resolutions of about 0.2 eV (He I) and 0.1 eV (He II) could be obtained. Only for the determination of the work function from valence band spectra, UPS were taken in constant pass energy mode because this yields a sharper cut off at low kinetic energy due to the better transmission of electrons with low kinetic energy in this mode.



### 5.5 Determination of work functions by UPS

Due to the electrical insulation between sample and spectrometer it was possible to apply a voltage between them during measurements. This was a prerequisite for the determination of electronic work functions from valence band spectra measured with UPS in the constant pass energy mode, cf. chapter 8). In the standard setup with the sample on the same potential as the spectrometer, it usually is the spectrometer work function which defines the lowest kinetic electron energy which can be detected. By applying a known offset voltage between sample and spectrometer, this limit can be overcome and the work function of the sample itself becomes accessible (fig. 5.3) which equals the energy difference between the Fermi level of the sample and the vacuum level.

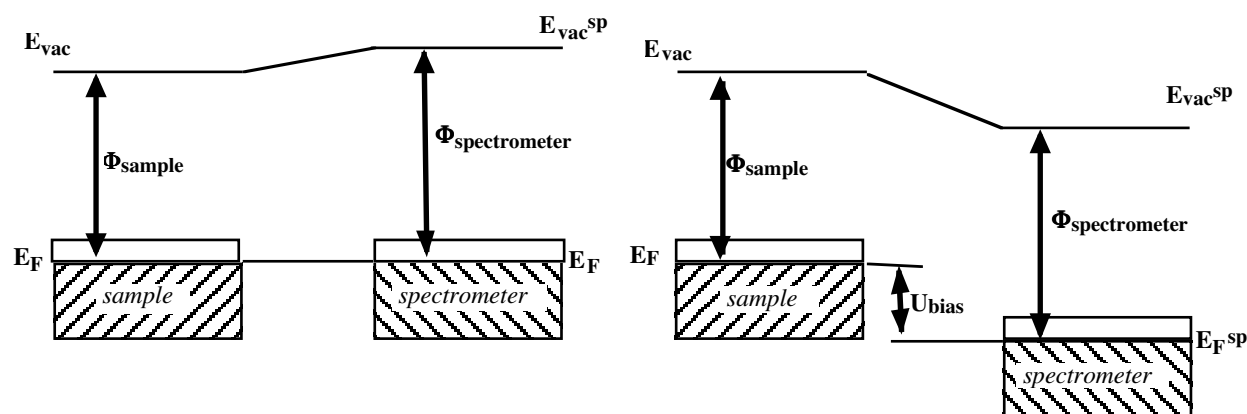


**fig. 5.3:** schematic of the energy levels with electronic contact between sample and spectrometer (left) and with a voltage applied between them (right); in the latter case, it is no longer the work function of the spectrometer, but the one of the sample which defines the cut off at low kinetic energy and can therefore be determined.

The energy value at half maximum height was taken as measure to compare between the samples. This approach is justified by the steepness of the slope in this cut-off region (cf. fig. 8.2). For comparison with values from other sources, this yields work functions which are rather too high. On the other hand, work functions derived from photoelectron spectra may just reflect a property of a small part of the investigated surface namely the one with the lowest work function which defines the cut off. The value for the rest of the surface can be higher.



## 6 Results: metal-carbon interaction in a-C:Na

Some of the experimental series performed within this study comprise numerous single steps in changing order (cf. fig. 5.2). Any representation of these procedures and even more so of the respective results encounters problems due to this diversity. This chapter, e.g., deals with pristine metal-free carbon films and with pure metal-containing ones. In this context "pure" denotes those films which consist of carbon and alkali-metal atoms and do contain oxygen only as a minor contamination of less than about 2 at%. This condition could be maintained for several hours when the cooling trap of the vacuum chamber was cooled with liquid nitrogen. This was a prerequisite for the investigation of lithium in particular which required long recording times due to its small cross section.

### 6.1 Deposition

According to the outline given in chapter 5.2, a-C films were deposited by electron beam evaporation of graphite on silicon substrates which were left at room temperature (r.t.) or heated to 300°C, 550°C, and 800°C. Samples from this temperature range were employed in the analysis of the structural properties of the carbon matrix after incorporation. For most other experiments samples deposited at either room temperature or at 800°C were used.

Comparatively thick films were produced for the analysis of film structure and chemical reactivity. They possessed sufficient thickness to fully suppress the silicon substrate's photoemission signal. Most of them were more than 10 nm thick. Some other experiments, however, relied on the substrate's signal being detected at the same time as the film's. They were meant to yield information on *changes* in film thickness due to erosion or other reactions of the material. In addition, this allows to control the depth down to which reactions occur or particles penetrate the layers.

### 6.2 Comparison of pristine carbons

Although they all consisted of the same element, samples of amorphous carbon deposited between room temperature and 800°C could be distinguished in XPS and UPS measurements. In fig. 6.1 C1s core level spectra of four pristine amorphous carbon samples which were deposited at room temperature, 300°C, 550°C, and 800°C, respectively are displayed. A C1s spectrum of polycrystalline graphite is also included for reference. Left and right part of the figure have been taken from the same spectra. In the left part, the energy range of the display is wider to include the weak feature at about 290 eV which starts to evolve at deposition temperatures of more than 300°C. It is attributed to a collective electronic excitation of  $\pi$ -electrons in the course of the relaxation process of the photohole (intrinsic plasmon). As the other features which are related to  $\pi$ -electrons, this plasmon gets more pronounced the more delocalised the electrons become in extended  $\pi$ -

systems (cf. EELS results 7.1.5.1). The following analysis mainly relies on the two parameters binding energy and full width at half maximum (FWHM).

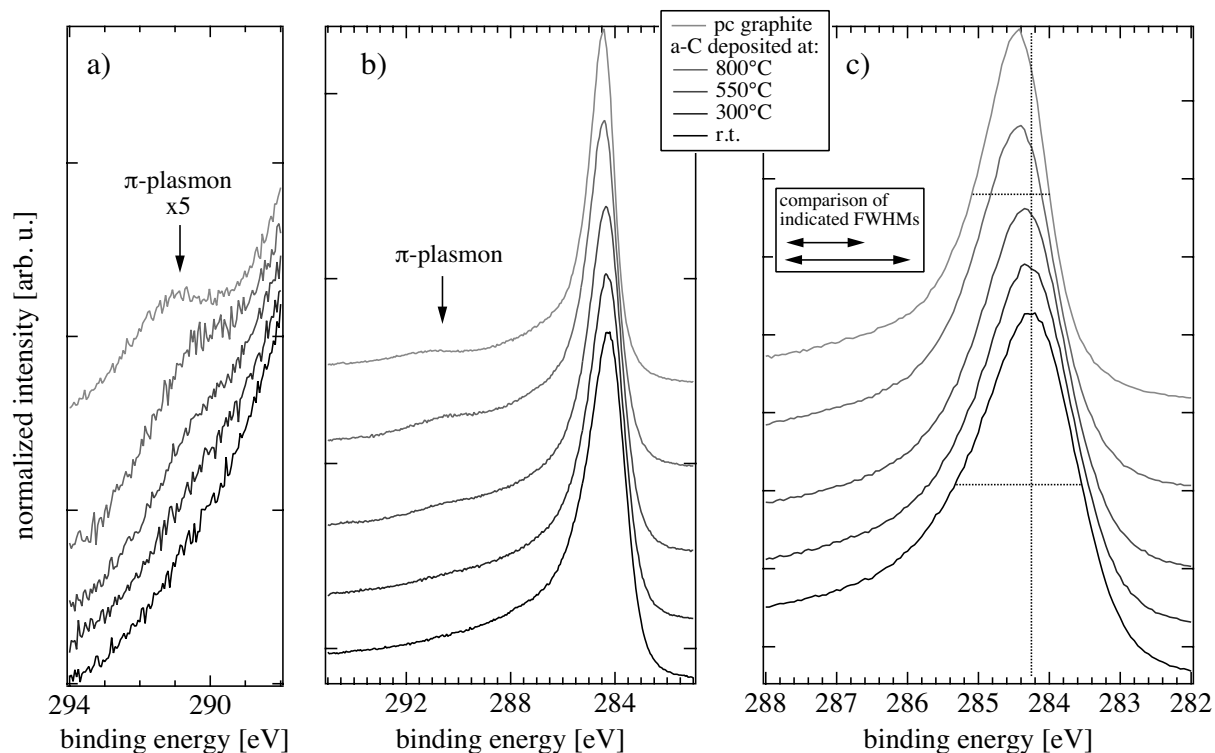


**fig. 6.1:** C1s core level spectra from XPS ( $MgK_{\alpha}$ , 1253.6 eV). **Middle:** wider energy range including the plasmon at 290 eV (-6 eV energy loss with respect to the main peak). **Left:** enlarged view of the plasmon region around 290 eV. **Right:** reduced energy range of the same spectra as in the other parts. Binding energy is indicated for the r.t. sample, FWHMs are compared for r.t. and polycrystalline graphite.

### 6.2.1 Binding energies

From what was said above about binding energies and chemical shifts, it would be surprising if binding energies varied significantly between materials which all contain only carbon atoms bonded to other carbon atoms. In fact, binding energies for all five materials did not differ much although a tendency to slightly higher binding energies with increasing deposition temperatures is just detectable. However, the effect was still small enough to be accounted for by the error of the measurement (cf. tab. 6.a and fig. 6.7). The binding energy of C1s in amorphous carbon deposited at room temperature was  $284.3 \pm 0.1$  eV and for both polycrystalline graphite and a-C deposited at 800°C it was 284.4 eV (tab. 6.a). For films deposited at intermediate temperatures, binding energies varied between both values. One must be aware of the fact that these are binding energies of peaks which might comprise signals of inequivalent carbon sites and with different binding energies as will be discussed in the following. Small contributions to a peak do not always influence the binding energy of the main maximum, but do well contribute to its shape as will be discussed below.

### 6.2.2 Full widths at half maximum (FWHM)

In contrast to binding energies, peak widths showed a significant decrease with increasing carbon deposition temperature (cf. tab. 6.a and fig. 6.7, respectively).

dep. T of a-C [°C]	FWHM pristine, [eV]	binding energy pristine, [eV]
HOPG	1.04 [76]	284.5/284.3
pc graphite	1.2±0.1	284.4±0.1
800	1.5	284.4
550	1.6	284.3
300	1.8	284.4
r.t.	1.8	284.3

*tab. 6.a: binding energies and full widths at half maximum for various  $sp^2$ -dominated carbon species. HOPG data only is taken from [76].*

While the most disordered room temperature deposited sample set the upper limit with 1.8 eV, polycrystalline graphite figured at 1.2 eV. Highly oriented pyrolytic graphite has been measured elsewhere with only 1 eV [76]. From what is known about the structure of amorphous carbon compared to the one of graphite, it is obvious that the width of the C1s peaks is closely related to the degree of order or disorder within the

respective carbon network. The sample which was produced farthest from equilibrium conditions, namely the one deposited at room temperature, is the one with the most disordered atomic network. The majority of its atoms (85-100 %, cf. chapter 3.2) is in an  $sp^2$ -hybridised state, the rest of the atoms is in the  $sp^3$ -state. However, only part of the  $sp^2$ -hybridised atoms could obtain the favoured arrangement in regularly stacked planar graphene sheets. There remained a large number of dangling bonds which could not be saturated during film growth due to the lack of mobility of the atoms arriving at the growing film's surface. The carbon film therefore contains only small clusters with graphitic order which are embedded in an amorphous matrix. Cluster diameter in this case has been observed to be about 2 nm [51]. When temperatures are increased towards equilibrium conditions, the graphite-like clusters grow at the expense of their amorphous surroundings and reach diameters of 20 nm at a temperature of 800°C and finally yield graphite itself at temperatures in excess of 1200°C. The effect of this transition from the predominantly amorphous to the more or less crystalline structure is reflected in the decrease in peak widths in carbon C1s spectra and can also be monitored in valence band spectra (see 6.2.3). There are a number of contributions to peak broadening or peak narrowing, respectively, in core level spectra. In some cases, a narrowing can be attributed to an increase in photohole lifetimes reducing the Lorentzian contribution to peak widths. This effect should yield a symmetric decrease in peak width [66] which is not observed here, but might well be obscured by other phenomena. Temperature dependent phonon-broadening must be considered as one of the effects contributing to increased peak widths [77, 78]. When measuring always at the same temperature, in the present case at room temperature, the (small) influence should be of similar magnitude. However, it is still possible that structural modifications depending on deposition temperature hinder or facilitate phonon excitation. With light atoms of the first period of the periodic table, the recoil of the escaping photoelectron can play a role in the generation of phonons [77-79]. These and other even more subtle effects cannot easily be identified or even

separated. In an independent approach, the decrease in line width with increasing deposition temperature is attributed to the development of a more uniform ordered environment for each carbon atom. In the least ordered material, dangling bonds, disordered regions and a non-negligible number (0 to 15 at%) of non- $sp^2$ -hybridised carbon atoms form the background for the  $sp^2$ -hybridised atoms. The bonding or just close contact of these different types of carbon atoms generates an additional wealth of carbon species with slightly varying properties. For example, the relaxation energies occurring during the photoemission process will vary. While formula (4) was based on the simplifying assumption of electronic states not being changed during the process according to Koopman's theorem, the loss of a photoelectron and the subsequent relaxation of the atom's energy levels in fact do enter into the energy balance of photoemission [62]. Consequently photoemission signals of atoms in different environments are not equivalent, either. Summing up all the signals, the overall binding energy hardly changes because the individual contributions are small. Nevertheless, the peaks of the individual species are positioned at slightly higher or lower energy with respect to the position of graphite and therefore yield a broader common maximum. With increasing deposition temperature, more atoms obtain the  $sp^2$ -hybridisation and a larger proportion of them arranges in a graphite-like manner so that the dominance of this species becomes more pronounced. In accord with this, photoemission peaks are mainly representing the properties of the majority species. Small quantities of other types of carbon are still present, but their small signal contributions do not alter the overall peak width any more.

### 6.2.3 Valence bands in UPS

In the various carbon allotropes, the geometric structure is closely related to the electronic one which is determined by UPS. This is due to the different degrees of electronic delocalisation which can be achieved depending on the respective atomic structure. UPS favours emission from p-symmetric states [72] and is therefore particularly suited for the analysis of the binding states in carbon. Here, both  $sp^2$ - and  $sp^3$ -hybridized atoms are involved in bonding and the more "p-like" their character is, the closer they are to the Fermi energy and the more they are subject to changes in their bonding environment. Another important observation in valence band spectra would be the presence of direct transitions which can only occur in crystalline materials. However, the feature visible for graphite at 13.7 eV in fig. 6.4 is not actually such a direct transition, but a secondary electron peak. It is due to the scattering of electrons into a well defined final state in  $\sigma$ -bands with low dispersion (" $\sigma$ -peak") [74, 80] which also explains why it is missing in He II spectra: its position is pinned on the *kinetic* energy scale at 7.5 eV and therefore not within the *binding* energy range measured in routine He II spectra. As it is related to the presence of the bands mentioned, this feature is also indicative of the material's crystallinity, although in a different way than direct transitions are. Graphite as well as all the amorphous carbon spectra show a shoulder at binding energies of about 3 eV which develops into a sharper feature with increasing deposition temperature. This peak is due to valence electrons originating from the p- $\pi$ -band, while the main maximum of the spectra is caused by emission from the p- $\sigma$ -band [81]. These bands are formed by the interaction of atomic orbitals with p-symmetry. In the case of  $\sigma$ -bands, they interact along their longitudinal axis with rotational symmetry with respect to this axis, while in  $\pi$ -bands, the direction of interaction is perpendicular to the main axis of the orbitals and thus lacking rotational symmetry. It is the formation of extended p- $\pi$ -bands which enables the high electric conductivity along the planes in graphite, whereas  $\sigma$ -bonds are responsible for the bonding of carbon atoms within the

graphite planes. Where no regions with long range graphitic order are present in the material, spectra lack a distinct peak at 3 eV. No major contribution of s-electrons is found in UPS because of the much smaller photoionisation cross sections for those states in this energy range of excitation. The p- $\pi$ -band related feature is observed in both He I and He II modes, but as even the two helium discharge lines differ in their interaction with electronic states depending on their symmetry, the feature is more distinct in He II (fig. 6.2 to fig. 6.4). For the investigation it serves as an indicator of crystalline character because it is connected to the presence of extended graphitic arrays of sp<sup>2</sup>-hybridised atoms. It also serves as a marker structure in the valence band to which changes in other features can be referred. The latter point is of importance for the analysis of charge transfer interactions with other atomic species (see 6.3.1).

### ***6.3 Carbon structure probed with sodium atoms***

For the application under consideration, lithium appears as the most favourable reactive metal while the other alkali metals are under investigation with respect to the development of other functional materials, e.g. for electron emission (mainly Cs) or sensing devices (Na) [55]. In spite of this, we employed sodium in some experiments in order to gain additional information on the interaction of alkali metal guest atoms with the carbon host matrix. On the one hand, rather minute differences between the spectra of the pristine carbon films are enhanced when sodium atoms interact with the carbon network. On the other hand, sodium facilitates the analysis for merely practical reasons because its much larger photoionisation cross section yields higher signal intensities in photoemission. Sufficiently intensive signals are a prerequisite to establish peak features such as peak width or binding energy with reasonable certainty after limited measuring times. For the routine analysis of lithium containing material, the lithium 1s signal could usually not be measured until a signal to noise ratio comparable to a routinely recorded sodium 1s peak was achieved. One has to keep in mind, however, that due to the different atomic sizes of the alkali metals, results cannot be transferred to all other elements of the first group of the periodic table. Nevertheless, some principles concerning charge transfer between carbon host network and donor guest atoms can be elucidated in this way. Sodium containing carbon films were prepared in the same way as the lithium containing ones under clean UHV conditions with a stepwise increase of metal concentration in the films.

#### **6.3.1 a-C:Na - valence bands**

Complete sets of He I and He II valence band spectra with increasing sodium content are displayed in fig. 6.2 and fig. 6.3 for carbon matrix deposition at room temperature and 800°C, respectively. Spectra for polycrystalline graphite are added in fig. 6.4. The room temperature sample exhibits valence bands with rather round shapes which mainly consist of the p- $\sigma$ -band related maximum at about 7 eV. At 3 eV, a shoulder of considerable intensity can be found for this most amorphous sample of the series. The spectra show only minute variations in shape with increasing sodium content and any shifts are not easy to establish on the weak shoulder.

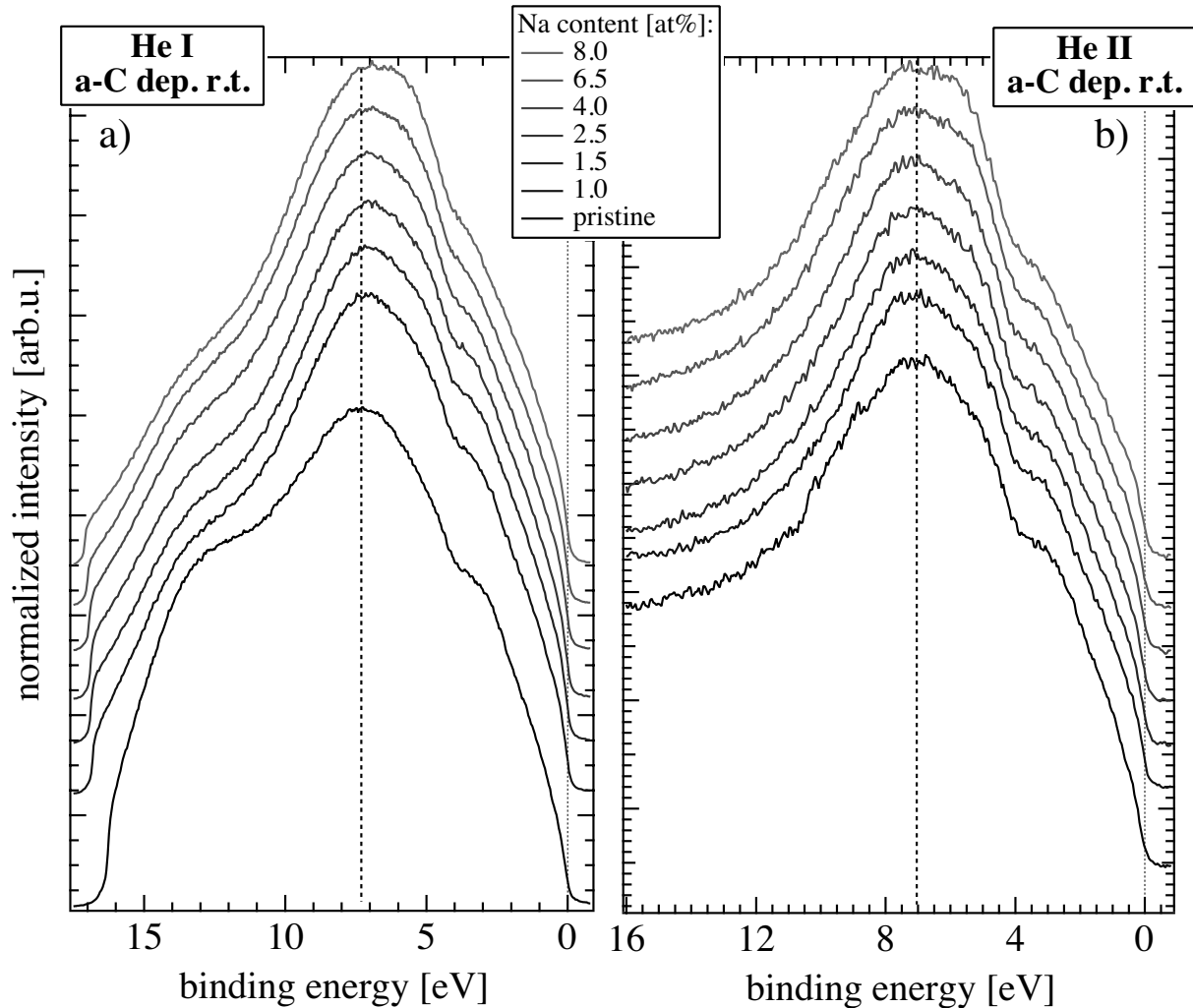


**fig. 6.2:** Development of valence band spectra with sodium addition to a carbon thin film deposited at room temperature. **Left:** He I excited spectra with the almost unstructured  $p$ - $\sigma$ -dominated valence band. **Right:** He II excited spectra of the same experimental series. Only a round shoulder is visible where more ordered material exhibits an albeit small peak (see fig. 6.3).

Both the 800°C sample (fig. 6.3) and polycrystalline graphite (fig. 6.4) show much more structured valence band spectra with a distinct feature at about 3 eV which allows a more reliable determination of the energy shift of this peak and therefore of the Fermi level as discussed in 6.3.1. Only graphite reveals the strong secondary " $\sigma$ -peak" in its He I excited spectra (fig. 6.4, 13.7 eV) although in the pristine 800°C sample its development has already begun in accord with the presence of crystalline regions of sufficient extension. As this peak is due to unoccupied states above the Fermi energy, its position on the *kinetic* energy scale remains fixed [82, 83].

Graphite itself and the amorphous carbons are classified as more or less semi metallic due to a finite overlap of conduction and valence bands even at low temperature. The addition of alkali-metal atoms induces increasingly metal-like characteristics as can be followed in the development of UPS measurements. Most obviously, a distinct Fermi edge is forming in the spectra of the 800°C sample already at low sodium concentrations. For well comparable films of lower carbon deposition temperature, formation of a Fermi edge usually requires higher percentages of sodium in the samples (see chapter 8).



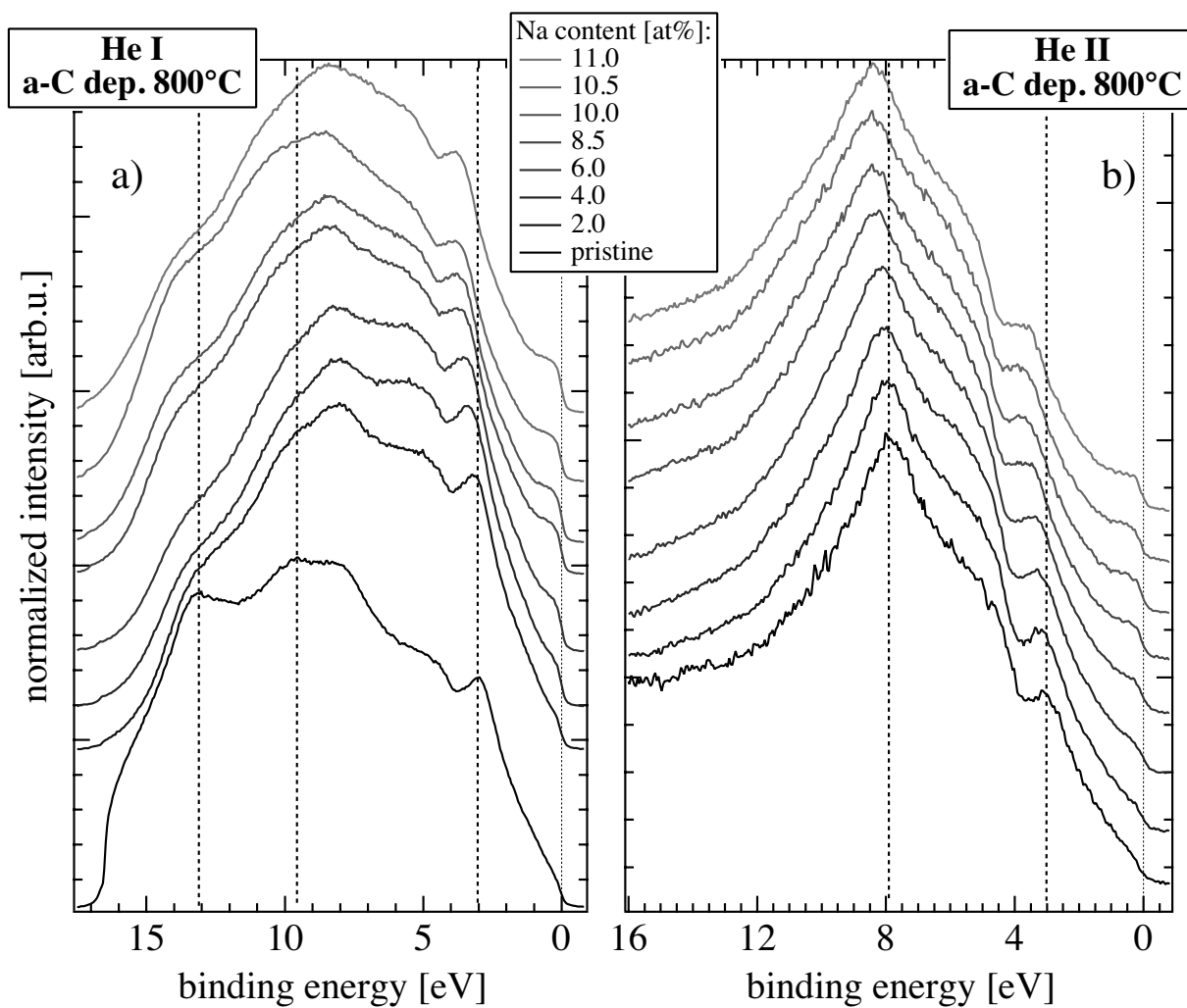


**fig. 6.3:** Valence band spectra of a carbon thin film deposited at 800°C. Spectra were recorded during sodium addition. **Left:** He I excited spectra with the  $p$ - $\pi$ -band feature at 3 eV binding energy which is shifting to higher binding energy and becomes less pronounced with increasing sodium content. **Right:** He II excited spectra of the same experimental series.

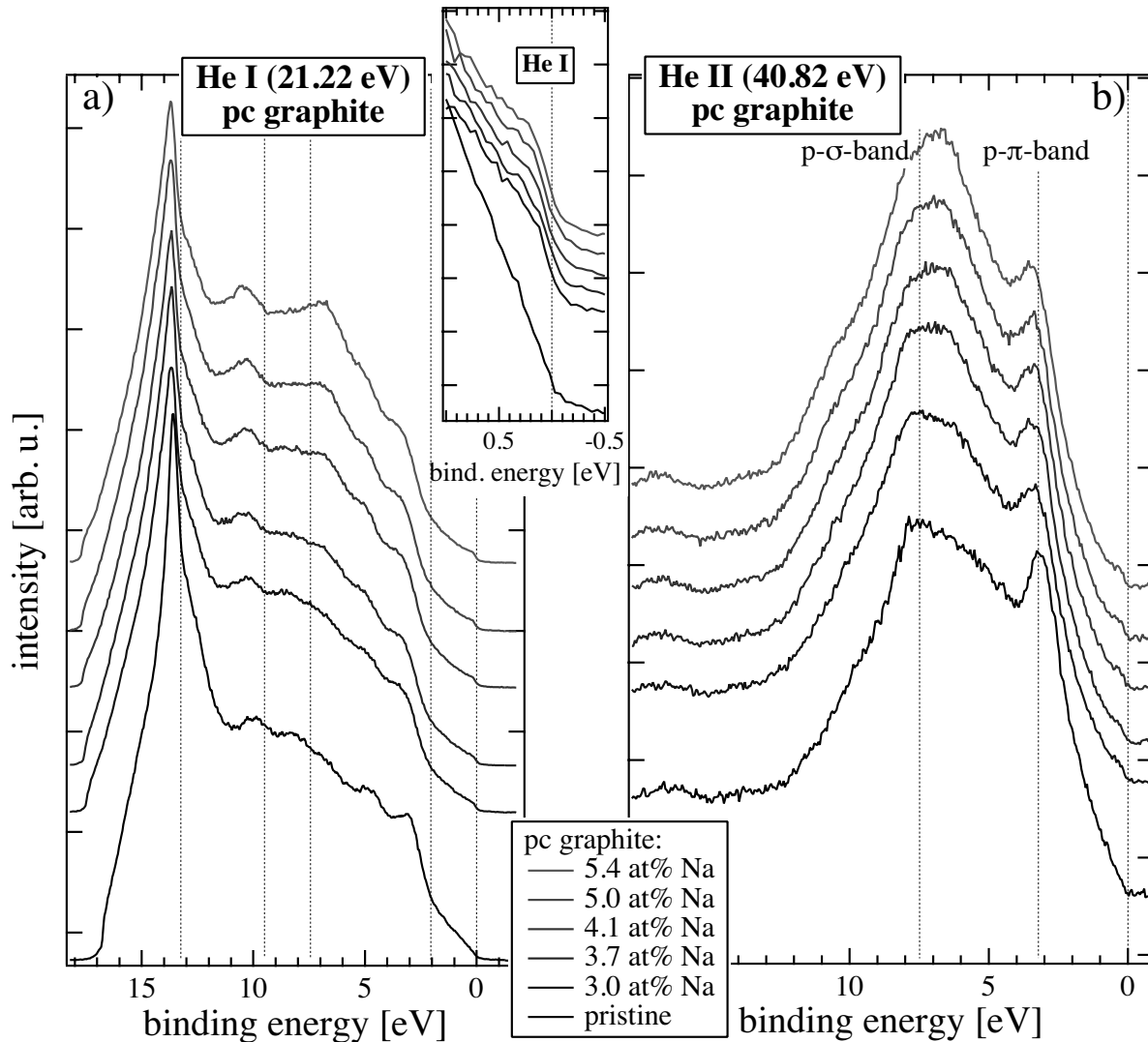


**fig. 6.4:** Valence band spectra of polycrystalline graphite during sodium addition in both UPS modes. **Left:** He I excited spectra with the secondary electron peak at 13.7 eV binding energy (or more precisely at 7.5 eV kinetic energy independent of excitation) [80]. Again, the width of the valence band increases with sodium concentration. The inset shows the Fermi energy region of these spectra. **Right:** He II excited spectra with the p- $\pi$ -band feature at 3 eV which becomes less pronounced with increasing sodium concentration. The secondary peak is missing because of the higher excitation energy. In this case it would appear outside of the measured binding energy range.

In all the spectra of figures 6.2 to 6.4, one can observe a loss of intensity in the p- $\pi$ -related feature with increasing sodium concentration. At the same time, this peak is shifting to higher binding energy. The latter effect in particular is indicative of charge transfer taking place between the metal atoms and the carbon network. The observed shift of the p- $\pi$ - and other features is the effect of the occupation of formerly unoccupied electronic states in the material. This extends the range of occupied states and consequently moves the Fermi energy upwards and closer to the vacuum level (fig. 6.5), which results in a broadening of the valence band's width when a rigid band behaviour is assumed. As the Fermi energy is the zero point of the energy scale in our spectra, peaks and other features appear at higher binding energies at the same time. For the determination of the respective shift from the spectra, a marker structure is chosen from the spectra, in this case the feature at 3 eV, which is assumed to be pinned to its position [84]. Its apparent shift is consequently equal to the

one induced by the electron transfer. One should realize that the denomination of this shift as 'apparent' is as ambiguous as the term 'Fermi level shift'. Nevertheless, both phrases might be used in this work for the sake of brevity.

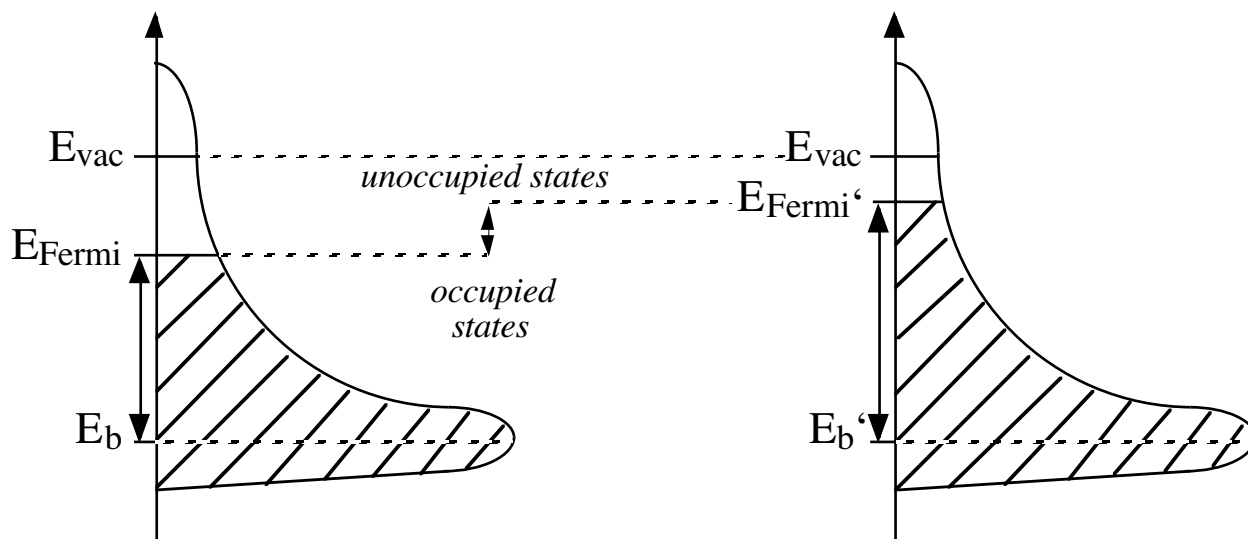


**fig. 6.5:** Schematic representation of the effect of the filling of previously unoccupied electronic states, in this case for a metal. Although the maximum in the electron distribution curve remains at its energetic position  $E_b$  with respect to the vacuum level, it is at a larger energetic distance from the Fermi energy. In photoemission spectra, this yields a shift of the respective feature to a higher binding energy  $E'_b$ .

The described effect is one of those which have previously been observed with graphite intercalation compounds [84]. For the concept of carbon host-reactive guest compounds, the GIC mark the borderline case of composites well defined in both structure and composition. They served as indispensable reference materials for the present investigation wherever the properties of the crystalline clusters of  $sp^2$ -hybridised atoms were concerned. Graphite possesses a low density of states symmetrically around its Fermi energy [85]. Therefore, in a "rigid band" view [86], already the transfer of a small number of electrons into these empty states yields a considerable shift in valence band spectra (fig. 6.4). This argumentation relies on the "rigid band"-model. In other materials and in amorphous ones in particular, there are more electronic states available above the Fermi energy and the same number of electrons transferred does not cause an energy shift as large as the one observed in graphite (cf. fig. 6.2 to fig. 6.4; note the different sodium concentrations). In tab. 6.b the shifts are listed for the amorphous samples and for graphite in relation to the sodium content of the material.

sample	Na-content [at%]	VB-shift [eV] (with vs. without Na)	C1s shift [eV] (with vs. without Na)	Na1s shift [eV] (most vs. least Na)	Na1s shift [eV] (a-C:Na vs. Na metal [87])
pc-graphite	5	0.3	0.2	-0.2	1.5
a-C, 800°C	11	0.8	0.7	0.1	2.1
	5	0.3	0.5		
a-C, 550°C	12	0.6	0.5	0.7	1.7
	4	0.2	0.3		
a-C, 300°C	12	0.5	0.3	0.1	1.5
	6	0.4	0.2		
a-C, r.t.	8	0.3	0.2	0.2	1.1
	5	0.3	0.2		

**tab. 6.b:** Energetic shift of valence band features, respectively of the Fermi edge, for samples with the given sodium content in comparison to the metal free a-C. Right columns refer to the discussion of shifts in core level spectra which do not simply match the ones observed in valence band spectra (cf. 6.1.3.2). The reference value for metallic sodium (1071.8 eV) is taken from [88]).

In fact, the samples deposited at higher temperatures show larger shifts. Even taking into account the higher sodium content of the a-C samples, the observed shifts in those materials are larger than expected from comparison with graphite (cf. second lines in tab. 6.b indicating values for approximately 5 at% sodium in all samples). Accordingly, the assumption of an increased density of states above the Fermi energy might not apply in the described manner for all the samples although it is in agreement with the observations on the low temperature deposited samples. It is possible that the polycrystalline graphite used in this study and the high temperature deposited samples with a "mixed" amorphous/crystalline composition have similar properties also in this respect. One can even imagine that cluster sizes in the a-C samples were larger than the ones of crystallites in polycrystalline graphite. With respect to intercalation the coexistence of crystallites with an amorphous fraction might be more favourable than a polycrystalline sample with small crystallites and a lot of disturbing grain boundaries. A strong indication to this is the polycrystalline graphite's density which is much lower than the one usually accepted for graphite ( $1.83 \text{ g}\cdot\text{cm}^{-3}$  versus  $2.27 \text{ g}\cdot\text{cm}^{-3}$  [89]).

### 6.3.2 Core level spectra

Firstly, XPS was applied to establish the elemental composition of the samples. In our case, the increase in sodium content was monitored and the uptake of oxygen was controlled to ensure reproducible conditions. Fig. 6.6 depicts the development of compositions with carbon concentrations on the ordinate. The oxygen concentration was essentially independent of the increase in sodium content.

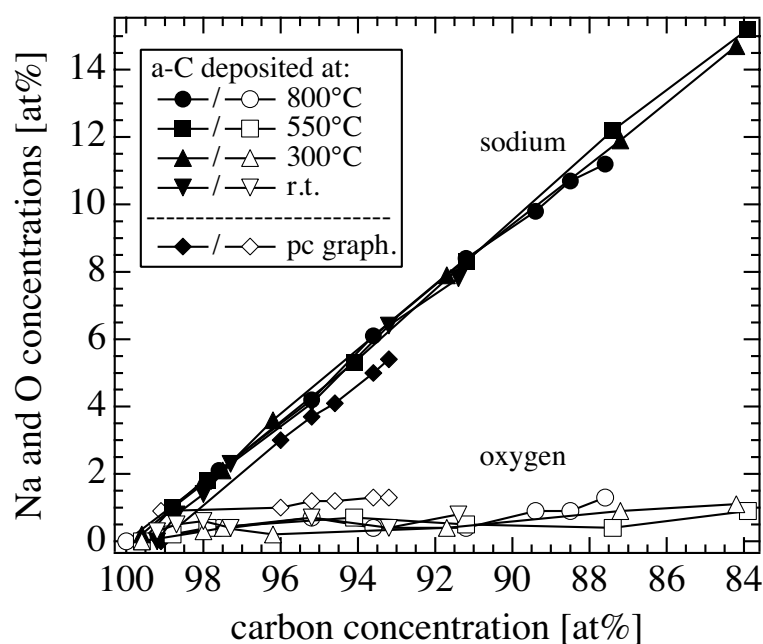


*fig. 6.6: atomic concentrations from Na1s (filled symbols) and O1s (open symbols) core levels. Data is referred to the decrease in carbon concentration. The oxygen uptake was kept independent of the increase in sodium content.*

From a closer investigation of binding energies and peak widths in carbon and sodium core level spectra, information about the binding situation inside of the films can be gathered. The according values for C1s and Na1s core levels are given in tab. 6.c. The values refer to the respective peaks after background subtraction. Of course it would be desirable to obtain data for the different components of each peak. Therefore, deconvolution procedures using Doniach-Sunjić type peak shapes were performed which have been used successfully in earlier studies of a-C:H and many other carbon based materials (see, e.g. [23]). However, these yielded either no or more or less arbitrary results. As no physical significance could be attributed to this kind of results, we prefer to base the interpretation on the measured data alone.

dep. T of a-C [°C]	C1s		Na1s		metal content [at%]
	FWHM in C+metal [eV]	binding energy in C+metal [eV]	FWHM in C+metal [eV]	binding energy in C+metal [eV]	
HOPG[76]	1.98	285.0			11.1 (Cs)
pc graphite	1.4-1.5	284.6-284.6	2.5-2.4	1073.5-1073.3	3-5 (Na)
800	1.6-2.0	284.6-285.1	2.4-3.2	1073.8-1073.9	2-11 (Na)
550	1.7-2.1	284.4-284.9	2.3-3.0	1073.2-1073.5	1-15 (Na)
300	1.8-2.0	284.3-284.7	2.3-2.6	1073.1-1073.3	2-15 (Na)
r.t.	1.9-2.0	284.3-284.4	2.1-2.3	1072.7-1072.9	1-8 (Na)

*tab. 6.c: ranges of full widths at half maximum and binding energies for C1s and Na1s signals in  $sp^2$ -based carbon materials. Only values for HOPG are taken from [76]. Note that values for the metal-containing state in this case refer to cesium intercalation.*

In fig. 6.7 the development of C1s binding energies (left) and full widths (right) with stepwise increasing sodium concentration is displayed. The values for the pristine carbon materials which appeared in tab. 6.a are included at [Na] = 0 at%. Part b) of the figure clarifies the ranges of binding energies by only showing minimal and maximal values observed on the five materials.

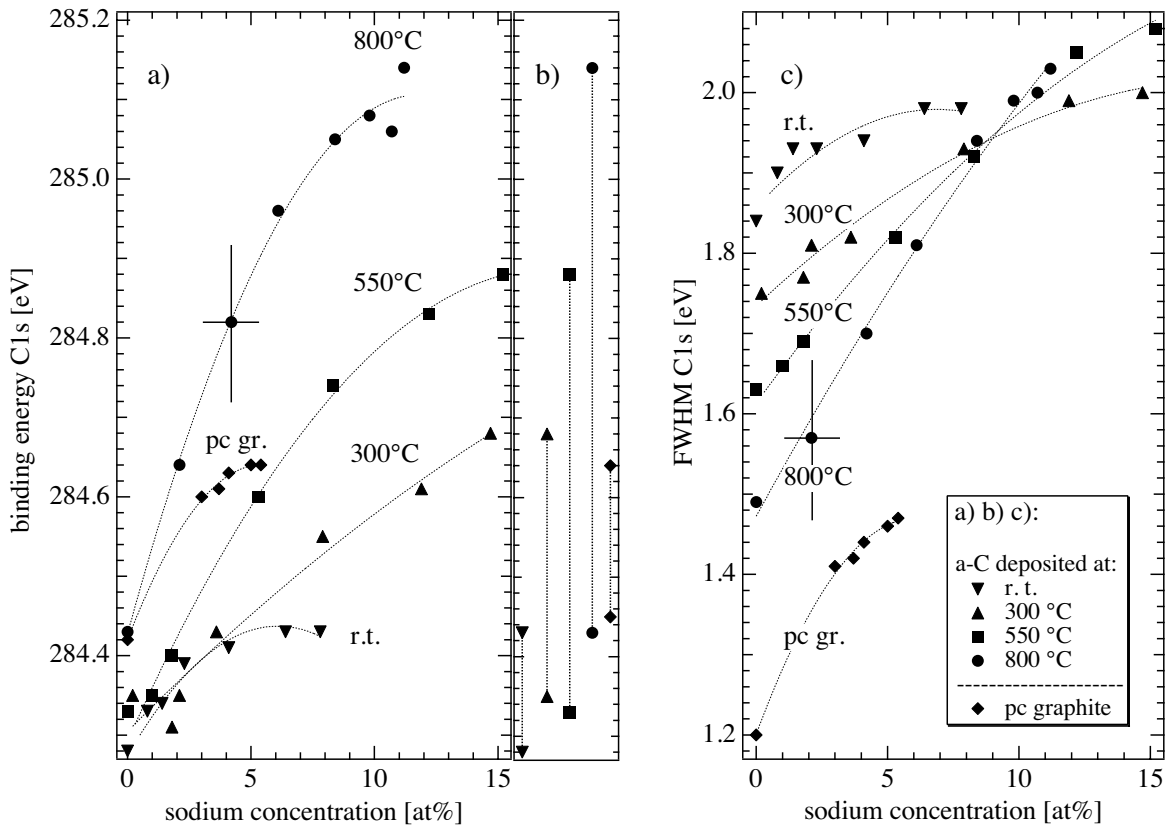


**fig. 6.7:** development of binding energies (a), their minimal and maximal values (b), and development of FWHMs (c) for C1s signals of amorphous carbons deposited at room temperature, 300°C, 550°C, and 800°C and graphite.

Here, smallest peak widths are observed for highest deposition temperatures, as discussed above. With increasing sodium concentration, all samples showed a trend towards wider peaks and higher binding energies, although not at the same rate. Among the amorphous carbons, peak width increases the most for the one deposited at 800°C (by more than 0.5 eV between 0 and 11 at% Na) and the least for the room temperature deposited one (by about 0.1 eV between 0 and 8 at%). As a result, the order of the samples according to their C1s peak widths changes for sodium concentrations of more than about 9 at%. From there on, peaks for the higher carbon deposition temperatures are wider. Graphite itself shows a step increase of its originally narrow C1s peak width with sodium concentration, too, but although the concentration range covered in the experiment is rather small, it seems probable that the overall change of peak width for larger concentration ranges is smaller than at least in the 800°C film. In contrast to the thin amorphous carbon films, graphite was used in the form of a bulk sample of 0.5 mm thickness. According to our observations, large quantities of sodium diffuse into the bulk of the material. Therefore, by the method used here concentrations achievable in graphite must be lower than the ones in the amorphous films. This must be considered in the interpretation of the results.

C1s binding energies follow a parallel trend: the largest increase is observed for the 800°C a-C (0.7 eV between 0 and 11 at% Na) and the smallest is found for room temperature a-C with less than 0.2 eV between 0 and 8 at%. As can be seen in fig. 6.7 (left) this difference is not due to the smaller concentration range, but to the different concentration dependence. The C1s binding energy in pristine graphite is about the same as the one in 800°C a-C. Its change with addition of about 5 at% sodium, however, is considerably smaller than in the 800 and even slightly smaller than in the 550°C amorphous carbon.

A complication occurs because of the rise of the Fermi level into formerly unoccupied states as described above. In the most simplest model, one should expect the same shift which was observed in UPS also in the core level spectra. This is not the case as can be seen in tab. 6.b. Binding energy shifts on individual core level signals comprise the described effect on the Fermi energy *and* chemical shifts. While the former is a property of the interaction of the bulk material with guest atoms, the latter are due to the interaction of individual atoms with each other and include contributions from core hole relaxation energies. With carbon's 1s electrons, the effect of electron transfer to unoccupied states above the Fermi level increases binding energies. Quantitatively, it outweighs the effect of increased photohole screening on individual carbon atoms due to charge transfer from sodium which is expected to decrease C1s binding energies. Therefore, shifts of the valence band and the C1s peak actually observed are of roughly the same magnitude when referred to the metal free material (tab. 6.b).

Both FWHM and binding energy also change on the sodium 1s signal (fig. 6.8). Higher binding energies are observed on the amorphous carbons deposited at higher temperature and the order of the four samples according to the Na1s binding energy is preserved over the sodium concentration range. While binding energies of the C1s peak seem to approach some kind of plateau, Na1s binding energies even pass through a maximum which is, however, not very pronounced in the lower temperature deposited samples. Because of this maximum, the binding energy ranges for Na1s given in tab. 6.c are not representative because the difference between smallest and largest values is much larger in some cases (cf. tab. 6.d). Again, graphite does not figure where it might be expected from the considerations regarding its structure in comparison to the amorphous carbons. Its Na1s binding energies range between the ones for the 800 and the 550°C materials and although the concentration range is small, the values tend to fall with increasing concentrations. In the case of the Na1s signal the same considerations with respect to the Fermi level shift and the observed peak shift apply as detailed before. The comparison of both values (tab. 6.b) does not yield an easily understandable relation in the case of these materials. However, reference of the signal shifts observed in a-C:H to the binding energy of pure metallic sodium (1071.8 eV [88]) again shows the clear trend of increasing shifts with higher deposition temperatures. Graphite figures at a value comparable to the one of the 300°C sample. We suspect that a large number of grain boundaries in the polycrystalline graphite used for this work might inhibit access of the intercalant species. In this respect, the mixed materials containing larger clusters and a certain fraction of an amorphous phase seem to be more favourable for the intercalation. Intuitively, one might think of a more "open" structure with less restrictions for atomic diffusion in these materials.

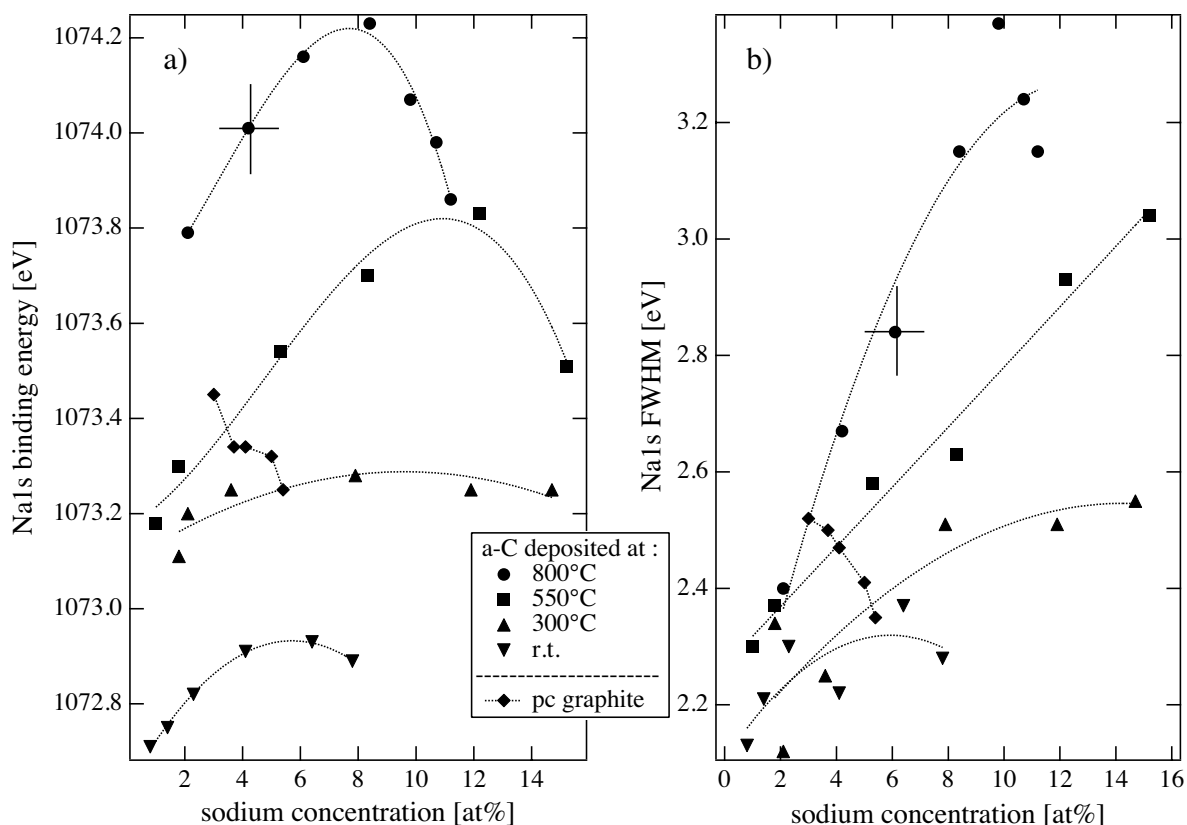


**fig. 6.8:** development of binding energies (a) and FWHM (b) for the Na1s peak in the four different amorphous carbons and graphite. Note the deviating behaviour of signals for sodium in graphite.

Unlike the FWHMs for C1s, the ones for Na1s at low concentrations in all samples fall in the same range. With increasing sodium content, they diverge because of the different dependence on metal concentration. For all the amorphous materials, peak widths grow. Again it is the high temperature deposited materials which show the most pronounced effects while the room temperature deposited one only exhibits a rather minute tendency towards broader peaks. Polycrystalline graphite behaves differently with its Na1s FWHM decreasing with slightly increasing metal content.

	lowest binding energy [eV]	highest binding energy [eV]	sodium content for maximal binding energy [at%]
pc graphite	1073.3	1073.5	3
800	1073.8	1074.2	8
550	1073.2	1073.8	12
300	1073.1	1073.3	8
r.t.	1072.7	1072.9	6

**tab. 6.d:** extreme values for Na1s binding energies in various samples. Data refers to the same measurements as those in tab. 6.c. Note that the behaviour of graphite deviates in that the higher value was obtained at lower concentrations fig. 6.8.



#### ***6.4 Carbon and metal: interpretation***

A conclusive interpretation of these observations must take into account the structural peculiarities of the materials and the various forms of interaction between the carbon host structure and metal guest atoms. In particular, the dualism of binding environments between the clearly covalent attachment to dangling bonds and an intercalate like insertion into the spacings of layered clusters are discussed. The latter mechanism is best known from graphite, which is the prototype host material for intercalation reactions. From what was said above about rather extended graphite-like clusters in the high temperature deposited amorphous carbons, a considerable contribution of intercalation can be expected in these materials, too. With decreasing temperature during carbon deposition, the share of amorphous carbon with numerous dangling bonds in it increases strongly. This transition in the availability of coexisting binding sites for mobile guest species is reflected in the spectra. As a rule, the changes during metal incorporation are the smaller the more uniform the carbon's structure is. Therefore, both graphite and room temperature deposited a-C experience comparatively small changes because the one is almost entirely crystalline, whereas the other is predominantly a very disordered amorphous material with no long range order and only very small crystalline contributions. Both are very unlike in atomic order, but in themselves they are rather uniform with respect to the kind of binding environment they can offer to guest atoms.

The behaviour of polycrystalline graphite in some respect deviates from the one expected from a simple extrapolation of the amorphous carbons' characteristics towards higher crystalline order. This very interesting result indicates that additional factors must govern the interaction with metal atoms. The role of grain boundaries in particular must be taken into account, as they influence diffusion within the material and electron delocalization. The loss of metal into the bulk of these thicker samples which resulted in low surface concentrations may well be due to preferred diffusion along these grain boundaries (see, e.g. contributions in [90]). With respect to other properites, a material can be all crystalline, but due to the arrangement in a large number of very small crystallites with a lot of boundaries between them, only part of the typical "crystalline" features can be observed. A comparison with highly oriented pyrolytic graphite (HOPG) is therefore still of major interest.

For the structurally more mixed films, the mechanism of metal incorporation is understood in the following manner. When only a small number of metal atoms is added, they diffuse through the carbon matrix and attach to the first accessible binding site. In the more amorphous material, this is most probably a dangling bond, whereas in films with a larger fraction of graphite-like regions, this may be a site inside one of these clusters with similar probability. However, intercalation into graphite usually requires some activation [38] (p.143-148 and references therein). The introduction of a guest atom in any case induces a severe disturbance in both electronic and geometric respect. The host material's capability to accept and screen this disturbance is decisive for the ease with which the guest particle can be accomodated and for the difference between the properties of the pristine host material and the host-guest compound. Recently, an instructive example was given with the comparison of the lithium intercalation behaviour of the two chemically identical titanium-dioxide modifications anatase and rutile [91]. From experiments it was known that both materials intercalate different quantities of lithium and show a different temperature dependence. The theoretical study showed that apart from factors such as local distortions and the interaction of the

guest atoms with each other the kinetics of diffusion to the thermodynamically favoured intercalation sites is responsible for those observations. Where, e.g., a strong spatial anisotropy of diffusion constants restricts the penetration of lithium atoms through the network, the available channels for diffusion can be blocked by the formation of lithium-ion pairs without the chance of bypassing the blockade at low temperatures. As in our case the embedding of the clusters in an amorphous matrix restricts both the mobility of metal atoms at cluster edges and the free expansion of lattice spacings in the clusters intercalation is probably kinetically not favourable either. It can be assumed that at low metal atom concentrations usually dangling bonds are saturated preferentially as long as there are any of them available.

With respect to the photoemission spectra this assigns the low binding energy states of both carbon and sodium to electrons originating from atoms involved in this kind of covalent bonding. In the room temperature deposited material, there exists a large variety of binding environments for the atoms of the amorphous matrix which causes the large width of the C1s peak. However, in spite of this multitude of slightly different carbon atoms, Na1s peaks are among the narrowest ones in these experiments (though these peaks are still wider than the C1s peaks). Again, this is due to the fact that the majority of sodium atoms in the most amorphous material is covalently bonded with a degree of ionic character which depends on the atomic environment of both atoms. This includes the way the carbon atom is attached to its adjacent atoms (double bonds, single bonds, different hybridisations) and the proximity of other non-bonding neighbours with their influence on charge distribution in space. Necessarily, a large variety of atomic arrangements is present in a-C which leads to numerous different types of dangling bonds, e.g. those on the edges of clusters versus those inside of the matrix to name only the most basic distinction. For small graphitic clusters (about 2 nm in diameter which equals the one of clusters in the r.t. sample) it has been shown that the degree of charge transfer between - in this case - lithium and carbon atoms [52] is strongly dependent on such variations in the environment. Reactivity for bonding is enhanced at cluster edges which are supposed to play an important role in the uptake of excess metal. The bonds formed in these cases do not even allow a discussion in terms of a clear "covalent" versus "ionic" dualism.

Binding energies of Na1s electrons at maximal intensity in *all* the materials investigated in the present study cover a range of more than 1.5 eV. This is rather astonishing for bonds between the same two elements as long as only covalent bonds are considered. With additional contributions from intercalation these values can be understood much better. As described above for the amorphous materials, only a minor fraction of metal atoms can find its way into intercalated states because most of them bind elsewhere before. Accordingly, this picture changes for the materials with a larger fraction of graphite-like clusters. While the contribution of dangling bonds is still considerable, the spectra are strongly shaped by the higher probability of intercalation due to the increased graphite-like fraction. The increasing value for the binding energy of the peak maximum is indicative of the larger charge transfer from the metal atoms to the carbon matrix as observed in GICs [92]. The large peak widths are therefore due to the presence of sodium atoms in covalent bonds and intercalated ones at the same time and in roughly comparable quantities. Charge transfer in the intercalate depends on the concentration of metal atoms as has been shown theoretically for GICs in various stages [93]; the "stage" in the case of GICs denotes the number of carbon layers between adjacent intercalated metal layers. Stage-1 is the metal richest GIC which can for example

not be produced with sodium. In this case only stages equal to or higher than 4 are accessible [94] as binary compounds and even these were obtained in mixture with unreacted graphite. Such sodium GICs of stage 4 or higher possess a stoichiometry  $\text{NaC}_n$  with  $n \geq 32$  and contain 3 at% and less of sodium. A hypothetical first stage sodium compound would show the stoichiometry  $\text{NaC}_8$ . This would yield a concentration of 12.5 at%. In comparison, the ideal first stage lithium GIC  $\text{LiC}_6$  contains 14.3 at% of lithium. The different stoichiometry is due to the smaller size of lithium atoms in comparison to all other alkali metal atoms.

As mentioned above, the binding energy of the Na 1s peak passes through a maximum in some cases approaching a value comparable to the one in metallic sodium. Due to the restrictions in sodium uptake into clusters there might indeed be present sodium of more or less metallic nature at or close enough to the surface under these clean conditions. However, we do not see direct proof for this at the moment.



## 7 Reactivity of lithium containing amorphous carbon

The above discussion of metal-carbon interaction also applies to the a-C:Li-system in all essential points. In the following, the focus will be on the chemical reactivity of lithium containing amorphous carbon towards reactive gaseous species. The preparation was usually carried out in the same way as already described. Lithium was in most cases added to the amorphous carbon matrices after the carbon deposition was finished. Only in a few selected experiments the metal was deposited simultaneously with the carbon evaporation ("codeposition").

### 7.1 Chemical reaction with molecular oxygen

In the course of the reactivity experiments, the use of molecular oxygen marks the mildest treatment in that the particles are chemically reactive, but do not carry more than thermal energy. This corresponds to the situation of residual gas in an evacuated fusion vessel before any discharge is ignited which generates more energetic or reactive species.

Prior to oxygen exposure the a-C:Li contained less than 2 at% oxygen. For the following experiments, these clean samples were exposed to oxygen in a controlled way in the preparation chamber of the vacuum system (fig. 5.1). Exposures are given in Langmuir ( $1 \text{ L} = 1.33 \cdot 10^{-6} \text{ mbar} \cdot \text{s}$  or  $10^{-6} \text{ Torr} \cdot \text{s}$ ) accounting for different combinations of gas pressures and exposure times. In most cases, results are presented for room temperature deposited a-C and for material produced at  $800^\circ\text{C}$ . Again, graphite is included for reference.

The most striking effect of oxygen exposure of a-C:Li was observed commonly for all experiments performed: Lithium concentrations always showed a steep increase even at oxygen exposures as low as 1 L. The increase in lithium content was directly related to the uptake of oxygen by the films (fig. 7.1).

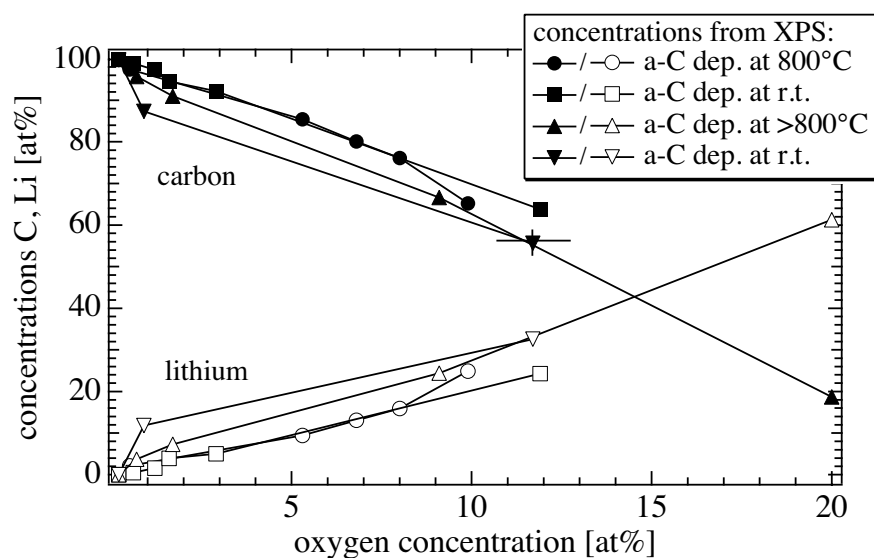


*fig. 7.1: examples for the relation between lithium and oxygen concentrations in amorphous carbon samples deposited at room temperature and at  $800^\circ\text{C}$ , respectively.*

From core level spectra it was evident that the vast majority of lithium and oxygen was bound in lithium oxide ( $\text{Li}_2\text{O}$ , free enthalpy of formation:  $-561.2 \text{ kJ}\cdot\text{mol}^{-1}$  [40]) (fig. 7.2 and fig. 7.3). During oxygen exposure only very small changes in C1s peak parameters were observed although during clean metal incorporation, the C1s signal experienced a binding energy increase and peak broadening comparable to those detailed for a-C:Na above. Li1s and O1s peaks not only gained in intensity, but also exhibited considerable chemical shifts and changes in peak shape. On a-C:Li and on as deposited a-C after some time an oxygen signal was identified at about 532.4 eV which originates from adsorbed oxygen containing species. During lithium addition and measurements a certain level of oxygen contamination cannot be completely avoided. In the case of a-C:Li this adsorbate sometimes already reacted to form lithium oxide and other products containing both lithium and oxygen. In spectra a to d of fig. 7.2 (top), the oxidic state is found at binding energies of 529.5 eV to 530.5 eV which is typical of many metal oxides [87]. It dominated the spectra when a concentration of about 8 to 10 at% of oxygen uptake was reached. The lower binding energy value usually dominated for carbon matrices deposited at room temperature, whereas the higher one was regularly observed on 800°C deposited samples. On graphite, both states were not separable (fig. 7.3, bottom). The assignment of the O1s state at around 533 eV is more difficult. It is observed at lower binding energy on room temperature deposited carbon and at higher energy on 800°C material. Different assignments are considered such as suboxides, hydroxides or unreacted adsorbed oxide [95]. As time of flight (TOF) mass spectrometry revealed, the SAES lithium dispensers also emit considerable amounts of hydrogen together with the desired metal atoms. Therefore, it can be assumed that hydrogen and residual water are involved in the formation of hydroxidic compounds. As an alternative or rather complementary assignment suboxides have been suggested as well as unreacted adsorbed oxygen [95] and under the given reaction conditions, the presence of suboxides from incomplete reactions is a likely assumption. They were observed on cesium GICs [96] and even on Cs multilayers [97]. The depletion of the high binding energy state after electron irradiation of the samples during EELS measurements also supports this view of less tightly bonded species (fig. 7.3). It is particularly tempting to connect the presence of suboxides with the ratio of lithium to oxygen which is usually higher than 1 : 2. However, when considering the lithium to oxygen ratio one has to keep in mind that the escape depth for Li1s photoelectrons is more than twice as large as the one for O1s electrons. As long as the distribution of lithium and oxygen is homogeneous throughout the information depth, this is already included in the calculation of the respective concentrations. The same values, however, could be obtained from the elements in an inhomogeneous, layerwise distribution which cannot be distinguished by concentrations alone. In addition to the lithium species mentioned, carbon oxidic species have also been discussed to form for sputtered amorphous carbon films [98]. From the spectra for carbon and from the high reactivity of lithium in our case it is unlikely that they contribute more than traces, if any, which has been checked by measurements of the oxygen exposure of pristine metal-free material.

Binding energies of the Li1s state in the non-oxidized material are between 56 and 57 eV close to results for the stage-1 graphite intercalation compound  $\text{C}_6\text{Li}$  (57.1 eV [99]). The oxidation shifts binding energies to lower values between 55 and 56 eV. These values are in agreement with data for  $\text{Li}_2\text{O}$  (55.6 eV [100]). Interestingly, exposure of a-C:H/Li to an oxygen plasma led to a small shift

to *higher* binding energy [23]. The observation of binding energies of 55 eV and below for the oxidized material, however, is intriguing. In carbon based material, formation of a carbidic compound has been observed [101], but neither is carbide formation expected under these very mild conditions nor is it observed in the carbon core level spectra. In chapter 7.1.2 the presence of unreacted metal with a binding energy of 54.4 eV [100] to 54.9 eV [99] will briefly be mentioned as a possibility in connection with the mechanism of oxidation.

Additional information is provided by fig. 7.2 which compares two samples of a-C deposited at room temperature. Top spectra were recorded for a sample to which lithium was added *after* the carbon deposition, whereas the bottom ones were measured on a sample in which carbon and lithium were deposited simultaneously. No major differences arose for the oxidation process, but recovery of the material by annealing seemed to proceed more readily in the sample with post-deposition lithium addition.

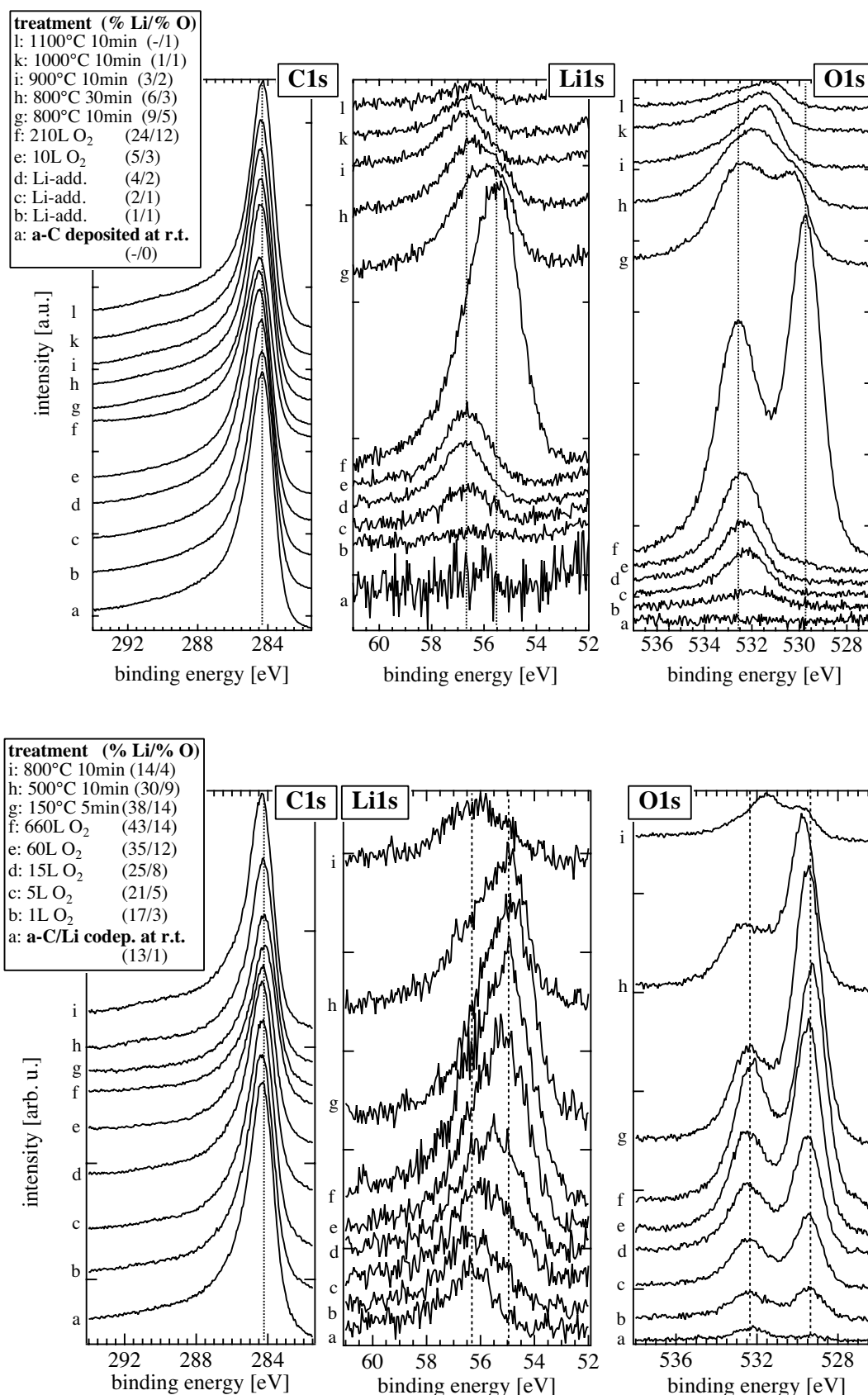


**fig. 7.2:** *top: r.t. deposited a-C, bottom: r.t. a-C codeposited with Li. See the coincidence of states in samples from both deposition methods. "Li-add." signifies the addition of lithium to amorphous carbon, "O<sub>2</sub>" marks exposure to the given number of Langmuir and the number pair in parentheses gives the percentages of lithium and oxygen, respectively. Measurements after annealing are included.*



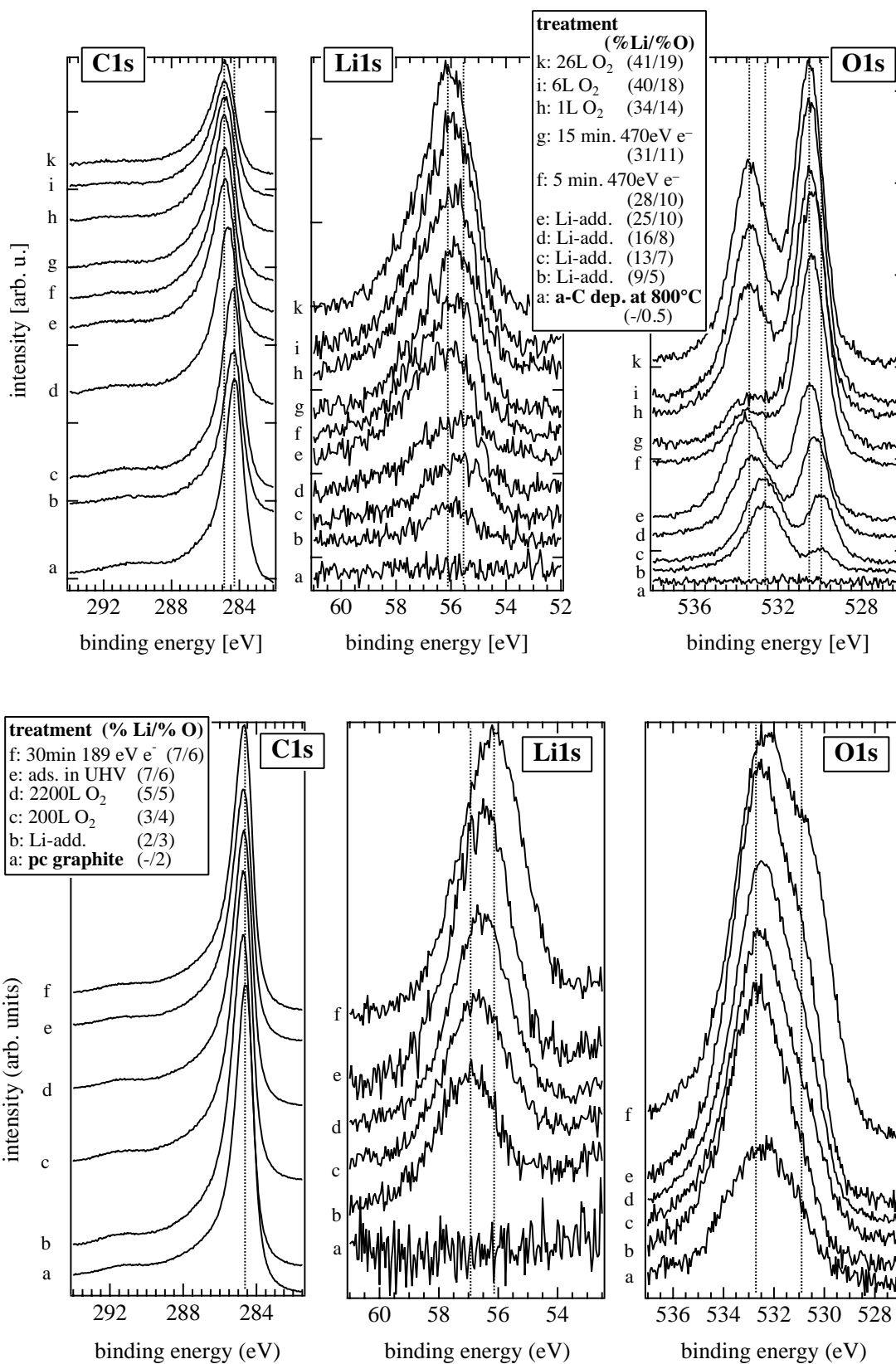


**fig. 7.3:** *top:* a-C deposited at 800°C. *bottom:* polycrystalline graphite. Same labelling as in fig. 7.2. Note the presence of the  $\pi$ -plasmon between 291 and 292 eV in the 800°C sample which is usually best developed in crystalline graphite. Both series include electron irradiation during EELS-recording, the top one also annealing steps (see 7.1.4).

### 7.1.1 Elemental distributions in the films

An essential question in connection with the observation of the oxidation process was, whether the dramatic increase in lithium concentration was merely due to the removal of the carbon matrix. This is of course closely related to the problem of *where* lithium and oxygen are actually located in the film. In principle, lithium oxide can be distributed throughout the film or it can be located just on top of the material and in both cases, erosion of carbon through the reaction has to be considered. For this purpose two different kinds of experiments were carried out, sometimes on the very same samples. Firstly, very thin films were used and secondly, samples were tilted with respect to the analyzer.

Very thin a-C films were deposited to allow photoemission detection of the silicon substrate underneath (thickness less than 3 nm). It was therefore possible to compare the development of the concentrations of carbon and silicon. Should a new layer form on top of the material, it must attenuate the signals of all the elements underneath. If mixing with the top phase (carbon) occurred, one would have to expect a different development for carbon and silicon. Erosion of the carbon layer, on the other hand, would yield an increase of the substrate's signal which would be less attenuated by the carbon cover.

In the experiment, one could observe that the signal intensity from the substrate decreased in parallel with the one of carbon when oxygen was offered and lithium oxide was formed (fig. 7.4).

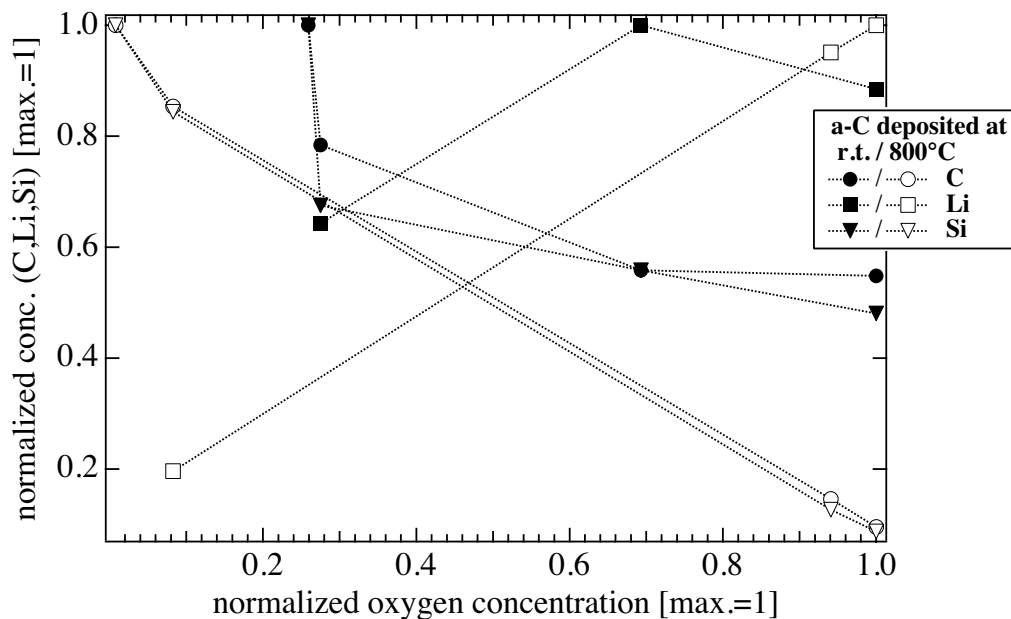


**fig. 7.4:** development of normalized carbon and silicon concentrations with increasing oxygen content in room temperature and 800°C deposited a-C. The normalization refers to the maximum concentration which was obtained for each element so that a value of 1 in the graph corresponds to the element's maximal concentration in this experiment. Data for lithium is included. Deviations at low oxygen content are probably related to different absolute film thicknesses.

As can be seen, a clear correlation between carbon and silicon concentrations was obtained. This means that both materials were covered by a lithium oxide layer forming on top of the film. Neither

erosion of carbon nor formation of lithium oxide inside of the carbon layer were the dominating process.

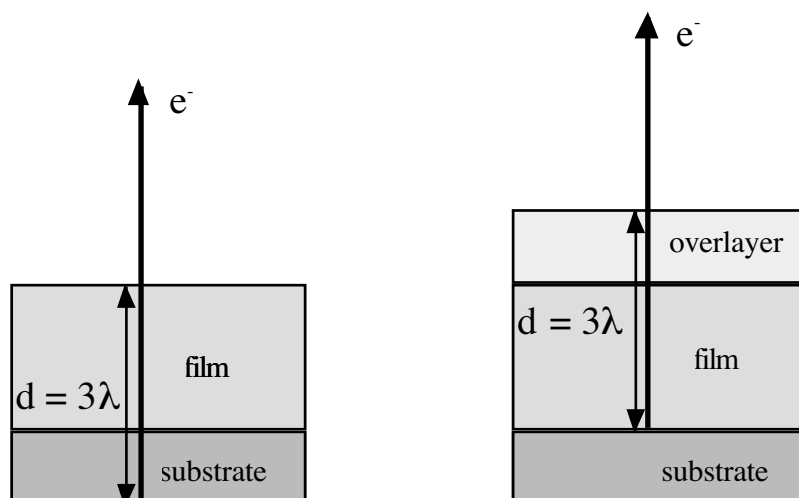


**fig. 7.5:** schematic of the effect of overlayer growth on substrate signal intensity. When an overlayer is developing, signals of the underlying materials are attenuated. This effect is even more pronounced, as the topmost regions contribute more to the overall signal than the lower ones according to the Lambert-Beer-law.

Further evidence for this was obtained from another set of measurements in which samples were rotated relative to the analyser's entrance axis by an angle  $\theta$  (fig. 7.6). Really angle resolved measurements could be used for a rather straightforward quantification of layer thicknesses provided that well defined interfaces exist [102]. For compositional gradients procedures become more complicated. Measurements presented here therefore serve as tests for the structure of the material and can help to decide between alternative models as in this case. The additional information compared to routine photoemission measurements results from the variation of the distance which photoelectrons have to travel through the solid before they leave its surface. In the routine measurement, the sample's surface normal is directed towards the analyser entry (left in fig. 7.6).

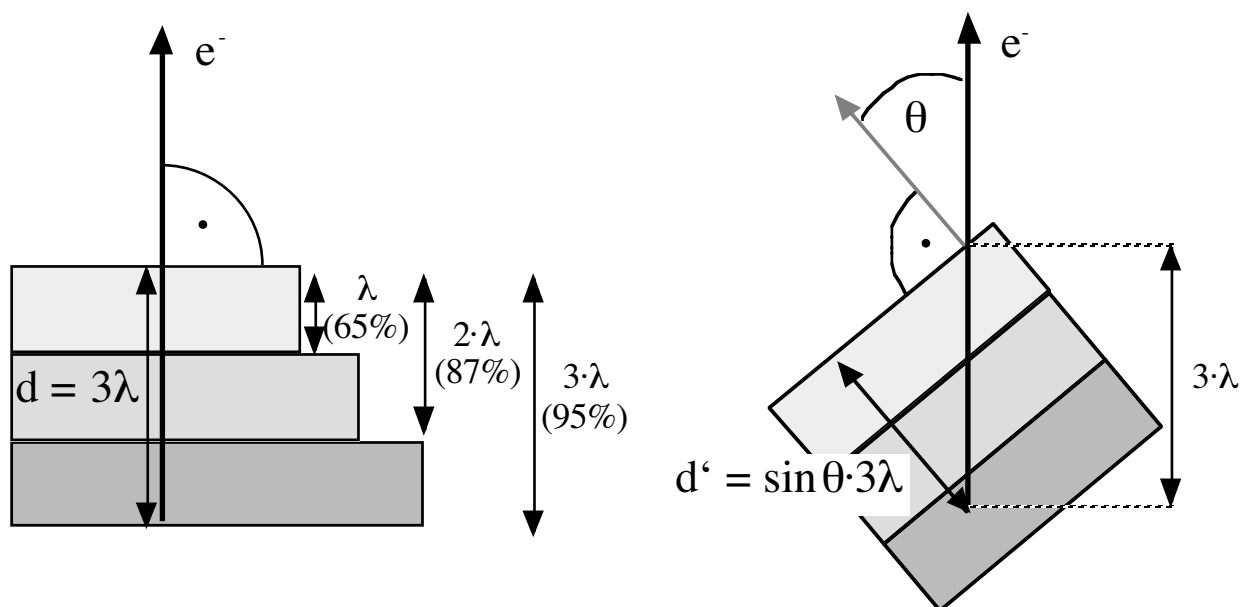


**fig. 7.6:** schematic of the background of photoemission experiments with samples rotated by an angle  $\theta$ . Left: standard setup, right: variation of the angle tunes the depth within the sample down to which the material is probed. Contribution of electrons from different depths are also indicated.

Although an analyser positioned in the direction of the surface normal also collects electrons emitted in many other directions due to the finite size of its entrance slit, the main weight is on those electrons which leave the sample along the surface normal. At an escape length  $\lambda$  given by the electron energy, these electrons carry information from the largest depth  $d = 3 \cdot \lambda$  inside the sample. According to geometric arguments, this means that in order to reach the surface of a sample tilted by the angle  $\theta$  with respect to the surface normal, electrons must originate from regions of the bulk which are closer to the surface within  $d' = \sin\theta(3\lambda)$  (see fig. 7.6). By variation of the tilting angle between  $90^\circ$  and  $40^\circ$ , one can vary the probing depth between  $3 \cdot \lambda$  and  $0.64 \cdot (3 \cdot \lambda)$ . One has to keep in mind that in any case photoelectron spectroscopy favours electrons from the near surface region according to the Lambert-Beer equation [63]. 65% of the emitted electrons originate from within a depth of  $\lambda$ , 87% from within  $2\lambda$ , and 95% from within  $3\lambda$ . These weights are conserved for any angle investigated though modified by the factor of  $\sin\theta$ .

Results are discussed for a metal free a-C thin film deposited on silicon at room temperature and for the same sample in the lithium containing and the oxidized state. The quantitative results of these experiments are summarised in fig. 7.7. Because the measurements required extended measurement times, the concentration data includes some variations due to deterioration of the material by further oxygen adsorption. However, control measurements showed that this did by no means account for the observed effects. The diagrams comprise the effects of the oxidation itself which is responsible for the different concentration levels in the untilted position ( $\theta = 90^\circ$ ) and of the tilting of the sample. With an equal distribution of all four elements, the rotation of the sample would reduce their intensities equally, but would preserve their concentration ratios, which is not the case here. For example, 21 at% silicon are detected under the pristine carbon film. When the sample is rotated, its concentration decreases to only 3 at% in the  $40^\circ$  Position. In the lithium containing state, the additional material on top reduces the silicon's signal intensity so far, that even in the  $90^\circ$  position only 7 at% are detected. Only 3 at% are found after oxidation. For the other elements a distinction must be made between angles  $\theta$  from  $90^\circ$  to  $60^\circ$  and those below this. Within the former range, carbon concentration is slightly decreasing in the lithium containing and oxidized states while the lithium concentration is growing in agreement with the view of an accumulation of lithium closer to the surface. As no lithium was added during oxygen exposure, the metal atoms must originate from within the bulk. At the extreme angles of rotation, the measurement is still becoming more surface sensitive and finally mainly probes the material on top of the film itself and yields an increase in carbon and oxygen concentrations at the expense of silicon and lithium. For the case of oxygen, for example, a look at the O1s spectra in fig. 7.8 confirms that it is in fact the oxygen state at higher binding energy which dominates at smaller  $\theta$ . This state was previously ascribed to partly or not reacted oxygen. At the same time, the C1s signal shifts to slightly lower binding energy which is less typical of amorphous carbon (284.5 eV instead of 285.0 eV), but rather of adsorbed hydrocarbons [87]. These observations together indicate that while lithium oxide is forming at and close to the film surface with a gradual concentration increase rather than a sharp interface, its outermost surface is covered by the surplus of adsorbed oxygen and carbon species at least in this case which allowed for the saturation with oxygen.

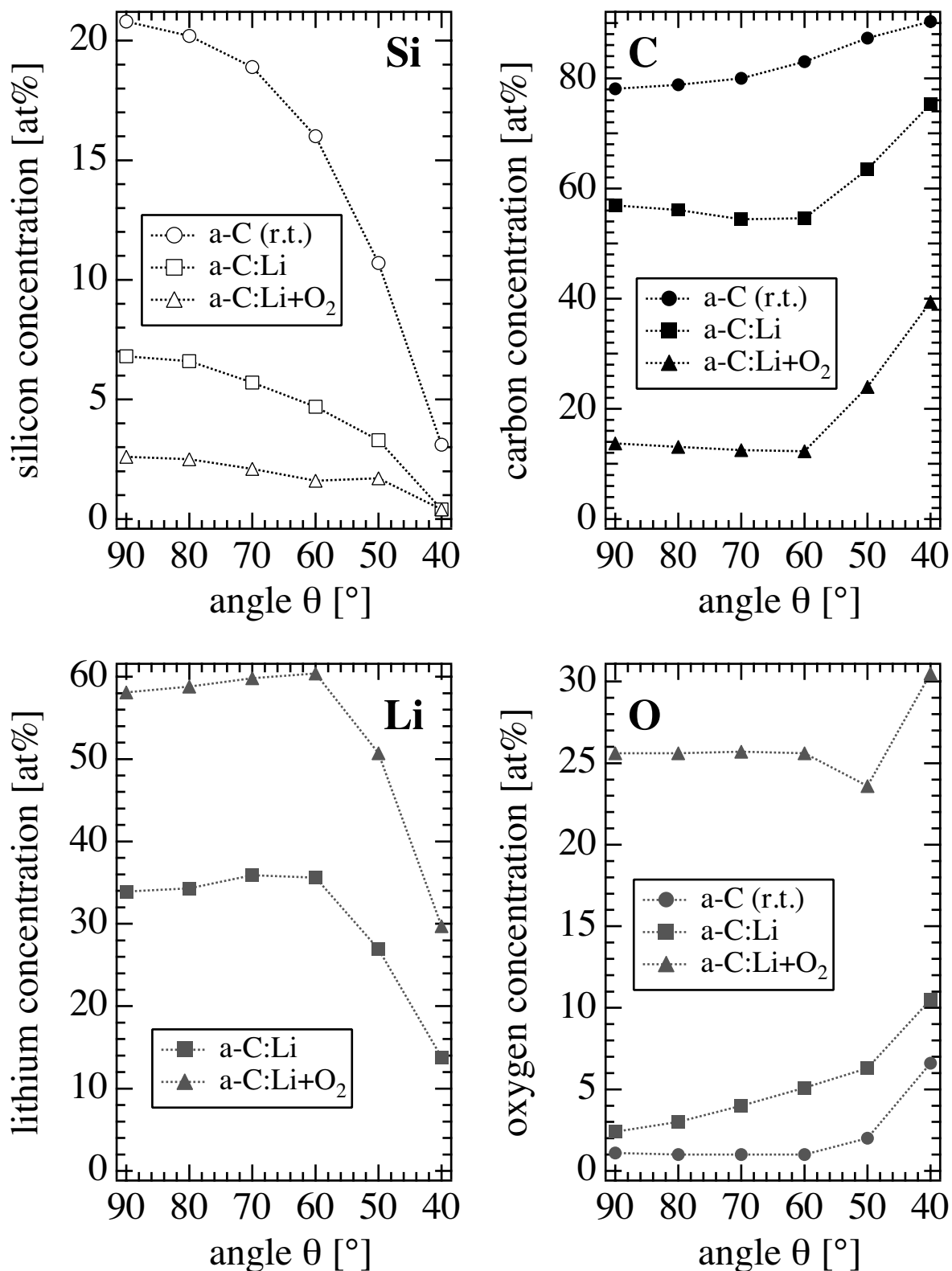


**fig. 7.7:** development of concentrations of silicon (top left), carbon (top right), lithium (bottom left) and oxygen (bottom right) in XPS measurements on a rotated thin film sample of a-C deposited at room temperature in the pristine (circles), lithium containing (squares) and oxidized state (triangles), respectively.  $\theta = 90^\circ$  corresponds to the untilted sample (cf. fig. 7.6). Note the different scales on the vertical axis.

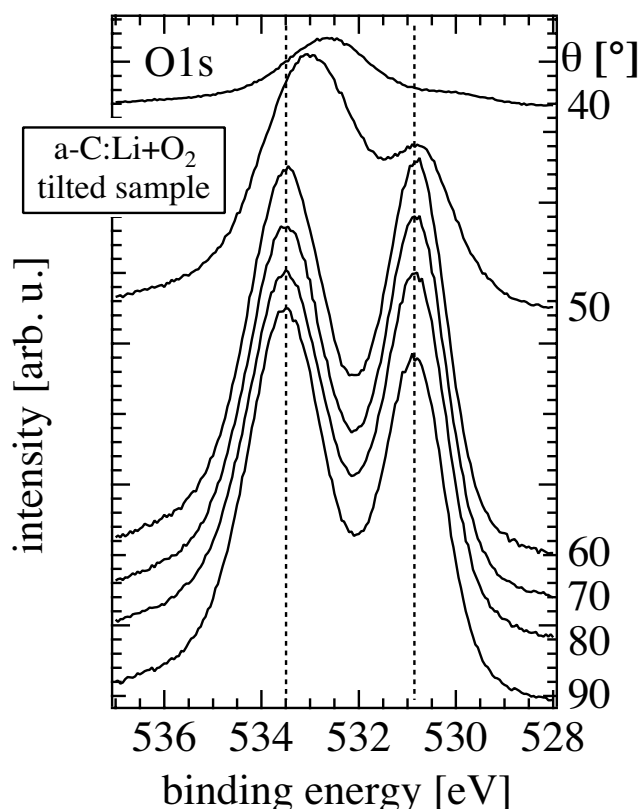


*fig. 7.8: development of O1s spectra for the oxidized a-C:Li sample with the tilt angle.  $\theta = 90^\circ$  corresponds to the untilted sample (cf. fig. 7.6). With tilt angles  $\theta$  of up to  $60^\circ$ , the state corresponding to the oxide (530.8 eV) is still growing, indicating the increasing weight of this state close to the surface. When the sample is rotated further, the adsorbed or only partly reacted states at higher binding energy gain in intensity and finally dominate the spectrum. This means that photoemission is no longer probing the film itself, but the material on top of it.*

### 7.1.2 Model for the oxidation driven segregation

From the results detailed above it is shown that lithium oxide is actually forming an overlayer on top of the carbon material. Obviously, an oxidation driven segregation of lithium from the carbon bulk takes place when oxygen is offered as a reactant. This behaviour is related to the instability of GICs towards oxygen-containing species [96].

Prior to the oxidation reaction, lithium atoms are incorporated partly as intercalants in the graphitic regions of the material and partly covalently bonded to dangling bonds of the amorphous matrix or at cluster edges (fig. 7.9a). When oxygen is supplied, the oxidation of superficial or surface near lithium atoms begins. It acts as driving force for the diffusion of lithium from the bulk of the material towards the sample surface (fig. 7.9b). The reason for this can be found in lithium oxide's high standard molar enthalpy of formation  $\Delta_f H^\circ$ , which is given as  $-597.9 \text{ kJ}\cdot\text{mol}^{-1}$  [40], equalling approximately  $-6.2 \text{ eV}$ .

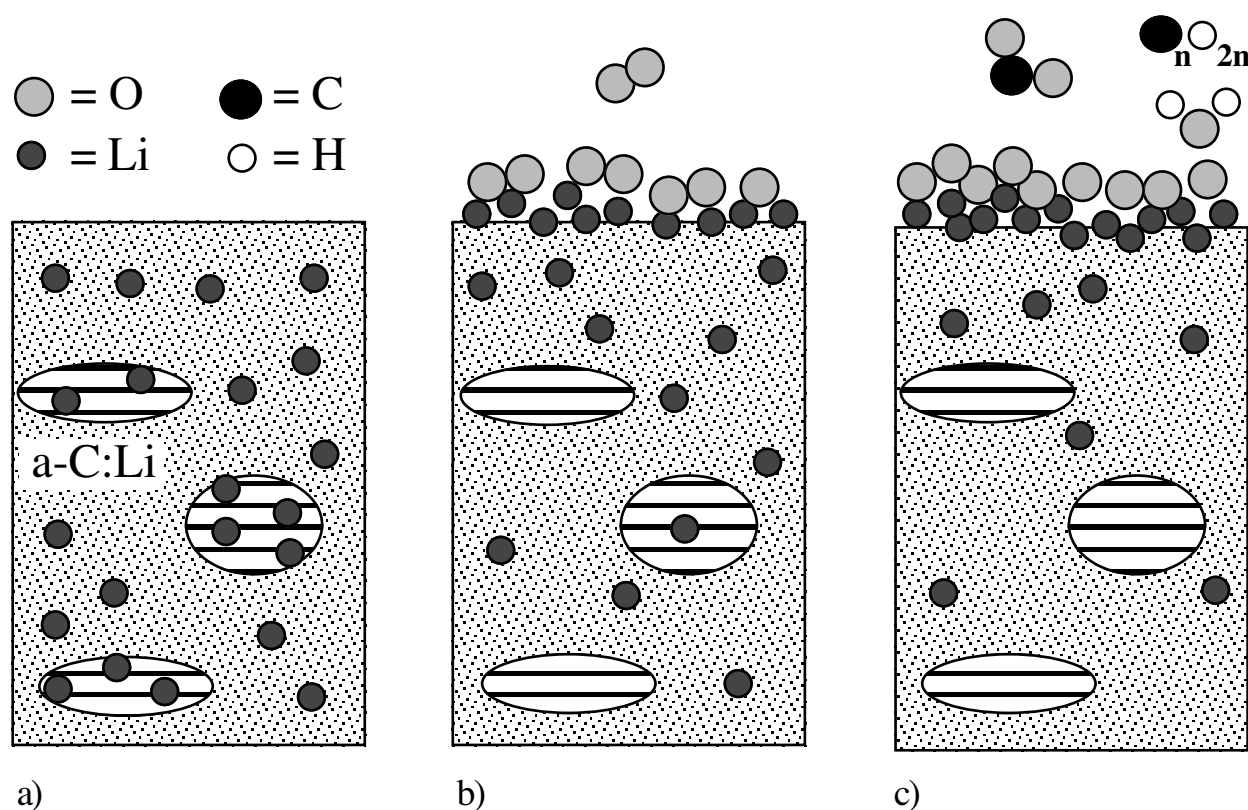


**fig. 7.9:** model representation of the oxidation driven segregation on a-C:Li. **a)** a-C:Li with lithium intercalated into clusters and bonded to the amorphous matrix. **b)** Begin of the segregation of lithium from the bulk under the influence of the oxidation reaction on the surface. **c)** Formation of a closed oxide overlayer and depletion of lithium in the bulk. In the figure, the additional adsorption of species from air is shown which is relevant for the experiments on air exposure (see 7.1.3).

Obviously, the mobility of lithium atoms is sufficient for this, which indicates that the formation of the oxide is energetically more favourable than the intercalation into carbon. While the oxidation reaction is progressing, most of the lithium from the sample is accumulated close to the samples surface. A lithium oxide surface layer is formed (fig. 7.9c) which influences the electronic properties of the material (see chapter 8). From the photoemission spectra of some of the samples one might even suspect that the oxide surface layer is dense enough to inhibit further progress of the reaction by acting as a diffusion barrier for either oxygen or lithium. In such a scenario one could imagine the presence of some unreacted and basically metallic lithium underneath the oxide film. This would account for surprisingly low Li1s binding energies at some stages of the experiments (fig. 7.2 and fig. 7.3). Binding energies of the Li1s state were observed to fall to as little as 55 eV with the literature value for  $\text{Li}_2\text{O}$  being 55.6 eV [100] and the one of metallic lithium being 54.4 eV [100] to 54.9 eV [99] (all data referred to gold  $\text{Au}_{4f7/2}$  at 84.0 eV). No proof for this can be given so far. It should be pointed out that in contrast to what was observed with a-C:H films [101] no formation of lithiumcarbide could be proven for these materials. The presence of the carbide would in principle account for lower Li1s binding energies, but C1s spectra did not show signs of carbide formation. Numerous attempts of numerical fits to the spectra were performed, but they gave no indication of the presence of either carbide or any other chemically distinguished carbon species in the films. Comparing the deposition methods of a-C and a-C:H, this is not surprising. Ion beam deposition and plasma activated chemical vapour deposition with lithium

already present were employed in the production of a-C:H/Li [103]. Both methods involve the impact of energetic particles to the films. In contrast, the a-C samples were deposited by evaporation of graphite and therefore experienced the influence of particles with merely thermal energies.

### 7.1.3 Exposure to air

The oxidation experiments reported so far were carried out under controlled vacuum conditions carefully avoiding any contact of the samples with air. In contrast to this, some of the samples were removed from UHV after the oxidation and stored in the laboratory for hours, days and even months. Some were also taken out immediately after lithium addition. The chemical state of oxidized samples did not change much any more, while the non-oxidized ones became subject to the oxidation reaction in air (fig. 7.10). Compared to the results obtained in situ, one difference was the appearance of carbon 1s states at a binding energy of about 290 to 292 eV.

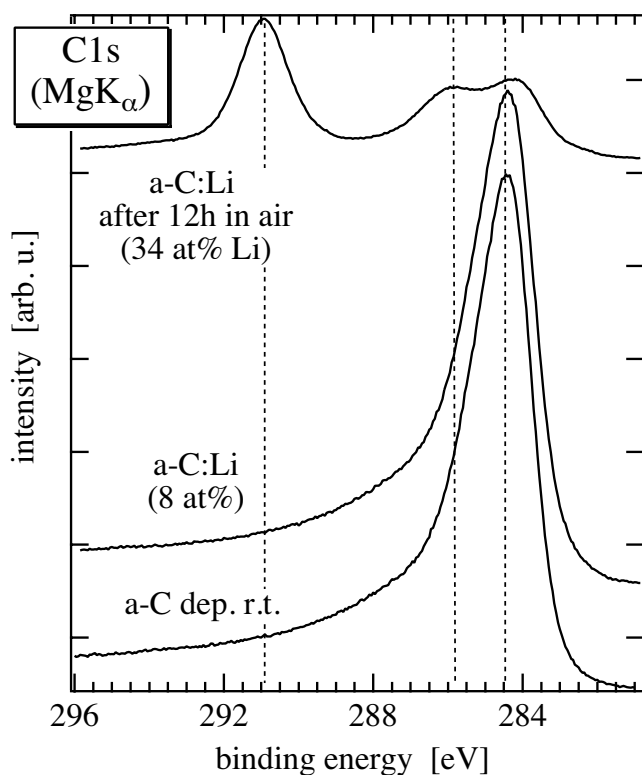


*fig. 7.10: C1s spectra for a-C deposited at room temperature in the pristine, lithium containing and air-oxidized state. Note that after several hours in air, the carbon-oxidic state is even dominating the spectra (however, again its weight in photoemission is too high due to its position on the sample surface which contributes most to the signal).*

These are not to be mistaken for the  $\pi$ -plasmon of the C1s peak which is found on graphite and on some high temperature deposited amorphous carbons at a similar position at about 7 eV from the photoemission maximum (cf. fig. 7.2 and fig. 7.3). The according O1s spectra, of course, show unambiguously that a new compound is formed. The states on the air exposed samples are related to the presence of carbon-oxidic species, but this still leaves the two possibilities of adsorption of carbon oxides and of the formation of lithiumcarbonate [23]. Not only the reaction, but also the adsorption is induced by the presence of alkali-metal atoms because no equivalent bonding state was observed on any metal-free carbon samples. This is in agreement with the role of metals for carbondioxide activation in general [104] and of alkali-metal atoms in carbondioxide adsorption in particular (see, e.g.[105] and references therein). The fact that after long-time air exposure, two high



binding energy C1s state could be distinguished supports the view that both adsorption and carbonate formation can play a role at different stages (fig. 7.11). The following mechanism is suggested for the processes occurring in air: hydroxidic lithium on the sample surface can react directly with carbon dioxide. As lithium oxide ( $\text{Li}_2\text{O}$ ) is hydrolysed by water [106], it can first form hydroxides which then react to form the carbonate. The formation of metalcarbonates from hydroxides is a basic mineralisation process in nature and plays a major role in the fixation of carbon dioxide. More carbon dioxide is adsorbed, but cannot react any more. It is responsible for the additional high binding energy state at about 290 eV (fig. 7.11, left). During long-time storage in air, however, hydrocarbons and other carbon containing adsorbates from the laboratory air accumulate and tend to dominate the spectrum. The right panel of fig. 7.11 connects this to the elemental composition: while the  $\text{Li}/\text{H}_2\text{O}/\text{CO}_2$ -reaction is proceeding, the oxygen concentration is increasing at the expense of carbon as one should expect from the reactants' stoichiometry. Afterwards, when the reaction is completed, both oxygen and lithium signals are attenuated by the adsorbing carbon species. In fact, this may just be regarded as an illustration of the basic necessity of UHV-conditions in photoemission experiments.

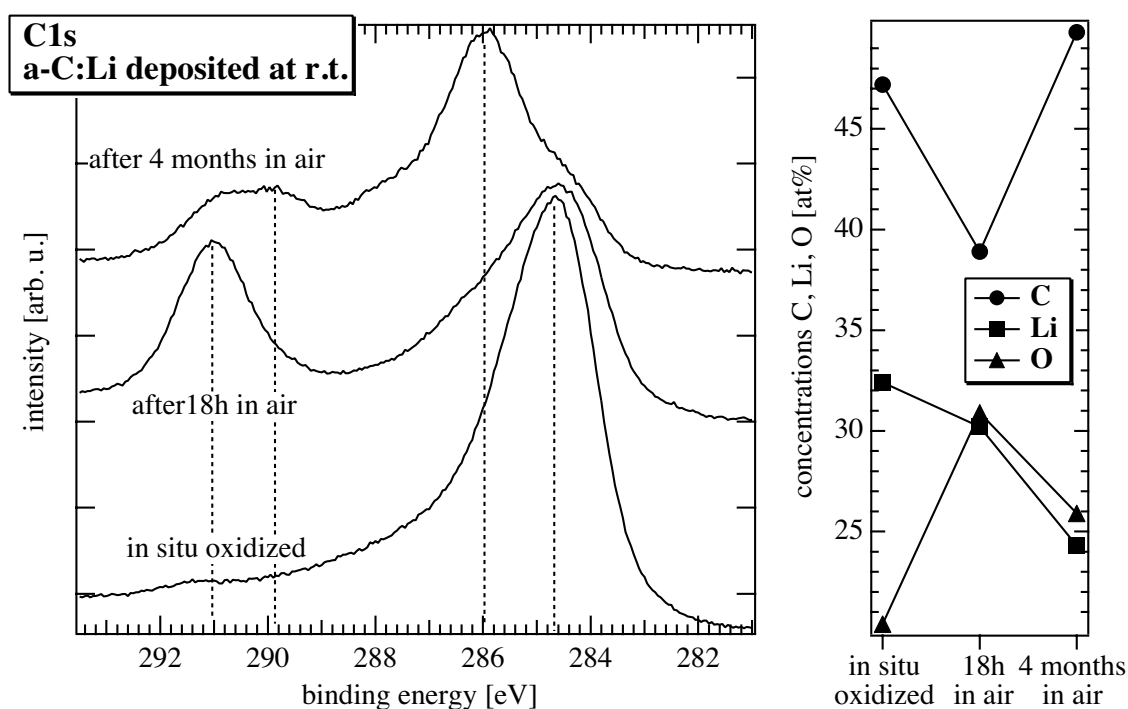


**fig. 7.11:** C1s spectra for an a-C:Li film deposited at room temperature and oxidized with  $\text{O}_2$  in situ. After storage in air, the carbon oxide state becomes prominent fast, but after a longer period of time, hydrocarbons and other adsorbates begin to dominate the spectrum. The display on the right summarises the development with respect to the elemental composition (see text).

Because of the major influence of the topmost atomic layer(s) on the results of photoelectron spectroscopy (see above), one has to be aware that in this case, the coverage with adsorbate species prevents a representative analysis of the underlying film itself.

As was expected, the lithium containing carbon materials cannot be prepared or handled in air because neither their composition nor their structure are preserved. This does not rule out their applicability in the vacuum vessel of a fusion device where regular in situ conditioning procedures are common practice.

#### 7.1.4 Oxidation and annealing - UPS

In fig. 7.12 a series of valence band spectra from UPS for the oxidation and subsequent annealing of lithium containing amorphous carbon deposited at room temperature is shown. The addition of lithium to the pure carbon matrix exhibited only a limited effect on the spectra. A shoulder was evolving at 11 eV. As this feature became much more pronounced with oxidation, it cannot be decided whether it is due to the influence of oxygen or to the increasing lithium concentration. Oxygen concentrations at the beginning were very low so that it may well be lithium that is responsible for this feature. During metal addition the main maximum which is predominantly due to  $\sigma$ -bonding electrons became narrower because one of its states at 7 eV became more intensive than its companion at 5.5 eV (cf. fig. 6.2 to fig. 6.4 with sodium). The  $\pi$ -electron related shoulder at 3 eV which is already low in intensity due to the amorphous character of this material was preserved, but in more crystalline materials its intensity and sharpness were reduced at this stage. The oxidation had a different effect in that it favoured the lower binding energy state of the main maximum. The overall intensity of the main maximum was increasing to a multiple of its original value (spectra in fig. 7.12 are normalized to the intensity at 7 eV). As a consequence of the oxidic character of the sample surface, no Fermi edge was detected any more even in the strongly graphitic and previously intercalate-like material.

Some samples were heated stepwise beginning either with the oxygen-free metal-containing state or the oxidized one. Pure carbon samples were used for comparison. As can be seen in the core level spectra of fig. 7.2 and fig. 7.3, the main result of these experiments was the removal of both lithium and oxygen from the surface of the carbon films. The loss of these elements was already beginning at temperatures as low as 150 to 200°C, and it was not completed even when temperatures of 1000°C were exceeded. Probably, longer heating times would facilitate the removal. There is some indication that the removal of lithium proceeded less readily in material produced by *c*odeposition of carbon and lithium. This would be in agreement with the view of a carbon network to which lithium is covalently bonded and therefore not mobile at insufficient temperatures. In UPS the reverse of the development during metal addition and oxidation was observed with a depletion of the lithium and oxygen related features (fig. 7.12). While core level and valence band spectra were largely restored to the state of the original pristine material (fig. 7.2 and fig. 7.12), a certain degree of graphitization is observed in the valence band spectra and in electron energy loss spectroscopy (see chapter 7.1.5) as has been reported before upon thermal treatment [81].

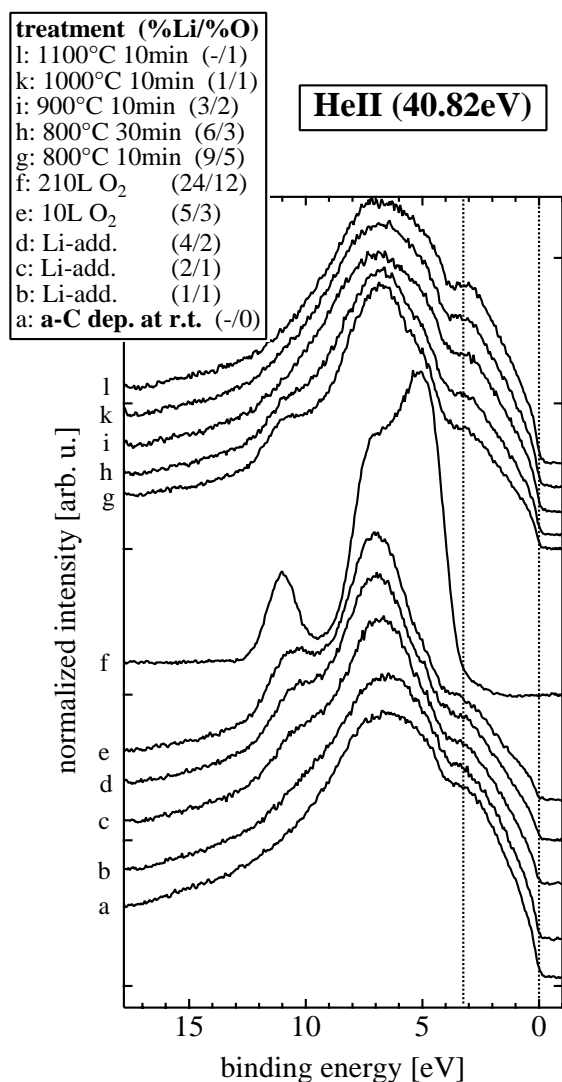


**fig. 7.12:** UPS valence band spectra for a-C deposited at room temperature. Spectra are for the pristine, lithium containing, oxidized and annealed state (cf fig. 7.2, top).

At a binding energy of 3.2 eV, the shoulder which is characteristic for more graphitically ordered carbons begins to evolve at temperatures above 800°C.

Note the markedly different spectrum for the oxidized material.

With respect to the application in question, the reversibility of lithium incorporation and oxidation could offer the possibility of a regeneration of the gettering material after its first use. To a limited extent even a structural restoration of the material seems possible, if sufficiently high temperatures can be achieved in a locally controlled way.

### 7.1.5 EELS measurements - electron irradiation

The recording of electron energy loss spectra on in situ produced a-C, a-C:Li and oxidized samples had to be carried out with some caution. As has been mentioned above, the impact of electrons on the materials induced some changes in the chemical states, though not in elemental composition. For this reason, both the EELS results themselves and the influence of their recording on the samples must be discussed.

#### 7.1.5.1 EELS

Electron energy loss spectroscopy exploits some of the energy loss effects which have been discussed for photoelectrons emitted from the bulk. In this case, a beam of electrons of a known primary energy is directed towards the samples surface and the kinetic energies of the inelastically scattered electrons are analysed. A large fraction of the electrons is elastically scattered and

therefore these electrons maintain their primary energy. Other electrons are scattered inelastically and suffer more or less large energy losses. In energy loss spectra they appear at lower kinetic energies with respect to the primary energy. For the analysis of amorphous carbons, both hydrogenated and hydrogen-free, EELS offers the opportunity to estimate the material's density [89]. This is even more attractive for the hydrogen-free carbon which avoids the complication arising from the presence of a usually not very well known quantity of hydrogen as a constituent. This was already shown in [51] for amorphous carbons very similar to the ones investigated here. Note that the polycrystalline graphite employed in this study has a density of  $1.83 \text{ g}\cdot\text{cm}^{-3}$  (measured and producer data) which deviates considerably from the one usually assumed for graphite ( $2.27 \text{ g}\cdot\text{cm}^{-3}$  [89]). This must be taken into account when using the position of graphite's loss maximum at 27 eV as reference point for the relation of energy loss and atomic density.

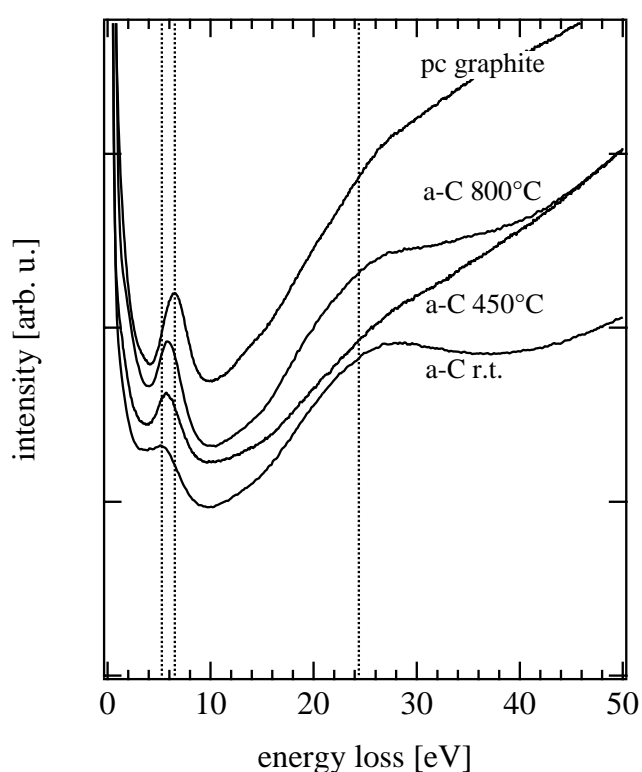


**fig. 7.13:** EEL spectra for pristine amorphous carbons deposited at r.t., 450°C, 800°C and polycrystalline graphite. The  $\pi$ -plasmon peak at 5 to 6 eV is shifting visibly while the position of the  $(\sigma+\pi)$ -plasmon's position is hard to establish in this qualitative manner because of its convolution with higher order loss peaks [107]. Considering the low density of the graphite used in this case, it is not even to expect that the position of this loss peak should vary much from the one of the amorphous carbons. Graphite and the 450°C sample were measured with a primary electron energy of 189 eV, the other samples at 470 eV which accounts for the different slopes of the background.

The first, smaller loss maximum at 5 to 6 eV is due to the excitation of collective oscillations of  $\pi$ -electrons (" $\pi$ -plasmon"). This one was already observed in the photoemission spectra where the photoelectrons undergo the same loss processes. Graphite and some of the higher temperature samples showed a plasmon loss maximum at 290 to 291 eV in photoemission (see fig. 6.1). The second, broad maximum is assigned to a loss due to  $\sigma$ - and  $\pi$ -electrons (" $(\sigma+\pi)$ -plasmon"), which involves all valence electrons of the carbon atoms [107]. The contribution of all valence electrons in this loss maximum gives at least an intuitive understanding why this maximum can be used for the purpose of density determination with reference to graphite. In the present case of the comparison of a low density graphite and  $sp^2$ -rich amorphous carbons, however, it is not surprising that the position of this maximum does not seem to change much. The density of this particular graphite is closer to the ones of the amorphous carbons than usual. While the  $\pi$ -plasmon loss peak is

increasing in intensity and energy due to the growing *delocalisation* of  $\pi$ -electrons, the ratio of  $sp^2$ - to  $sp^3$ -hybridized atoms is not expected to change much for the various films and the  $(\sigma+\pi)$ -plasmon peak should suffer only limited changes. An additional loss signal for graphite in this energy range is known to occur at 10.0 eV, but its intensity is too low to be detected here [108, 109].

In the context of this work, some new observations on the metal-containing and particularly on the oxidized material are of further interest.

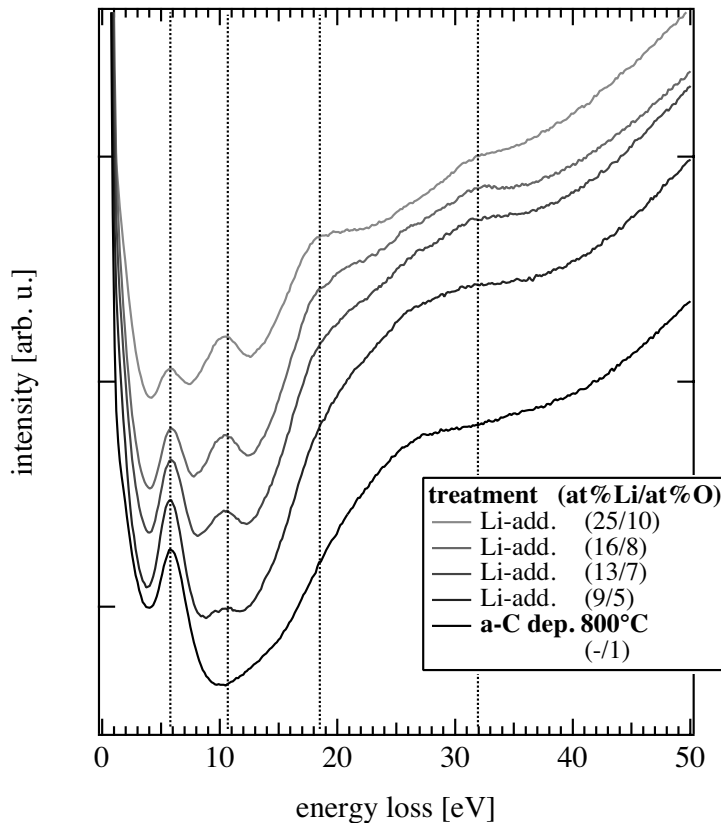


**fig. 7.14:** EEL spectra ( $E_p = 470$  eV) for amorphous carbon deposited at 800°C and incorporated with increasing quantities of lithium and oxygen. While the  $\pi$ -plasmon's intensity is reduced with the progress of lithium oxide formation, new loss maxima are evolving at 10.5, 18.5, and 32 eV.

In the course of the oxidation reaction on the sample surface, the characteristic  $\pi$ -plasmon loss peak at 5.5 eV is attenuated and new loss states appear at 10 to 10.5, 18 to 18.5, and 32 to 34 eV. A reduction of this first loss peak was also reported for the formation of the stage-1 intercalation compound  $C_6Li$  [99] as predicted theoretically [110]. As can be seen from the comparison of fig. 7.14 and fig. 7.15, at low oxygen concentrations the  $\pi$ -plasmon is already losing intensity while the new states have not yet developed. The low - if any - oxide thicknesses at these stages are not sufficient to generate the respective plasmons. With thicker films (1 to 2 nm) it should be possible to observe both bulk and surface plasmons of the oxide layer [66, 109]. In contrast to the simple relation of bulk and surface plasmon energies in metals ( $E_s = E_p / \sqrt{2}$ ) [62], the dielectric constant  $\epsilon$  enters to the formula for oxides ( $E_s = E_p / \sqrt{1 + \epsilon}$ ) [109]. Assuming the maxima at 18 and 33 eV to be due to bulk plasmon excitation, the one at 10 eV could match a surface plasmon with unusually high intensity. This would yield an  $\epsilon$  for lithium oxide of 2.24 which compares not too badly to an  $\epsilon$  of 2.70 obtained as the square of the index of refraction for  $Li_2O$  of  $n=1.644$  [111]. As this relation ( $\epsilon=n^2$ ) is only valid for ionic crystals and bound to further conditions, neither the

agreement nor the discrepancy should be overrated [112]. This would also explain the lack of a second surface plasmon as this would coincide with the bulk plasmon at 18.3 eV. A corresponding assignment has been made for  $\text{Li}_2\text{O}$  on the surface of aluminium-lithium alloys with a bulk plasmon at 18.3 eV, a surface plasmon at 10.7 eV and an interband transition at 6.0 eV [113] (18.6 eV and 10 eV in [114], respectively). The higher energy loss is not mentioned though visible in some of the spectra therein. It is most probably related to the alkali metal itself which is known to exhibit pronounced plasmon signals [115]. The interband transition's signal is weak and coincides with the graphite loss plasmon on our samples. Its signal can be seen to evolve in the oxidized states as the growing shoulder at 6 eV (fig. 7.15, top curves). In this measurement, the lower primary electron energy makes the method more surface sensitive and therefore enhances the surface plasmon's contribution.

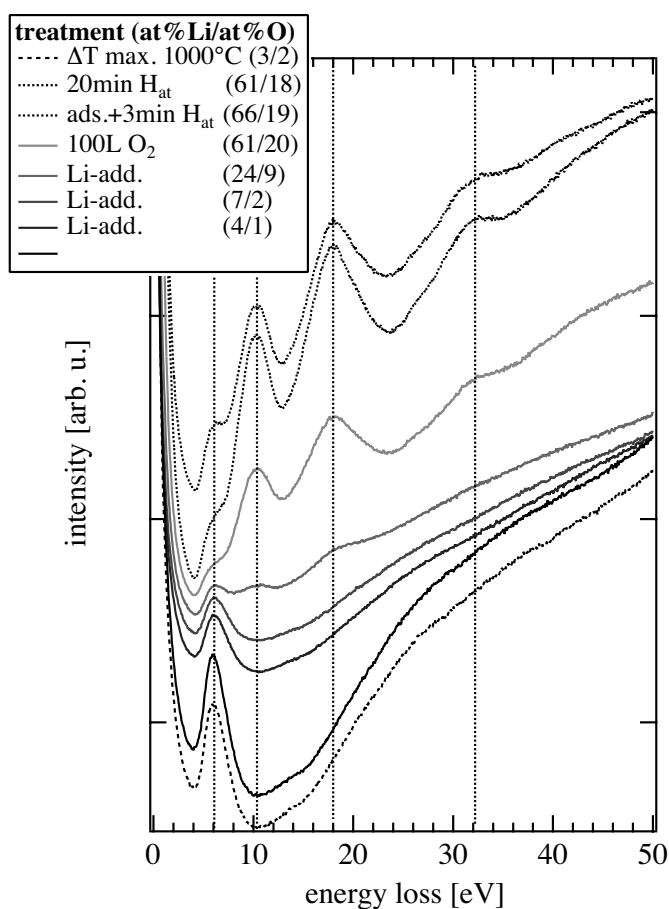


**fig. 7.15:** EEL spectra for amorphous carbon deposited at even higher (though less well controlled) temperature than the one in fig. 7.14. Electrons with a primary energy of 189 eV were used. The lower primary energy makes the measurement more surface sensitive and therefore enhances the surface plasmon at 10 eV.

In contrast to fig. 7.14 this experiment includes lithium containing, but fairly oxygen-free samples and the state after annealing (dashed curve at the bottom). In the phases of treatment with atomic hydrogen after further in situ adsorption, the thermal influence of the hot filament might be the decisive factor.

### 7.1.5.2 Effects of electron irradiation

Chemical effects of the irradiation of samples with electrons in connection with photoemission measurements are a long known phenomenon [109]. In that particular case, sodiumthiosulfate ( $\text{Na}_2\text{S}_2\text{O}_3$ ) was irradiated with low energy electrons from a spectrometer flood gun (about 0 V, 0.5 mA) which led to the formation of additional oxidation states on a time scale of half an hour to hours. In the experiments reported here, an electron gun with electron energies of 470 or 189 eV, respectively, was employed at an electron current of 75 to 80  $\mu\text{A}$ . With the higher electron energies one must be aware that any observed effect possibly includes the chemical effect of electron

addition at the surface, i.e. reduction of some chemical species. The penetration depth of the electrons, however, is limited in the present case between about 0.5 nm (189 eV) and about 1 nm (470 eV). In addition, the contribution from energetic impact is not at all comparable to the one of ion sputtering because of the electron's small mass. Results were already briefly mentioned in connection with fig. 7.3 which included photoemission spectra recorded before and after EELS measurements. These are displayed in fig. 7.16. The high binding energy state at 533.5 eV is depleted during irradiation while the low binding energy state of the oxide at 530.5 eV is gaining intensity. As the oxygen concentration in the film is only increasing from 10 to 11 at% while lithium content increases from 25 to 31 at%, the segregation of lithium is continuing as well as the decrease in work functions (included in fig. 7.17). However, lithium concentration increases more slowly than before due to the lack of further oxygen supply.

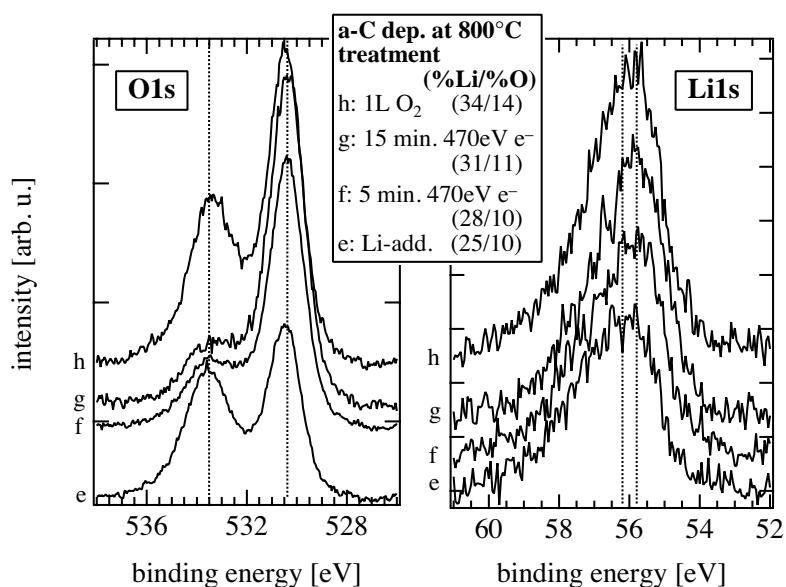


**fig. 7.16:** oxygen and lithium core level spectra for a-C deposited at 800°C. The sample was measured in the oxidized and electron irradiated state. Spectra are taken from fig. 7.3 with identical labels to enable quick reference.

Electron impact certainly induces some desorption of loosely bound oxygen species, particularly of those which are still essentially molecular entities. To a certain (small) degree reactions can be imagined which transform some of the oxygen from only partly reacted states to the oxide. Quite in accord with the core level measurements, valence band spectra exhibit a redistribution in the occupation of electronic states, but no overall change of the valence bands (fig. 7.17).

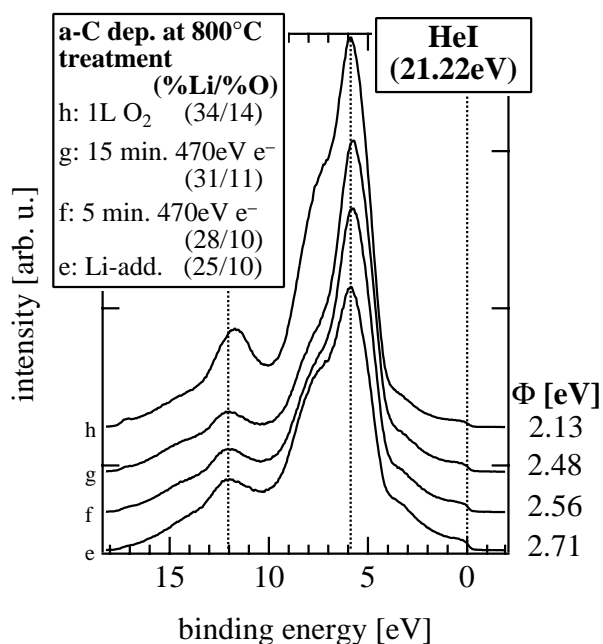


*fig. 7.17: valence band spectra for the same processing steps as above. A change of the relative intensities of the feature at 8 eV and the peak at 6 eV occurs, but no principle change is observed. Work functions are noted at the bottom (see chapter 8).*

For the sake of completeness it should be mentioned that under *strong* electron irradiation of Li<sub>2</sub>O crystals (1 MeV, 40 μA·cm<sup>-2</sup>), both the formation of lithium colloids [116] and even the development of inclusions of molecular oxygen [117] have been reported. This is just an indication of the multitude of effects which are possible.

An increase in the lithium concentration at the surface *without* a simultaneous growth in oxygen content as observed under these very mild conditions could be of importance for an in situ regeneration of a gettering wall material by superficial lithium enrichment. From the point of view of possible damage to the material other processes are certainly of much greater importance. This is true in particular for the impact of ions which can cause erosion and other damage on materials' surfaces and was investigated in separate experiments.

## 7.2 Irradiation with oxygen ions

The use of oxygen ions combines the chemical reactivity of oxygen with the physical effects of the impact of energetic particles onto the samples surface. As the ignition of the ion source required rather high oxygen pressures in the chamber (in the 10<sup>-4</sup> mbar range), one cannot really speak of the irradiation of a-C:Li with oxygen ions, but rather of the treatment of oxidized material. In fact, the procedure for the experiments often began with the exposure to molecular oxygen of this pressure and were subsequently continued with the actual ion treatment. Apart from the known oxidation effect, the physical modifications of the material include the amorphisation of the carbon matrix and the begin of erosion of the compounds of the films. In the following, the term "oxygen ions" comprises all the products of the ion source which can be both mono- and diatomic.

The ion irradiation was carried out in the preparation part of the vacuum system and made use of a Penning-type ion source (Leybold-Heraeus IQP 10/63) with ion generation in a gas discharge, extraction from the plasma and subsequent acceleration. Ion energies between 50 eV and 5 keV



were applied for periods of 100 s to several hours. The electric current between the sample holder and the grounded transfer rod was measured to give an upper limit for the ion flux onto the sample. For oxygen ions the relation of this current with the ion energy is displayed in fig. 7.18.

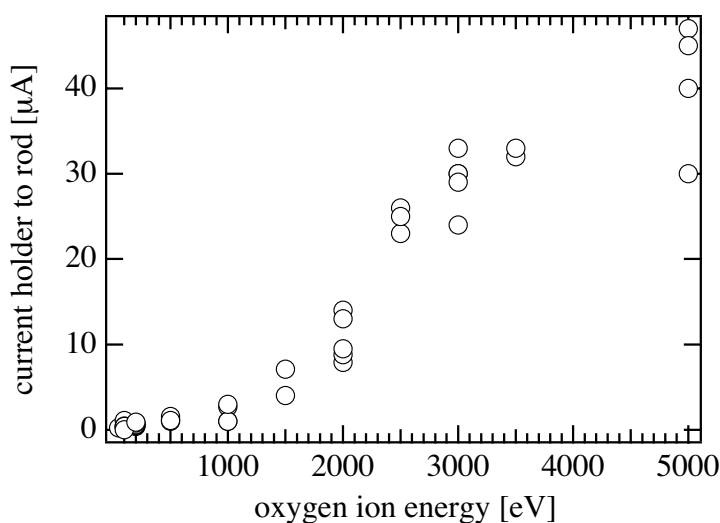


*fig. 7.18: dependence of the current measured between sample holder and transfer rod on the oxygen ion energy.*

This method is rather uncertain because it determines an "integral current" which is not corrected for secondary ions or stray electrons from the source. However, a comparison with the manufacturers data on the ion source showed a reasonable agreement. As the diameter of the ion beam depends on the acceleration voltage, the current density according to the manufacturers data varies from  $7 \mu\text{A}\cdot\text{cm}^{-2}$  for 3 keV to  $55 \mu\text{A}\cdot\text{cm}^{-2}$  at 5 keV for defined discharge current and voltage (4.5 mA and 500 V) and appropriate distance between source and sample (20 cm). The settings chosen for these experiments were close to this (around 5 mA and 5 keV) so that similar values for the current density are achieved.

### 7.2.1 Amorphisation of graphite

In this work, amorphous carbons were used to approximate the structural properties of graphite materials which were superficially damaged by particle impact and therefore became amorphous at least in their topmost regions. The principle justification of this approach has been illustrated in earlier chapters and in other works [118, 119]. In fig. 7.19 the valence band spectra of polycrystalline graphite before and after ion irradiation are compared to the one of an amorphous carbon sample deposited at room temperature. The spectrum recorded after hydrogen ion treatment (3 keV, 10 min.) shows a change towards a more amorphous character of the material. With the much heavier oxygen the effect is already more pronounced after the application of 2 keV ions for only 100 s in accordance with the much larger mass of the ionic particles. Even at much lower ion energies than this (down to 100 eV, not shown), ions penetrate the material deeply enough to effect the disturbance of crystalline order within the range of photoemission. Long range crystalline order is the prerequisite for the presence of the secondary electron peak 13.8 eV and the  $p$ - $\pi$ -shoulder at 3 eV as discussed above which accordingly vanish during the treatment. After the irradiation, the spectra of a-C and of "graphite" show a strong resemblance although the main maximum of the graphite spectrum remains broader and the density of states at the Fermi energy is slightly different.

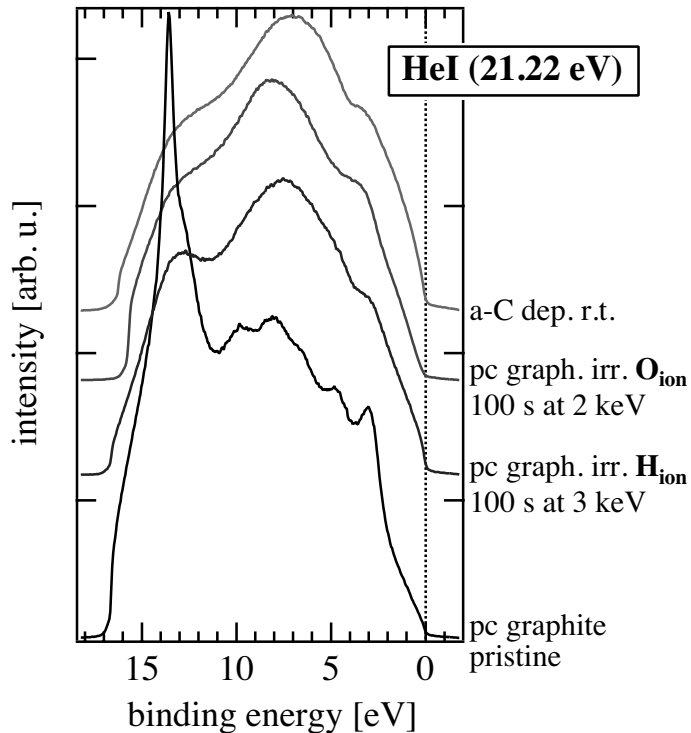


**fig. 7.19:** valence band spectra of polycrystalline graphite prior to and after irradiation with hydrogen (3 keV, 10 min), and oxygen ions (2 keV, 100 s), respectively. The disappearance of the secondary " $\sigma$ -peak" at 13.8 eV and of the  $p$ - $\pi$ -peak at 3 eV as well as the overall change of spectral features testify for the increasing disorder within the range accessible to photoemission measurements. For comparison, the spectrum of amorphous carbon deposited at room temperature is added at the top.

The loss of structural order is not the only effect of the irradiation. Ion impact also generates additional vacancy sites and dangling bonds which are so characteristic of "genuinely" amorphous material. At the same time, oxygen and hydrogen atoms are implanted into the irradiated material. The bombardment damages the graphene sheets contained in the material and creates new edges (cf. fig. 3.3) where there used to be a continuous network of bonded carbon atoms.

### 7.2.2 Irradiation of oxidized a-C:Li

It has been observed that lithium intercalation into graphite strongly reduces erosion due to chemical and physical sputtering [20, 21]. These studies refer mainly to the bombardment with hydrogen ions with the formation of hydrocarbons as erosion products. In the following these results are complemented by studies using oxygen ions. These should only be a minority species in any fusion vessel, but due to their high reactivity and much larger mass they cannot be neglected in this context.

In order to monitor both changes in the elemental composition of the material and to distinguish between stages of deposition or erosion, thin amorphous carbon films (less than 3 nm) were deposited on silicon substrates. As described before, this enabled the detection of substrate and film signals at the same time. In fig. 7.20 results obtained on a room temperature deposited sample are summarised which, however, also applied for other samples. Concentrations of the film constituents and of silicon are displayed for each experimental processing step. The respective treatments are listed in the box on the right and include irradiations with oxygen ions of 50 eV to 3.5 keV. The development of concentrations allows to distinguish between three major regimes of the ion irradiation. At ion energies of less than 2 keV, the irradiation does not change the result of the chemical reaction of lithium and oxygen with the accumulation of both elements on top of the carbon film. This can be monitored by the simultaneous decrease of silicon and carbon intensities

during the purely "chemical" phase which is followed by a period of more or less stationary concentrations during low energy ion irradiation. At around 2 keV, lithium oxide begins to be eroded, as can be seen by the increase of carbon and silicon concentrations at the same time. In spite of the loss of lithium oxide, the oxygen concentration slightly increases due to the implantation of more energetic ions deeper in the film. When the ion energy is even more increased, the carbon film itself is eroded together with lithium oxide. At this stage both silicon and oxygen concentrations increase at the cost of lithium and carbon. As can be seen from core level spectra in fig. 7.21, oxygen ions are penetrating the carbon film to form silicondioxide.

It must be pointed out that the effect of increased ion energy is certainly convoluted with the one of extended irradiation times. However, the periods of time required to obtain the same effects at much lower ion energy were probably too long to be observed on the time scale of our experiments. In chapter 7.2.3, the influence of prolonged irradiation time will be briefly discussed in connection with hydrogen ions.

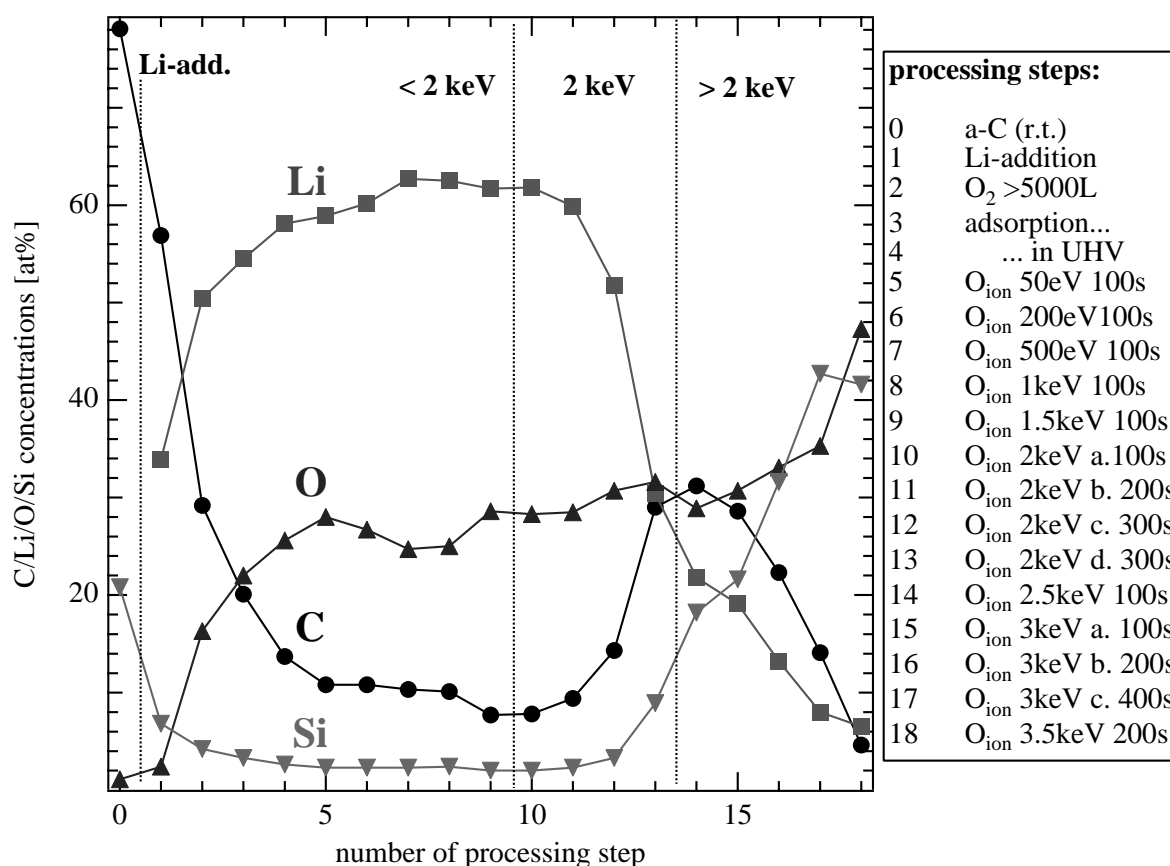
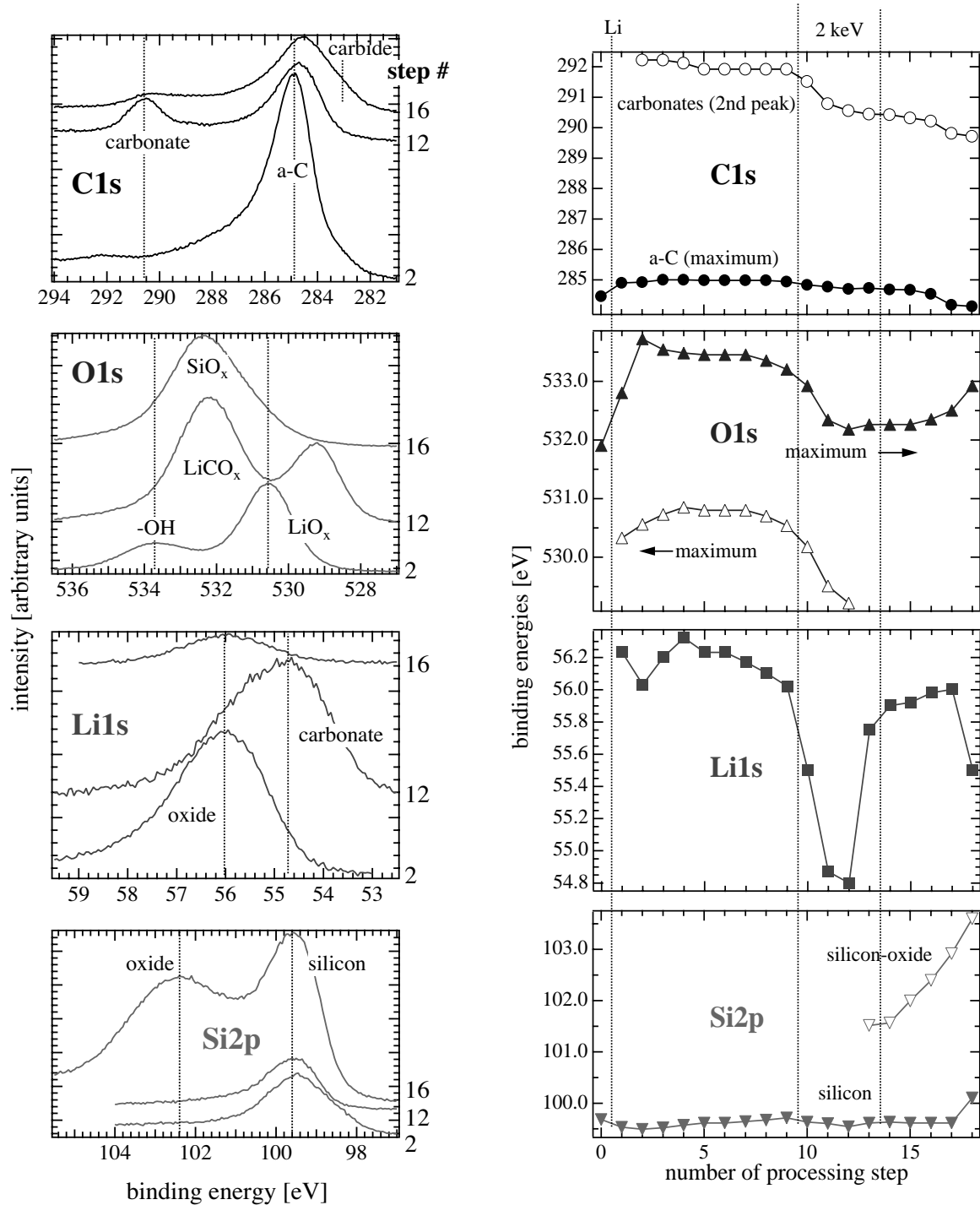


**fig. 7.20:** development of concentrations of film constituents and silicon substrate for an amorphous carbon deposited at room temperature. Lithium was added after the deposition and oxidized in situ. During the oxygen ion irradiation, three stages are distinguished. At energies below 2 keV, the oxide overlayer growth dominates; around 2 keV, erosion of lithium oxide begins and at more than 2 keV, carbon is eroded as well.

Spectra in fig. 7.21 refer to the same experimental series and include selected spectra for the four core levels and binding energies for all steps. Spectra are shown for an early stage (no. 2), at 2 keV

irradiation (no. 12) and at 3 keV treatment (no. 16). They allow to add a view of the chemical processes to the quantitative aspect of layer formation and erosion.



processing steps:					
0	a-C (r.t.)	5	O <sub>ion</sub> 50eV 100s	10	O <sub>ion</sub> 2keV a. 100s
1	Li-addition	6	O <sub>ion</sub> 200eV 100s	11	O <sub>ion</sub> 2keV b. 200s
2	O <sub>2</sub> >5000L	7	O <sub>ion</sub> 500eV 100s	12	O <sub>ion</sub> 2keV c. 300s
3	adsorption...	8	O <sub>ion</sub> 1keV 100s	13	O <sub>ion</sub> 2keV d. 300s
4	...in UHV	9	O <sub>ion</sub> 1.5keV 100s	14	O <sub>ion</sub> 2.5keV 100s
				15	O <sub>ion</sub> 3keV a. 100s
				16	O <sub>ion</sub> 3keV b. 200s
				17	O <sub>ion</sub> 3keV c. 400s
				18	O <sub>ion</sub> 3.5keV 200s

**fig. 7.21:** Left: selected core level spectra, right: binding energies for the same experiment as in fig. 7.20. The same labelling applies. See text for details.

After the oxidation, lithium oxide is the major chemical compound, accompanied by other oxidic or hydroxidic species. Binding energies figure at 56 eV for Li1s, 99.2 eV for the Si2p of the clean silicon underneath, 530.3 eV for O1s of the oxide and 532.8 eV for O1s in minor species. C1s is found at 284.9 eV. Ion irradiation in the intermediate energy range produces another compound which involves lithium, oxygen and carbon. A second C1s signal which is a minor shoulder at lower ion energies evolves close to 291 eV while the Li1s broadens towards lower binding energies. Its maximum shifts by more than 1 eV to as little as 54.8 eV. O1s is still growing in intensity and its two maxima appear at lower binding energies (532.5/529 eV). The one at higher binding energy is now dominating immediately after the Li1s peak's binding energy has reached its minimum. We attribute this one to oxygen which is implanted into the bulk of carbon and at sufficient ion energy and penetration depth into silicon, too, because the same development was found on lithium-free amorphous carbon and graphite samples during ion irradiation.

The changes described for the other core level spectra showed that the low energy shift of lithium and the different occupation of oxygen states is connected to the formation of lithiumcarbonate [23]. The energy of the impinging ions induces the reaction of carbon, lithium and oxygen which was otherwise only observed after air exposure due to the reaction with carbondioxide (7.1.3). The carbonate formation with oxygen ions has previously been observed on a-C:H/Li materials [24]. A further increase of energy enables the ions to penetrate the material even more deeply. They impinge into the silicon and very readily silicondioxide is formed as can be detected by its Si2p-signal at 102.4 eV [40]. From fig. 7.20 we saw that at this stage lithium and carbon concentrations are decreasing because of erosion. Accordingly, the majority of oxygen is now bonded to silicon. A contribution of a carbidic compound to the C1s signal at 283 eV [40] shows that now the impact of energetic ions also induces the reaction of carbon and silicon which otherwise requires increased temperatures. Again, one has to be aware that the physics of the photoemission process influences the apparent intensities: The contribution of the interfacial layer to the photoelectron spectra increases with reduced overlayer thickness due to erosion.

Irradiation experiments with polycrystalline graphite yielded similar results (fig. 7.22). Here, no substrate can be detected and erosion of carbon from the surface only exposes more carbon to the measurement. Given enough time, its concentration must therefore rise to unity and cannot fall as observed for the thin films. The decrease in oxygen content might be due to the fact that the faster oxygen ions penetrate the graphite so deeply that they travel out of reach of photoelectron spectroscopy [15]. Above the saturation limit of oxygen in carbon, even atoms from the upper regions of the film will diffuse into the bulk.

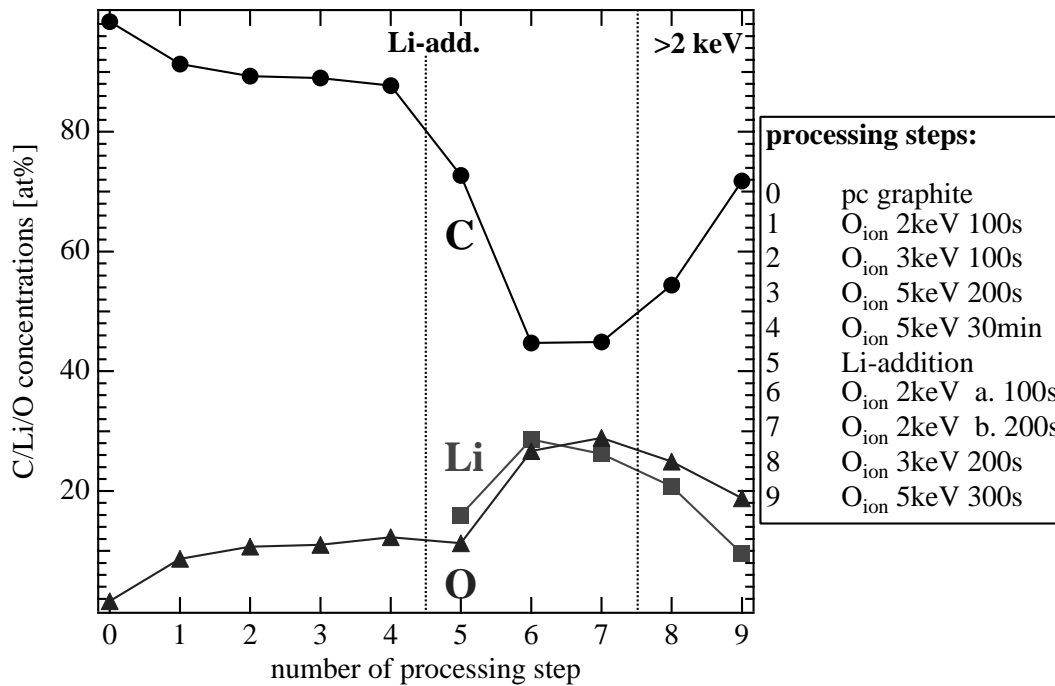


*fig. 7.22: changes of composition during treatment of a polycrystalline graphite sample irradiated with oxygen prior to the incorporation of lithium.*

Although there exist results for the erosion of carbon materials under ion irradiation [24, 120], the kind of compound material under investigation here requires a careful evaluation of the different regimes to consider if and in which position in a fusion device such materials could be used. This even includes the question whether it is favourable to dispense lithium into the fusion plasma. In connection with observations of the beneficial effect of lithium addition on plasma performance this will be of further interest [18, 19].

### 7.2.3 Oxygen ion irradiation after hydrogen ion treatment

In another experimental series, hydrogen ion irradiation was applied to the metal-free carbon film prior to lithium-addition (fig. 7.23). Hydrogen ions of energies between 3 and 5 keV were applied for periods of time between 5 minutes and 4 hours. In this case, the role of extended irradiation times becomes obvious. While concentrations could be regarded as more or less constant during the first 25 minutes of irradiation at increasing ion energies (steps no. 1 to 5), the next step of 1 hour duration definitely started the erosion of carbon with the simultaneous increase in the silicon substrate's signal intensity. Carbon erosion in this case is progressing via both chemical and physical sputtering [15]. Lithium addition and the following short hydrogen irradiation steps (no. 10 and 11) interfered with the erosion process. Due to lithium's high reactivity, oxygen content rose as soon as lithium was present (from 1.8 at% before lithium addition to 6 at% after step 11). The parallel increase of lithium and oxygen concentrations showed that it was again the formation of lithium oxide at the sample surface which caused the decrease in both carbon and silicon concentrations. This development obscured any erosion which might still have occurred during the short hydrogen irradiation cycles after lithium addition. The concentration of lithium still increased during the following short oxygen ion irradiations at 1.5 and 2 eV which indicates that the oxidation was still going on. The following steps led to a decrease in lithium content caused by erosion with an increase of oxygen content due to implantation. The increase in silicon and even carbon

concentration indicates that the lithium oxide layer is at least eroded faster than the rest of the film, it may even be the only component eroded at this stage because the still very high concentration of 26 at% lithium reflects a considerable thickness of the surface layer.

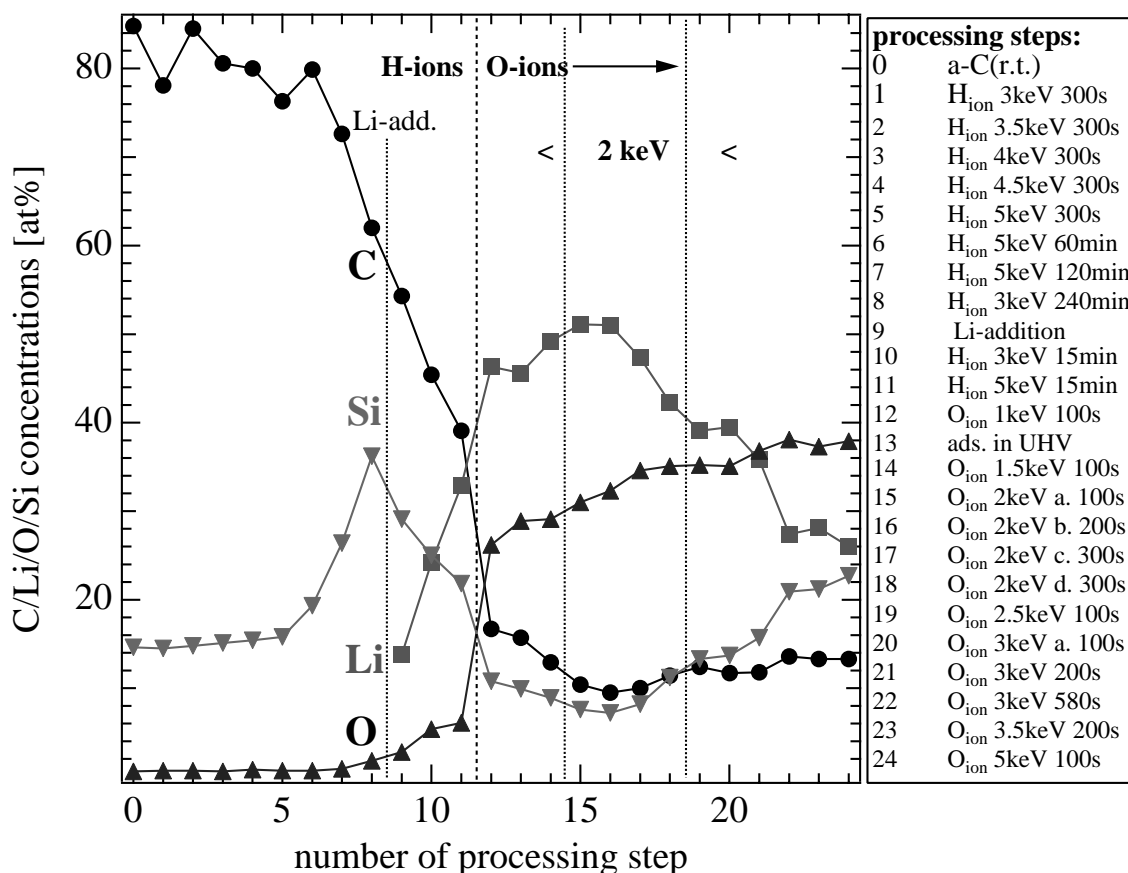


**fig. 7.23:** development of elemental composition of an amorphous carbon sample deposited at r.t. during irradiation with hydrogen ions (no. 1 to 8 and 10 to 11), lithium addition (no.9) and oxygen ion treatment (no. 12 to 24).

Although open questions remain, these experiments clearly show that the addition of lithium can delay the ion induced erosion processes when an oxidic surface layer is formed with residual oxygen.

### 7.3 Reactivity and implications for fusion

The results presented in this section bear some significance with respect to the general aim of the application of contamination gettering materials in fusion devices. The most basic result was, that lithium containing amorphous carbon in fact is a getter material for oxygen and oxygen containing species. This was basically a confirmation of what is known about lithium and its reactivity. While reacting in the desired way, the composite material showed a much more unusual behaviour in that it released unreacted lithium atoms to the surface region under the driving force of the reaction with oxygen containing molecules. These lithium atoms were provided from regions more deeply in the bulk through a process of reaction driven segregation. Possibly, the storage capacity could be

expanded when thicker films or an all carbon tile was employed. A lithium containing carbon first wall covering would therefore serve as a dynamic contamination getter with the capability of adjusting the amount of reactive atoms at its surface to the demand according to the progress of the surface reaction.

As was shown, the preparation of the materials must be carried out under good vacuum conditions. This does not pose a principle problem as the successful operation of different tokamaks with regular in situ conditioning procedures under vacuum conditions has proven. For the complex operation of in situ processes it is of great interest that the principle result of the reaction driven segregation of lithium from the bulk of amorphous carbon did not show any significantly critical dependence on preparation conditions such as temperature. The behaviour of polycrystalline graphite in our experiments, however, indicates that it might be necessary to carefully choose the basic wall tile material and control its structure in order to achieve optimal results. This would at least be the case if no additional amorphous carbon film similar to the ones produced here was deposited, but the graphite wall material itself was to host the lithium reservoir.

Furthermore, the reversibility of lithium incorporation and oxygen gettering appears as a very attractive feature of the procedure. This opens up the chance for removal of the lithium oxide formed during gettering in a principally simple thermal process. Afterwards, the carbon walls could be "recharged" with lithium for renewed use. The thermal regeneration could even be used for a partial structural recovery of the carbon host material if sufficiently high annealing temperatures were used in a controlled way. However, in a vacuum device with different materials on its walls, the risk of redeposition of the evaporated lithium and oxygen elsewhere in the vessel must be carefully observed.

The experiments concerned with hydrogen- and oxygen ions, respectively, provided other valuable pieces of information: The influence of energetic ions is not detrimental to the performance of the gettering material although structural damage and erosion are observed. Erosion might, however, become a problem in a reactor with a first wall made from a combination of materials. Carbon erosion-redeposition processes have been one of the major issues of research in plasma-wall-interaction for a number of years. The discussion is still open whether constructive measures and operation modes can be found in which the erosion-redeposition problem can be avoided or at least reduced below a critical limit. The answer to this question is of course decisive for all carbon based features inside the vacuum vessel.



## 8 Electronic effects

The changes in chemical composition and film structure discussed so far are accompanied by changes of some of the electronic properties of the carbon materials. With photoelectron spectroscopy e.g. the absence or presence of a Fermi edge as marker of metallic behaviour can be observed and the value of a material's work function is accessible in an appropriate experimental setup [74].

In fig. 8.1 the regions of the Fermi energy in valence band spectra of two amorphous carbon samples deposited at r.t. and 800°C, respectively, are compared. In this case, sodium was incorporated. At equal concentrations of 8 at%, the 800° sample developed a distinct Fermi edge, whereas the r.t. sample did not display any change, at all. At intermediate carbon matrix deposition temperatures, a Fermi edge was formed in some cases. However, higher sodium concentrations were required in the materials deposited at lower temperatures. For example, in a 550°C sample, the edge was still not fully developed even at 15 at%, while in a 300°C a-C, it just began to form at this stage (not shown here).

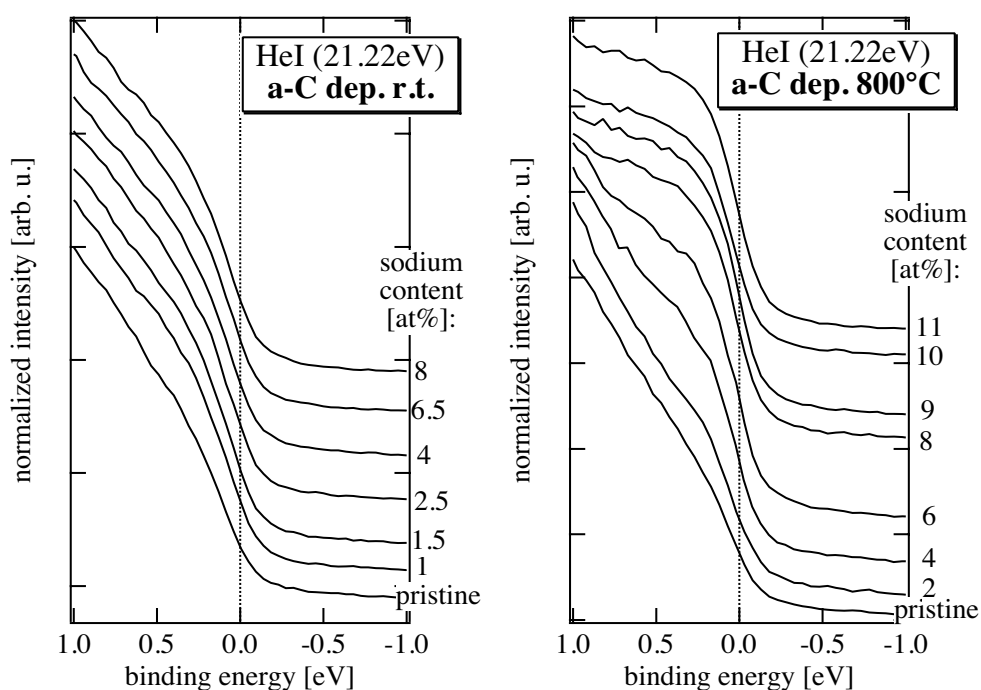


**fig. 8.1:** comparison of the development at the Fermi energy in carbons during sodium incorporation. **Left:** room temperature deposited a-C; no clearly visible change. **Right:** a-C deposited at 800°C; a Fermi edge evolves with increasing sodium concentration.

The reason for these different behaviours is that samples deposited at higher temperatures are structurally already more similar to graphite which due to its particular structure is a semi-metal. In the amorphous carbons, the electron transfer is more effective when more extended graphitic regions exist which allow intercalation of donor lithium atoms. Where disorder restricts the extension of such host regions for intercalation, the character of bonding between carbon and lithium is a more covalent one. In this case, charge transfer from metal atoms to carbon is a local effect and metal-like electron delocalization is not achieved.

For the determination of work functions, UPS measurements were performed in the constant pass energy mode (CPE). In this mode, the analyser transmission is proportional to the reciprocal of the kinetic energy. This is also the standard mode for XPS measurements since it yields a constant resolution over the whole XPS measurement range. UPS is usually recorded in the constant retardation ratio mode (CRR), in which the transmission is directly proportional to the kinetic energy. For the determination of the work function, the low kinetic energy region of the spectra is of interest. In the CPE mode, this part of the spectra has the largest weight (fig. 8.2). Work functions measured by photoemission are determined by those regions of the surface which possess the lowest work function. The values obtained therefore need not be representative of the surface as a whole.

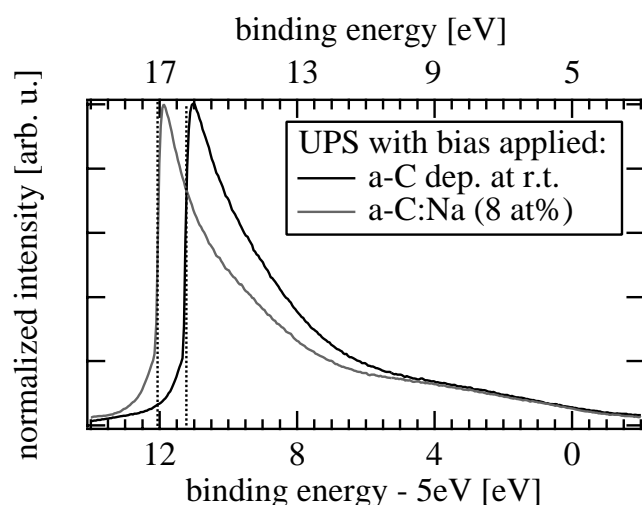


**fig. 8.2:** comparison of valence band spectra in the low-energy cut-off region measured in constant pass energy mode for pure amorphous carbon and after incorporation of 8 at% sodium. The low kinetic energy region with the spectral onset is much more pronounced than in measurements in constant retardation mode (cf. fig. 7.12). Both samples were biased by 5 V during the measurement.

Even the pristine amorphous carbons showed small differences in work function (fig. 8.3). In spite of the small differences, the values fit in the range of those determined for other carbonaceous materials, such as diamond (which are extremely sensitive to the surface preparation) and graphite. This illustrates rather well that all of the amorphous carbons investigated still differ considerably from either of the crystalline modifications.

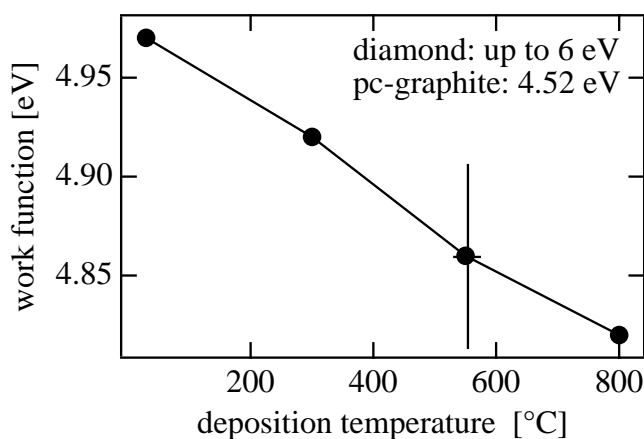


**fig. 8.3:** work functions of pure amorphous carbons deposited at r.t., 300°C, 550°C, and 800°C, respectively. Values for diamond and graphite are included for comparison.

When lithium or sodium was added to any of the amorphous carbons or to graphite, the work function of the resulting compounds was decreasing. In fig. 8.4 this is shown for a-C samples with up to 15 at% of metal incorporated and oxygen concentrations of below 2 at%. In all cases the work function values obtained for such clean samples were still higher than the one of the respective polycrystalline metal (sodium: 2.36 eV; lithium: 2.93 eV [40]).

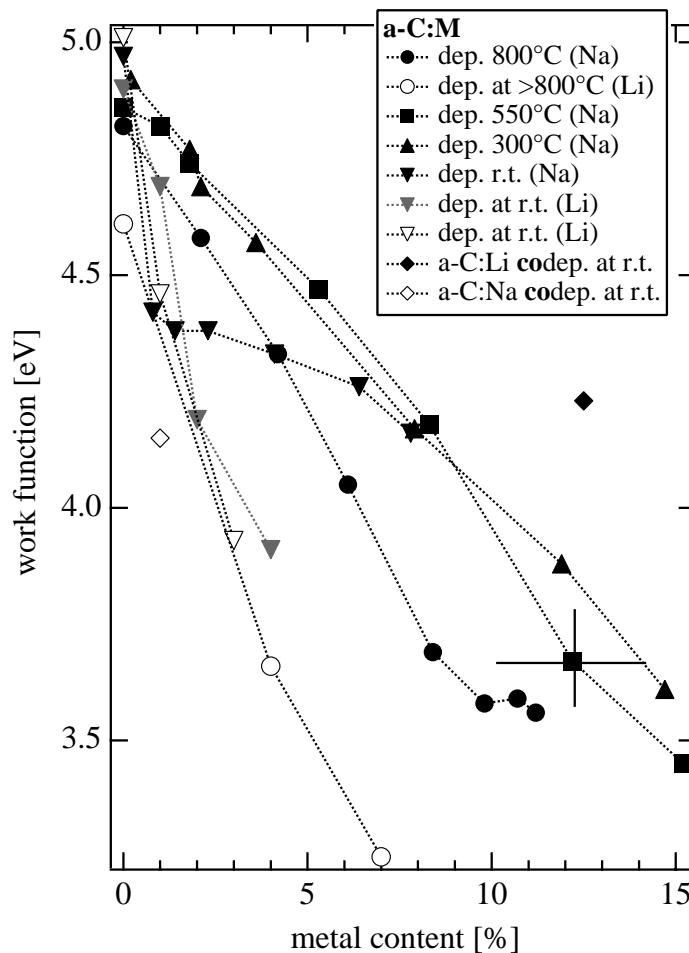


**fig. 8.4:** work function decrease in amorphous carbons during sodium or lithium incorporation, respectively, in the oxygen-free state (less than 2 at% oxygen). Samples were deposited at r.t., 300°C, 550°C, and 800°C, and >800°C, respectively, including two codeposited ones. The work function of polycrystalline sodium is reported as 2.36 eV, the one of lithium as 2.93 eV [40].

A decrease in work function is one effect of the adsorption of alkali metals in general due to the formation of a surface dipole moment when metal atoms transfer charge density towards the surface [121]. For example, it was already reported for lithium containing a-C:H films [101]. In that case of ion beam deposited films, the relation between work function and lithium concentration was shown to be non-linear for concentrations between 8 and 35 at% approaching a saturation value. For the amorphous materials from carbon evaporation presented here, no higher metal concentrations than 15 at% could be achieved for the clean films. A comparison is therefore restricted. Within the given concentration range, the correlation is roughly linear, but deviations e.g. for the first r.t. and the first 800°C sample of fig. 8.4 (with Na) are observed and indicate a possible saturation of dipole density at the surface.

It is a well known property of alkali metals to activate substrates by transferring charge to the surfaces on which they adsorb ([105] and references therein). While the lowering of the work functions of various surfaces is a physical effect of huge technological importance in past and present for any application exploiting electron emission, the activating effect has also been

successfully exploited in the use of alkali metals as promoters in heterogeneous catalysis in industrial chemical production [122]. Carbon based materials with low work functions are of particular interest for the development of field emission devices [123], e.g. for the use in displays. The use of air sensitive alkali metal-containing material, however, is hardly an attractive perspective from a technological point of view. Therefore, the observation of still much lower work functions on oxidized and therefore stable a-C:Li films was intriguing (fig. 8.5).

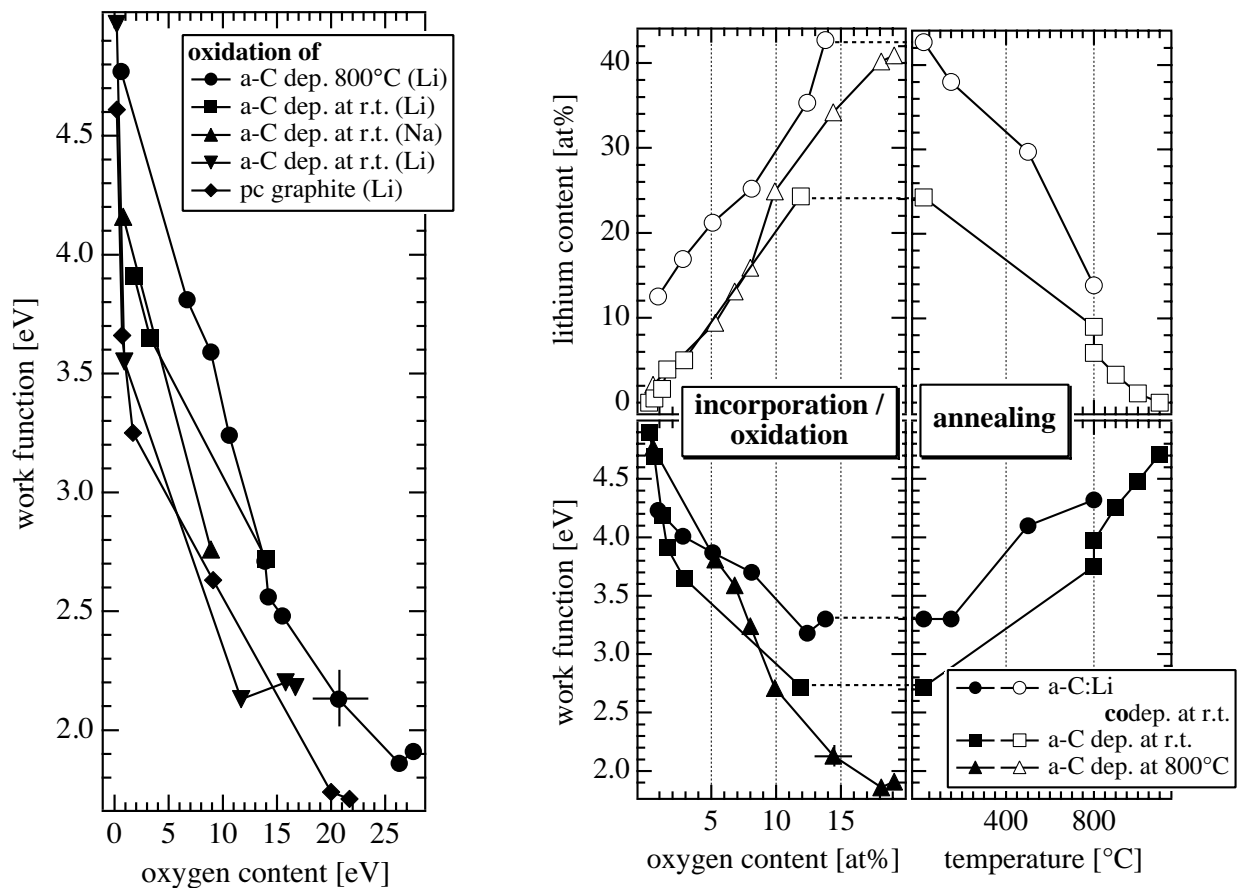


**fig. 8.5:** *Left:* development of work functions during oxidation of various carbon materials. In this case, work functions fall below the values of the metals (Na: 2.36 eV; Li: 2.93 eV [40]). **Right:** Correlation of lithium concentration (top) and work functions (bottom) with the oxygen concentration during the oxidation process (left) and during annealing (right).

In fig. 8.5 data for increasing oxygen concentrations in several samples is included and a representation is given of the dependences between lithium and oxygen concentrations during addition and removal by annealing in relation with the work functions observed during both processes. Work functions in this case even fell below the ones of the alkali metals. The reason for the lowering of work functions lies probably in the formation of the oxidic overlayer on the a-C:M films (fig. 8.6). This layer is even more effective in the generation of a surface dipole moment than the pure metal because of the larger spatial separation of charges. Again, the dipole moment lowers the surface potential barrier and effects the emission of electrons through the surface. For the measurement, however, it does not matter whether the electrons are emitted from the film beneath the oxide or from the oxide itself.

At a certain dipole density on the surface, the decrease in work function cannot proceed any further. The change in slope of the curves in fig. 8.5 already indicates the beginning of such a saturation which was clearly observed for the system a-C:H/Li [101].

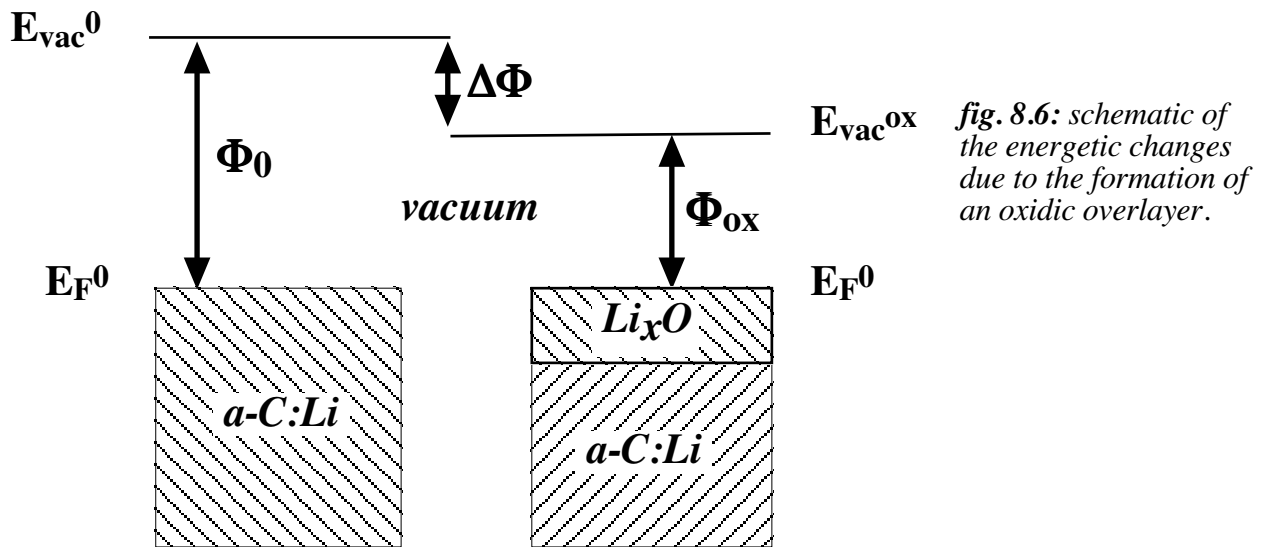


*fig. 8.6: schematic of the energetic changes due to the formation of an oxidic overlayer.*

From what was said above about the behaviour of oxidized material in air the question of air stability of the low work function values arises. In fact, although work functions remained comparatively low, they nevertheless rose by up to 1 eV with respect to the minimal value. From what is known about the materials, the increase is partly due to a deterioration of the material itself by the hydrolysis of lithium oxide with moisture and in addition it is due to the adsorption processes discussed above. The adsorption of contaminants could probably be reduced if necessary for an application so that the low in situ work function values are conserved in a dry atmosphere. In spite of these promising observations, a low work function alone is unfortunately no sufficient prerequisite for the purpose of field emission on a technical scale. For a-C:Na films as discussed here, this was demonstrated by tests at the Philips Research Laboratories (Dr. P.K. Bachmann). In these tests, the films did not show particularly promising qualities as field electron emitting materials, but behaved more or less like any other carbon based material. Details of these test measurements can unfortunately not be reported and will not be made publicly accessible.



## 9 Samples from the TCV first wall

Photoemission measurements were performed on wall cladding material which was to be mounted in the tokamak, on material which was removed from it after plasma operation, and on special test substrates which were introduced to collect thin films deposited during wall conditioning (boronization) procedures. These measurements support the work at TCV in that they provide information on the success of wall conditioning and allow to check for impurities introduced into the wall materials. As the focus is on the elemental composition of the layers, usually only XPS measurements were carried out.

### 9.1 Graphite wall tiles

The TCV (tokamak à configuration variable) at the Centre de Recherches en Physique des Plasmas (CRPP) in Lausanne is unique in the large variety of plasma shapes which can be produced there [124]. To meet the special requirements of the diverse operation modes, 90 % of the vessel's internal surface are by now covered with graphite tiles [125]. Tiles typically measure roughly 100 cm<sup>2</sup> with large variations due to the complex equipment of the vacuum vessel with numerous diagnostics, ports and other constructive constraints which require different tile formats. For the same reason thicknesses range from about 1 to 2 cm. The numerous different tile formats limit the possibility to remove tiles for analysis because they are destroyed when samples for photoelectron spectroscopy are cut out of their surface and the respective replacement can be difficult.

As an example of surface analysis with photoelectron spectroscopy in this field, a series of investigations on a larger ensemble of graphite samples is presented. The samples were cut from tiles taken out of the vessel in autumn 2000. The tiles were originally distributed over all the parts of the first wall, namely the floor (9 tiles), the ceiling (2), the outer wall (1), and the central column (4) of the torus. For the central column tiles, two different zones must be distinguished. On the surface of these tiles, areas with net redeposition of eroded material exist in the vicinity of net eroded surface areas with only a few centimetres between both regions. This is impressively illustrated in fig. 9.1 where the net erosion zone appears as a light stripe in the middle of the tile. This is the region of the most intensive interaction of plasma and wall material on the central column. The darker zone above which is limited by an inverted L-shape is the net redeposition zone.

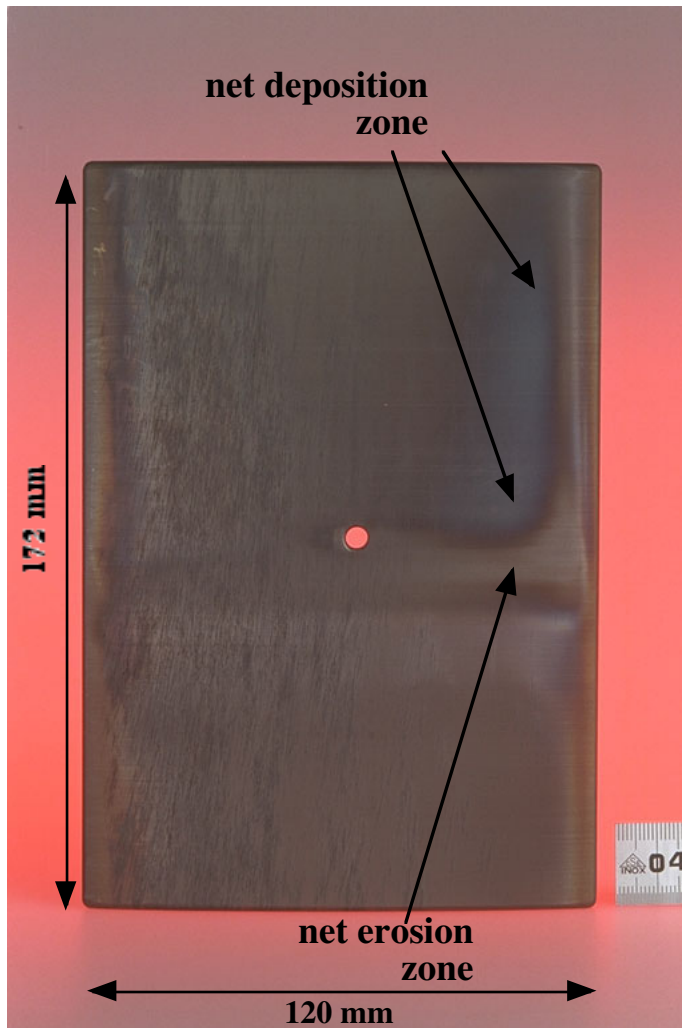


**fig. 9.1:** photograph of a graphite tile from the equator of the central column of the TCV torus after plasma operation. Its original size is 172 mm on 120 mm with a maximum thickness of 20 mm.

The light net erosion zone is the region of the central column with the most intensive interaction of plasma and wall material. The darker net redeposition zone is indicated above.

Photograph courtesy of Dr. R. Pitts, CRPP Lausanne; labels added by the author.

The aim of the study was to map the variations in elemental composition of the first wall boronization layer across the different regions of the inner vessel surface. Operation of TCV had led to another question. Laser ablation experiments were performed in the tokamak with aluminium and silicon and there was some concern whether deposits of the ablated material could interfere with plasma operation in other experiments, the ones with extremely elongated plasma cross sections in particular.

## 9.2 Aim of the investigation

In any fusion research device, the elemental composition of the plasma facing materials is of paramount interest for plasma operation. In TCV with its unique possibilities for operation with extreme plasma shapes, an additional interest in the tiles' composition arises from the possible interference of experiments on the device and the consequences of such interferences on experimental schedules. The question for the composition therefore was at least twofold, concerning both the elemental composition as a result of boronization and normal operation and the concentration of contaminations (mainly silicon and aluminium) from certain experiments carried out in the vacuum vessel. In an approach which has proven useful in recent years, photoelectron spectroscopy in the x-ray energy range ( $MgK_{\alpha}$ , 1253.6 eV) was used as a surface sensitive



analytical technique. By choosing tiles from different locations within the reactor, a locally resolved analysis was to be enabled. Parts of the following chapters were sent to Lausanne in the form of a report on the results.

### 9.3 Samples

During an opening of the tokamak’s vacuum vessel in winter 2000/2001, several graphite tiles were removed from the first wall of the machine. They had been mounted in different regions of the first wall according to tab. 9.a. The tile numbers signify a certain tile design and become unambiguous only by the combination with the respective sector number. For the preparation of the actual samples for the measurement, usually a stripe across the whole tile was cut and then dissected into smaller pieces of about 10·15 mm<sup>2</sup> and 1 to 2 mm thickness. For most tiles, the various samples produced from one stripe can be supposed to be equivalent with some deviations at edges etc. Usually, a sample from a position in some distance from an edge was preferred (normally no. 2 of 3). On the tiles originally mounted on the central column, however, zones with net-redeposition can be distinguished from those with net-erosion due to the non-uniform plasma-wall interaction. In tab. 9.a, sample 4 of these tiles originates from the net-redeposition zone, whereas sample 7 stems from the zone which had been subject to net-erosion under the influence of plasma surface interaction during plasma operation. In an abbreviated form, samples will be addressed as, e.g. #280 S5 2, denominating sample 2 taken from the tile with the design 280 in sector 5 on the reactor floor.

region	sector no.	tile no.	sample no.
floor	5	280	2
‘	5	281	2
‘	5	282	2
‘	5	286	2
‘	5	287	2
‘	5	285	2
floor	10	219	2
‘	10	220	2
‘	10	224	2
roof	5	225	2
roof	6	201	2
central column (CC)	13-B	371	4 (net redeposition)
‘	9-B	371	4 (net redeposition)
‘	5-B	371	4 (net redeposition)
‘	1-B	371	4 (net redeposition)
‘	13-B	371	7 (net erosion)
‘	9-B	371	7 (net erosion)
outer wall (OW)	3	349	3

*tab. 9.a: origin of the samples from the first wall tiles.*

## 9.4 Procedure

Every care was taken in the TCV's Lausanne workshop not to touch the surfaces to be measured. The samples were then transported to Basel through plain air. After an overall air exposure of several weeks, the samples were mounted in our spectrometer under ultrahigh vacuum conditions. Their surfaces had to be cleaned prior to a reliable determination of their surface composition. This was done by in situ argon ion sputtering beginning with a very mild treatment at low ion energies (500 eV) for a few (usually 5) minutes. This allowed to follow the removal of superficially adsorbed contaminants. With argon ion sputtering at 3 keV for ten minutes, part of the film material itself was removed and its elemental composition was determined. To make sure that no contaminants were buried more deeply in the film from earlier operation, further sputtering cycles with at least 3 keV for up to as much as ten hours were performed. They should, however, be understood predominantly as a check for these impurities, because the boronization layer's composition is not well preserved under these circumstances due to different sputter yields for the elements. The core level measurements involved the recording of survey scans and detail scans of the energy regions of interest as identified in the survey spectra.

## 9.5 Results

For all the measurements concentration values are given with one decimal digit. This does not claim the according precision of measurement, but is used to indicate trends in the results. The error of the measurement is usually of the order of  $\pm 0.5$  at% with some dependence on the respective core level's ionisation cross section. Data was obtained from the as measured spectra by subtracting the background (Tougaard) and weighing of the calculated peak area with the respective photoionization cross section. Results for the determination of surface compositions after removal of the topmost layer of adsorbed material are summarised in fig. 9.2 for all the samples from various locations within the vacuum vessel. At this stage of processing, the samples had usually been treated with argon ions of 500 eV for 5 minutes and for a further 10 minutes at 3 keV. Boron concentrations varied by a factor of 2 between about 5 and more than 10 at%. The lowest values were obtained for the net-deposition regions of tiles originally mounted on the central column of the reactor. In the net-erosion zone, boron concentrations were by 2.5 at% and 3.2 at% higher (samples #13B CC and #9B CC, respectively). While boron concentrations in the two roof tiles were relatively low (5.3 to 6.9 at%), all the floor tiles exhibited values in excess of 6.5 at%. An interesting observation was made for the tiles from sector 5 of the vessel's floor (##280 S5, 281 S5, 282 S5, 286 S5, 287 S5, 285 S5). These tiles had been positioned in the reactor side by side along the large radius of the torus. The lowest concentration of 6.5 at% was found on the tile mounted closest to the central column (#280) while the highest was found on the outermost tile (#285) with 10.5 at%. The intermediate samples followed a trend towards higher boron content with increasing distance from the central column, though not uniformly. The single sample from the outer wall (sector 3) contained 7.6 at% boron.

Oxygen concentrations in most of the samples were roughly correlated with the ones of boron as could be expected from boron's function as oxygen getter material. Usually, the oxygen content was

about 1.5 to 3 at% lower than the one of boron. Exceptions were floor sample #220 S10 and roof tile #225 S5 with almost equal concentrations of boron and oxygen (7.1/7.3 and 5.3/4.7 at%). Sample #285 S5 exhibited the highest difference with 4.7 at% less oxygen than boron. Carbon forms almost the entire rest of all sample materials. Nitrogen was usually present with about 0.6 to 0.7 at%. From the results presented in fig. 9.3 one might assume that nitrogen was actually pushed forward into the material by the sputtering process while it had originally been merely a surface contaminant. Traces of silicon and aluminium could only be identified in the low sub percent range (0.2 to 0.6 at%) where analysis becomes rather unreliable. A number of other elements which appear to be present in equally low concentrations according to the automated quantification procedure are not even included in the diagrams as their signals can no longer be distinguished from artefacts of the measurement. After some of the processing steps, silicon and aluminium concentrations could not be quantified, either, because the bad signal to noise ratio yielded deceptively 'high' concentrations of about 0.5 at%. For such measurements, no values are given in the diagrams.

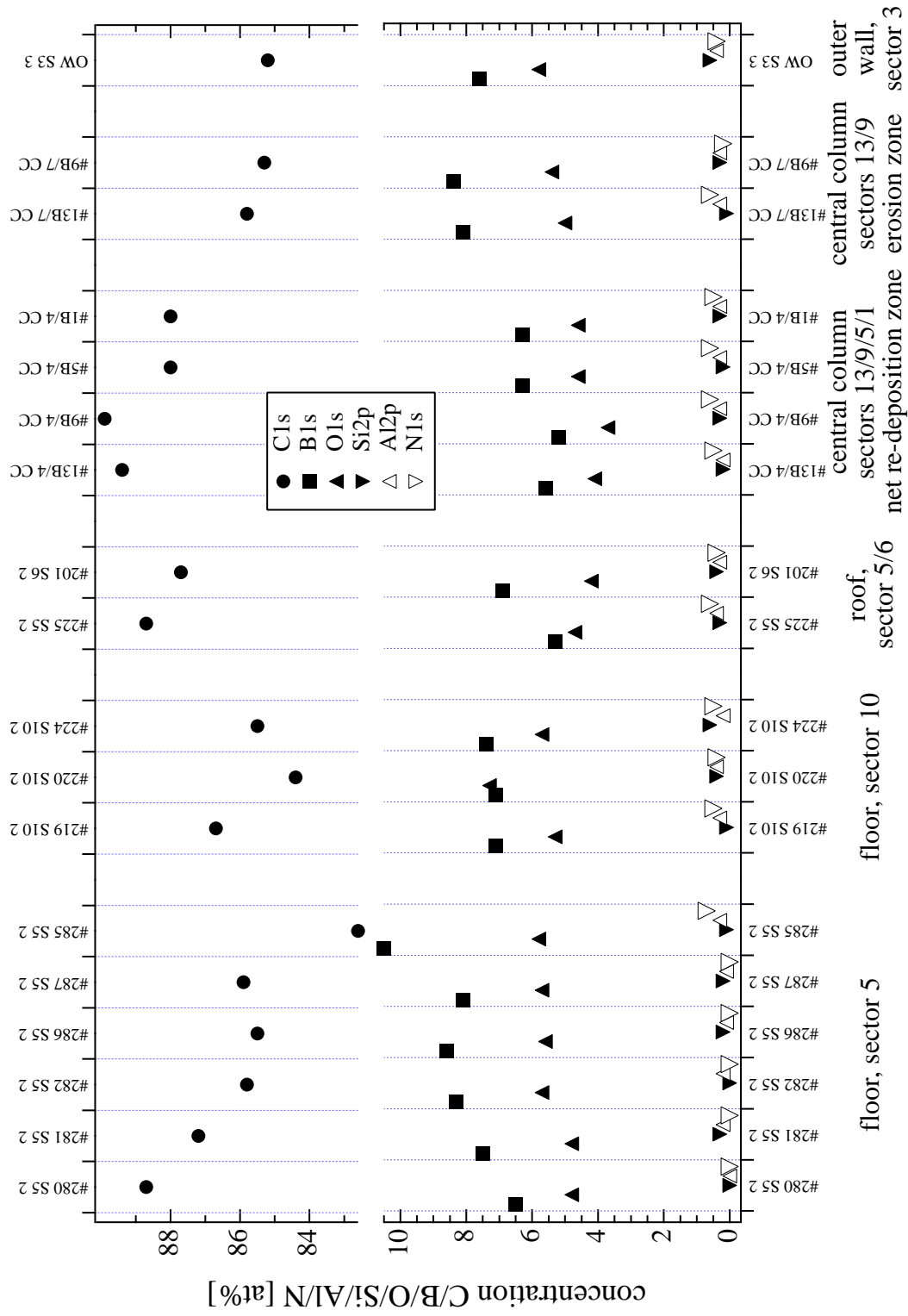


**fig. 9.2:** concentrations of boron, carbon, oxygen, silicon, aluminium and nitrogen in boronized graphite samples removed from different locations within TCV. Data refers to the state after removal of adsorbed contaminants by 3 keV argon ion sputtering for 10 minutes. The locations and sample numbers can be found in plans in the appendix.

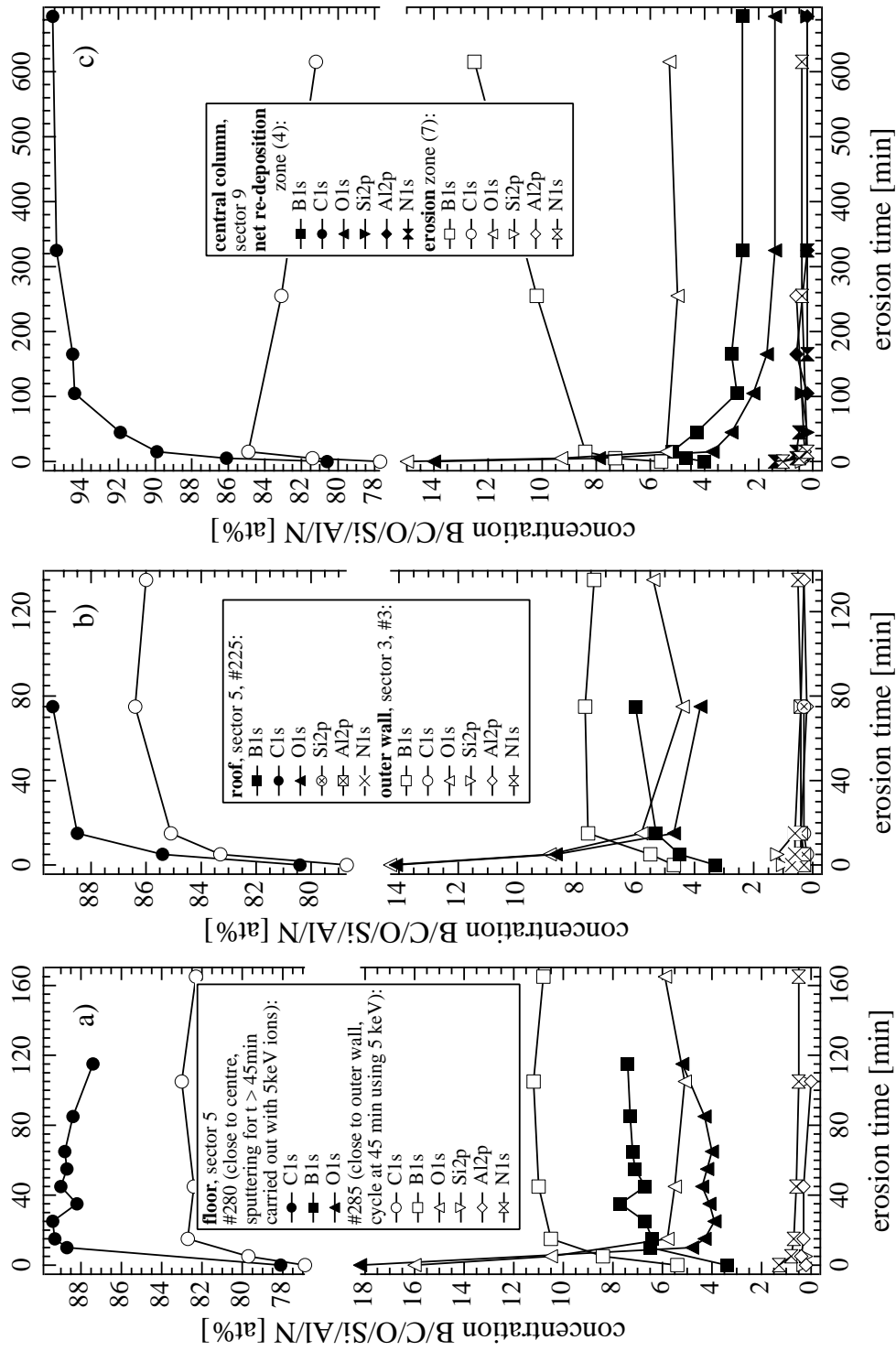


**fig. 9.3:** compositions of TCv graphite samples after argon ion sputtering. Note the fast stabilisation of concentrations at the beginning. The left panel compares two floor samples, one from close to the central column and one from near the outer wall. The graph in the middle contains data for a roof and an outer wall sample from near the equator. The right panel compares two samples from different areas of the same central column tile which differ in that the one was subject to net erosion (7) whereas the other experienced net-redeposition. The first cycle of five minutes sputtering was usually performed with 500 eV ions. Other deviations from the standard 3 keV ion energy are indicated, but show little effect.

Data in fig. 9.3 refers to the development of concentrations in the samples with extended irradiation times. As can be seen, the major changes in composition were usually achieved during the first minutes of irradiation at 3 keV. Afterwards, film material is removed and the concentrations must be considered with some care, as preferential sputtering of one compound might yield an apparent surplus of another one. However, for most of the samples only small changes occur during continued sputtering.

In the left panel of fig. 9.3, two samples from the same sector 5 of the reactor's floor tiling are compared. While one sample was taken from a tile close to the central column, the other one had been installed close to the outer wall. As described above, the concentrations of the elements are markedly different, but their development with ongoing sputtering is essentially in parallel. This is also true for the roof and outer wall tiles of the middle panel. In the right panel, however, one can observe a diverging trend for compositions in two spots of the same tile from the central column, one having been subject to net-redeposition in the reactor (no. 4), the other one having been exposed to net-erosion (no. 7). In this case, irradiation times were much longer than in the other experiments, but this applies for both samples and therefore does not explain the increase in boron and oxygen concentrations which is found. Obviously, redeposition of carbon on the surface has led to the formation of a more carbon rich material in this region. In the erosion zone, one can on the other hand expect a 'clean' carbon - boron film with its carbon content resulting mainly from the original boronization procedure. During the analysis with ion sputtering, carbon is removed more readily and a surplus of boron evolves compared to the initial composition. On the already eroded surface, there is no buffer layer of carbon deposits left which could delay this process.

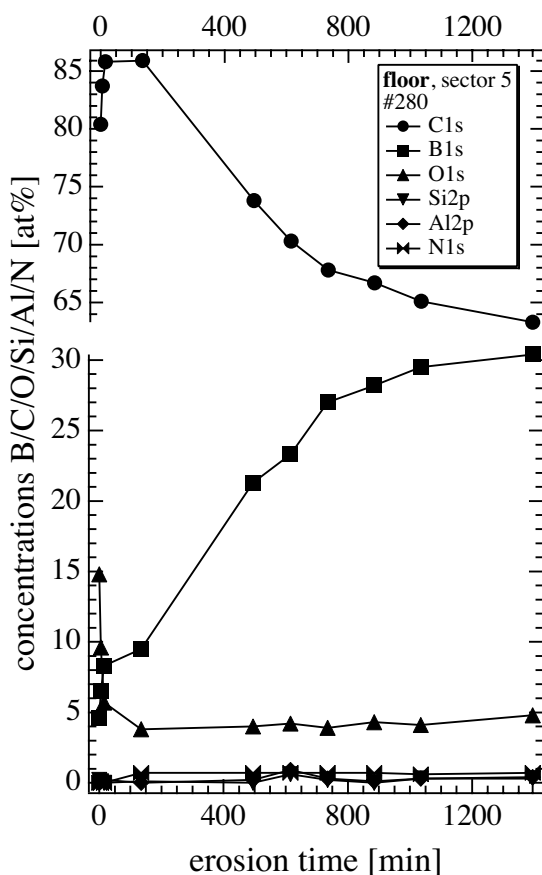


**fig. 9.4:** development of concentrations in floor sample #280 from sector 5 of the vessel. Note the very long irradiation times. The main increase occurs between 200 and 800 minutes. Before and after this, the increase is rather moderate and comparable to the ones observed in other samples.

For completeness we must briefly refer to one sample which yielded a dramatic increase in boron concentration during sputtering as can be seen in fig. 9.4. In the last step, the boron concentration in this floor sample exceeded 30 at%. Irradiation times in this case were excessive and preferential sputtering certainly had an influence, but the effect is still a very strong one and it is not uniform over the whole time range. Up to now, these measurements have not been repeated, but it is hoped that we will be able to use alternative analytical tools for verification.

### ***9.6 Summary of the TCV results***

The analysis of these 16 samples from different regions of the TCV did not yield any evidence for substantial contamination of the first wall material. Silicon and aluminium were identified in most samples, but only in minute concentrations in the sub-percent range below the ones observed in previous analyses of TCV graphite materials. The composition of the boronized graphite surfaces showed variations of a few percent depending on the location of the respective tiles in the reactor vessel. Oxygen concentrations were loosely coupled to the ones of boron. Lowest boron concentrations were found on the central column, higher values on the floor. There, boron content increased with distance from the central column. On the central column, adjacent erosion and deposition zones showed distinctly different compositions reflecting the history of these areas in the reactor.





## 10 Summary

This work comprises results from different experimental approaches in the characterization of carbon based oxygen gettering materials with photoelectron spectroscopy (PES).

Combinations of amorphous carbons (a-C) with sodium guest atoms were investigated in ultrahigh vacuum to gain deeper insight into the metal-carbon interaction in such materials with a particular focus on the role of structural modifications in the carbon host matrix. Experimentally, different degrees of crystallinity were achieved by variations of the carbon deposition temperature between room temperature and 800°C. The comparison with polycrystalline graphite material underlined the importance of a proper understanding of structural peculiarities in the research of carbon materials. It was shown that alkali metal atoms can successfully be employed as probes for these characteristics in combination with the analytical tool of PES: while binding energies of atoms in the pristine carbon materials show only small differences, the addition of alkali metal atoms as electron donors yields much more distinct features which can be used to assess the structural properties of the carbon host.

With this background information on the structure of the respective amorphous carbon matrix lithium containing samples were prepared with the objective of testing their ability to getter oxygen containing contaminants and their behaviour under the impact of energetic particles. Experiments with in-situ exposure to molecular oxygen, the bombardement with oxygen and hydrogen ions with energies from 100 to 5000 eV and additional ex-situ exposure to air were performed and each processing step monitored by subsequent analysis with PES. All the lithium containing carbons including polycrystalline graphite showed the desired ability to react with oxygen containing molecules and readily formed lithium oxide on their surface. The progress of the oxidation reaction in the surface region acted as driving force for the segregation of large quantities of lithium to the surface which had previously diffused into the bulk when lithium was offered to the sample surface. This lithium oxide layer was also formed with oxygen ions where it even served as protection for the carbon underneath at ion energies of not much more than 2000 eV. Hydrogen ion bombardement also led to structural damage and finally to erosion at higher kinetic energies. With respect to the application in a fusion reactor's first wall, the following points are the most important results:

- lithium containing amorphous carbon was prepared in situ under vacuum and acted as oxygen getter
- the gettering effect is not limited to the small quantity of lithium which is already close to the surface, but the whole film is a reservoir of metal atoms which are dispensed under the influence of the oxidation reaction
- the carbon material can be recovered after gettering by heating; such a procedure could be carried out in situ in a vacuum vessel which is of course an important criterion for the applicability of any process

- Taking into account the fact that several fusion facilities are equipped with the infrastructure for handling and dispensing lithium, carbon/lithium systems can be considered as an alternative to other low-Z systems.

Furthermore, the ability of the oxidized material to preserve very low work function values in air even pointed beyond the originally envisaged application towards the possibility of field emission from such materials. This effect found some external attention and the optimization of this effect could be an attractive task.

Studies of boronized graphite samples installed in the TCV in Lausanne during plasma operation complemented the work. They were carried out throughout the duration of the project with the main aim of ascertaining that contaminants were neither introduced from the outside nor produced inside the vacuum vessel. In the series presented here, an extensive locally resolved analysis of the elemental composition of the reactor's first wall was performed.

Considering the development in the field of plasma wall interaction in fusion research, the future of the application of carbon based materials has become less certain in recent years. Carbon in the form of graphite holds a firm place in many fusion research facilities worldwide, which alone would have been a good incentive to continue work in this field as these machines will be running for several more years. The discussion of alternatives for the next step device ITER-FEAT, however, is still open. For some regions of this large fusion facility, carbon cannot compete with other materials. For other areas of the vessel's inner surface, alternative concepts such as a liquid divertor have been developed. And even materials with high atomic numbers have returned into focus due to the much improved methods of controlling the dynamics of the plasma edge.

At present, the most probable outcome of this discussion might be the confinement of carbon in the form of graphite to only a small part of the first wall. In this case, the interaction of eroded carbon with other materials, such as the refractive metals tungsten or molybdenum becomes even more important. First studies in this field have also been performed in our group and it could be worthwhile to continue in this direction.

While this seems to point away from carbon in this very special field, carbon in all its various forms has attracted more and renewed attention due to its remarkable and unique properties. Some of them have been touched in this work pointing towards fields of interest like energy storage or microelectronics.

It would therefore be wrong to reduce this or any other work just to its original aim and outcome. In the best case, at least some piece of it might pop up in an unexpected place and fit in when needed - within fusion or elsewhere. In a way, this is part of what it is all about.

## 11 Zusammenfassung

Diese Arbeit umfasst Ergebnisse aus verschiedenen experimentellen Ansätzen zur Charakterisierung von kohlenstoffbasierten sauerstoffbindenden Materialien mit Photoelektronenspektroskopie (PES). Kombinationen von amorphen Kohlenstoffen (a-C) mit Natrium Gastatomen wurden im Ultrahochvakuum untersucht, um tieferen Einblick in die Metal-Kohlenstoff-Wechselwirkung zu erhalten. Der Blick richtete sich hier besonders auf die Rolle struktureller Modifikationen der Kohlenstoff Wirtsmatrix. Experimentell wurden verschiedene Kristallinitäten durch die Variation der Kohlenstoff Abscheidungstemperatur zwischen Raumtemperatur und 800°C erreicht. Der Vergleich mit polykristallinem Graphit unterstrich dabei die Wichtigkeit des Verständnisses der strukturellen Besonderheiten im Bereich der Kohlenstoffmaterialien. Es wurde gezeigt, dass Alkalimetallatome in Verbindung mit PES erfolgreich als Sonden für diese Eigenschaften eingesetzt werden können: Während die Bindungsenergien der Atome in den reinen Kohlenstoffmaterialien gering sind, führt die Zugabe von Alkalimetallatomen als Elektronendonoren zur Ausbildung deutlicherer Unterschiede, die herangezogen werden können, um die strukturellen Eigenschaften der Kohlenstoffmatrix zu bestimmen.

Auf Grundlage dieser Informationen zur Struktur wurden lithiumhaltige Proben erzeugt, um ihre Fähigkeit zu testen, sauerstoffhaltige Verunreinigungen zu binden und ihr Verhalten unter dem Einfluss energetischer Teilchen zu untersuchen. Es wurden in-situ Experimente mit Exposition gegenüber molekularem Sauerstoff und Beschuss mit Sauerstoff- und Wasserstoffionen mit Energien von 100 bis 5000 eV durchgeführt, sowie weitere ex-situ Versuche mit Luftexposition. Jeder einzelne Schritt wurde durch nachfolgende PES Analyse verfolgt. Alle lithiumhaltigen Proben einschliesslich polykristallinen Graphits zeigten die erwünschte Fähigkeit, mit sauerstoffhaltigen Molekülen zu reagieren und bildeten jeweils Lithiumoxid an ihrer Oberfläche. Der Fortgang der Oxidationsreaktion nah an der Oberfläche wirkte als Triebkraft für die Segregation grosser Mengen von Lithiumatomen, die zuvor in das Material diffundiert waren, als Lithium der Probenoberfläche angeboten worden war. Die Oxidschicht bildete sich auch mit Sauerstoffionen, wobei sie in diesem Fall bis zu Energien von etwa 2000 eV als Schutz des Kohlenstoffmaterials wirkte, bevor auch dessen Erosion begann. Auch Wasserstoffionenbeschuss führte zu struktureller Schädigung und bei höherer kinetischer Energie zur Erosion. Im Hinblick auf die Anwendung in der ersten Wand eines Fusionsreaktors sind die folgenden Punkte von besonderer Bedeutung:

- Lithiumhaltige amorphe Kohlenstoffschichten wurden in situ im Vakuum erzeugt und wirkten als Sauerstofffänger.
- Die sauerstoffbindende Wirkung ist nicht begrenzt auf die geringe Menge an Lithium, die sich unmittelbar an der Oberfläche befindet, sondern der ganze Film wirkt als Reservoir, das unter dem Einfluss der Oberflächenreaktion Lithiumatome abgibt.
- Das Kohlenstoffmaterial kann nach dem Einsatz durch Heizen erneut zur Verwendung aufbereitet werden; auch dieser Teil des Prozesses könnte in situ in einem Vakuumgefäss erfolgen, was ein wichtiges Kriterium beim praktischen Einsatz darstellt.
- Da einige Fusionsreaktoren zu diagnostischen und anderen Zwecken bereits über die nötige Infrastruktur zur Handhabung und Verteilung von Lithium im Reaktor verfügen, können

Kohlenstoff/Lithium-Systeme als Alternative zu anderen Systemen mit niedriger Ordnungszahl betrachtet werden.

Die Fähigkeit der oxidierten Filme, sehr niedrige Elektronenaustrittsarbeiten auch an Luft aufrechtzuerhalten, wies demgegenüber deutlich über die Anwendung in der Fusion hinaus auf die Möglichkeit der Feldemission aus solchen Materialien hin. Sie haben damit auch bei externen Partnern Interesse geweckt, und eine Optimierung des Effektes könnte eine reizvolle Aufgabe sein.

Die Untersuchung gleichfalls sauerstoffbindender boronisierter Graphitproben, die im TCV in Lausanne während des Betriebs installiert waren, ergänzte die Arbeit. Solche Analysen sind während der gesamten Projektdauer vorgenommen worden und sollten sicherstellen, dass Verunreinigungen weder von aussen in den Reaktor getragen noch in seinem Inneren freigesetzt wurden. Mit den hier vorgestellten Proben wurde eine aufwendige örtlich aufgelöste Analyse der elementaren Zusammensetzung der ersten Wand des Reaktors unternommen.

Im Hinblick auf die Entwicklung auf dem Gebiet der Plasma-Wand-Wechselwirkung in der Fusionsforschung scheint die zukünftige Anwendung von kohlenstoffbasierten Materialien heute als weniger gesichert. Kohlenstoff in Form von Graphit hat einen festen Platz in vielen Fusionsforschungsanlagen weltweit, und dies allein wäre genügend Anreiz, die Arbeit in diesem Bereich fortzusetzen, da diese Anlagen noch jahrelang weiterarbeiten werden. Die Diskussion der Alternativen für den nächstgrösseren Reaktor ITER-FEAT ist aber noch offen. In einigen Bereichen dieser Grossanlage kann Kohlenstoff dem Vergleich mit anderen Materialien nicht standhalten. In Teilbereichen sind sogar ganz andere Konzepte wie etwa ein „flüssiger Divertor“ mit sich erneuernder Oberfläche entwickelt worden. Und auch Elemente mit hoher Ordnungszahl sind in den Blickpunkt des Interesses zurückgekehrt, weil die Dynamik des äusseren Plasmas sehr viel besser kontrolliert werden kann.

Das zur Zeit wahrscheinlichste Ergebnis der Diskussion könnte die Verwendung von Graphit lediglich in einem kleinen Bereich der ersten Wand sein. In diesem Fall wird die Wechselwirkung von erodiertem Kohlenstoff mit allen anderen Materialien, unter anderem auch mit den refraktiven Metallen Wolfram oder Molybdän noch wichtiger werden. Erste Versuche in diesem Bereich sind auch in unserer Gruppe durchgeführt worden, und es könnte sich lohnen, in dieser Richtung aktiv zu bleiben.

Während die Aussagen in diesem speziellen Gebiet eher vom Kohlenstoff weg zu weisen scheinen, hat Kohlenstoff mit seinen bemerkenswerten und teilweise einzigartigen Eigenschaften in den letzten Jahren vermehrte und erneuerte Aufmerksamkeit auf sich gezogen. Einige wenige dieser Eigenschaften sind auch in dieser Arbeit berührt worden und verweisen auf das Potential bei der Energiespeicherung oder in der Mikroelektronik.

Es wäre darum falsch, diese oder andere Arbeiten lediglich auf das Gebiet zu reduzieren, von dem sie ihren Ausgang genommen haben. Im günstigsten Fall scheint ein Mosaiksteinchen des Inhalts an einem mehr oder weniger unerwarteten Ort auf und fügt sich dort ein, wo es gebraucht wird - egal, ob nun im Dunstkreis der Fusion oder andernorts.

## 12 References

- [1] J. Winter, *Journal of Nuclear Materials* **176/177** (1990) 14-31.
- [2] J. Robertson, *Diamond Films and Technology* **8** (1998) 225-236.
- [3] Q.H. Wang, M. Yan, and R.P.H. Chang, *Applied Physics Letters* **78** (2001) 1294-1296.
- [4] S. Flandrois, and B. Simon, *Carbon* **37** (1999) 165-180.
- [5] H. Oman, *MRS Bulletin* **24** (1999) 33-39.
- [6] M.S. Dresselhaus, K.A. Williams, and P.C. Eklund, *MRS Bulletin* **24** (1999) 45-50.
- [7] U. Schumacher, *Fusionsforschung - Eine Einführung*, Wissenschaftliche Buchgesellschaft, Darmstadt 1993, 216.
- [8] R.R. Weynants, *Fusion Technology* **37** (2000) 56-62.
- [9] G. Janeschitz, *Journal of Nuclear Materials* **290** (2001) 1-11.
- [10] S. Karamanolis, *Heisser als die Sonne - Energie aus Kernfusion?*, Elektra Verlag, Neubiberg b. München 1992, 182.
- [11] H.F. Dylla, *et al.*, *Journal of Nuclear Materials* **176/177** (1990) 337-342.
- [12] G. Saibene, *et al.*, *Journal of Nuclear Materials* **220-222** (1995) 617-622.
- [13] M.U. Valdes, *et al.*, *Journal of Nuclear Materials* **241-243** (1997) 750-754.
- [14] M. Ciotti, G. Franzoni, and G. Maddaluno, *Journal of Nuclear Materials* **220-222** (1995) 567-570.
- [15] E. Vietzke, and A.A. Haasz, *Chemical Erosion*, in *Physical processes of the interaction of fusion plasmas with solids*, W. Hofer and J. Roth, Editors. Academic Press 1995, p. 1-45.
- [16] N. Noda, V. Philipps, and R. Neu, *Journal of Nuclear Materials* **241-243** (1997) 227-243.
- [17] G. Janeschitz, *et al.*, *Journal of Nuclear Materials* **220-222** (1995) 73-88.
- [18] D.N. Ruzic, M.M.C. Allain, and R.V. Budny, *Journal of Nuclear Materials* **266-269** (1999) 1303-1308.
- [19] Y. Hirooka, *et al.*, *Journal of Nuclear Materials* **274** (1999) 320-328.
- [20] S. Kato, *et al.*, *Journal of Nuclear Materials* **266-269** (1999) 406-411.

- [21] N. Itou, *et al.*, *Journal of Nuclear Materials* **290** (2001) 281-285.
- [22] J.N. Brooks, *et al.*, *Journal of Nuclear Materials* **290** (2001) 185-190.
- [23] J.-U. Thiele, and P. Oelhafen, *Journal of Nuclear Materials* **220-222** (1995) 1047-1051.
- [24] J.-U. Thiele, and P. Oelhafen, *Journal of Nuclear Materials* **228** (1996) 290-301.
- [25] R. Zehringer, *et al.*, *Journal of Nuclear Materials* **176/177** (1990) 370-374.
- [26] H. Künzli, *et al.*, *Fresenius' Journal of Analytical Chemistry* **346** (1993) 41-44.
- [27] K. Tatsumi, *et al.*, *Journal of Power Sources* **68** (1997) 263-266.
- [28] H. Higuchi, K. Uenae, and A. Kawakami, *Journal of Power Sources* **68** (1997) 212-215.
- [29] S.M. Lee, *et al.*, *Hydrogen storage in single-walled and multi-walled carbon nanotubes*, in *Materials Research Society Fall Meeting 1999*, 2000, Boston, MA, USA, Materials Research Society, Warrendale, PA, USA 2000, p. 187-192.
- [30] B. Tsuchiya, and K. Morita, *Journal of Nuclear Materials* **220-222** (1995) 836-840.
- [31] R.E. Dickerson, and I. Geis, *Chemistry, matter and the universe: an integrated approach to general chemistry*, Benjamin/Cummings, Menlo Park 1979.
- [32] H.W. Kroto, *et al.*, *Nature* **318** (1985) 162.
- [33] S. Iijima, *Nature* **354** (1991) 56-58.
- [34] D. Ugarte, *Nature* **359** (1992) 707-709.
- [35] K. Sattler, *Carbon* **33** (1995) 915-920.
- [36] S. Iijima, *et al.*, *Chemical Physics Letters* **309** (1999) 165-170.
- [37] H.O. Pierson, *Handbook of carbon, graphite, diamond and fullerenes: properties, processing and applications*, Noyes Publications, Park Ridge, NJ, USA 1993.
- [38] M.S. Dresselhaus, and G. Dresselhaus, *Advances in Physics* **30** (1981) 139-326.
- [39] H. Zabel, and S.A. Solin, *Graphite Intercalation Compounds I*. Springer Series in Materials Science, ed. M. Cardona, Springer-Verlag, Berlin, Heidelberg, New York 1990.
- [40] D.R. Lide, ed. *CRC Handbook of Chemistry and Physics*. 78th ed., CRC Press, Boca Raton, New York. 1997.
- [41] R. Reichle, D.D.R. Summers, and M.F. Stamp, *Journal of Nuclear Materials* **176-177** (1990) 375-380.

- [42] J.P. Coad, *et al.*, *Journal of Nuclear Materials* **290** (2001) 224-230.
- [43] A. Kirschner, *et al.*, *Journal of Nuclear Materials* **290** (2001) 238-244.
- [44] P. Wienhold, *et al.*, *Journal of Nuclear Materials* **290** (2001) 362-366.
- [45] C.Z. Wang, K.M. Ho, and C.T. Chan, *Physical Review Letters* **70** (1993) 611-614.
- [46] G. Galli, *et al.*, *Physical Review B* **42** (1990) 7470-7482.
- [47] C. Gao, *et al.*, *Physical Review Letters* **62** (1989) 945.
- [48] S.T. Jackson, and R.G. Nuzzo, *Applied Surface Science* **90** (1995) 195-203.
- [49] G. Comelli, J. Stohr, and C.J. Robinson, *Physical Review B* **38** (1988) 7511.
- [50] *Amorphous Carbon: State of the Art*, in *1st International Specialist Meeting on Amorphous Carbon (SMAC '97)*, 1997, Cambridge, UK, World Scientific, p. 361.
- [51] S. Schelz, *et al.*, *Surface Science* **359** (1996) 227-236.
- [52] M. Nakadaira, *et al.*, *Journal of Materials Research* **12** (1997) 1367-1375.
- [53] J.R. Dahn, *et al.*, *Science* **270** (1995) 590-593.
- [54] K. Kanamura, *et al.*, *Chemistry of Materials* **9** (1997) 1797-1804.
- [55] J.P. Lukaszewicz, *Journal of Materials Science* **32** (1997) 6063-6068.
- [56] A. Bianconi, S.B.M. Hagström, and R.Z. Bachrach, *Physical Review B* **16** (1977) 5543-5548.
- [57] K. Siegbahn, and *e. al.*, *ESCA applied to free molecules*. 1. ed, North-Holland/Elsevier, Amsterdam, New York 1971.
- [58] R. Wahrenberg, *et al.*, *Europhysics Letters* **49** (2000) 782.
- [59] H. Hertz, *Annalen der Physik und Chemie, Neue Folge (Wiedemann)* **31** (1887) 983-1000.
- [60] P. Lenard, *Annalen der Physik, 4. Folge* **2** (1900) 359-375.
- [61] A. Einstein, *Annalen der Physik, 4. Folge* **17** (1905) 132-148.
- [62] M. Cardona, and L. Ley, *Photoemission in Solids I*. Topics in applied Physics, Springer, Berlin, Heidelberg, New York 1979.
- [63] J.F. Watts, *X-ray photoelectron spectroscopy*, in *Surface science techniques*, J.M. Walls and R. Smith, Editors. Elsevier Science, Oxford 1994, p. 5-23.
- [64] M.P. Seah, and W.A. Dench, *Surface and Interface Analysis* **1** (1979) 2.

- [65] S. Hüfner, *Photoelectron Spectroscopy*. Springer Series in Solid-State Sciences 82, ed. M. Cardona, *et al.*, Springer-Verlag, Berlin, Heidelberg 1995.
- [66] P.K. Ghosh, in *Introduction to Photoelectron Spectroscopy*. J. Wiley & Sons, New York, Chichester, Brisbane, Toronto, Singapore 1983, p. 160-178.
- [67] P. Reinke, and P. Oelhafen, *Surface Science* **468** (2000) 203-215.
- [68] P. Oelhafen, *et al.*, *Electron Spectroscopy on Carbon Based Films: Bulk and Interface Properties*, in *NATO Advanced Study Institute on Diamond and Diamond-like Films and Coatings*, 1991, Castelvechio Pascoli, Italy, Plenum Press, p. 377-415.
- [69] J.H. Scofield, *Journal of Electron Spectroscopy and Related Phenomena* **8** (1976) 129-137.
- [70] S. Tougaard, *Surface and Interface Analysis* **11** (1988) 453.
- [71] U. Gelius, *Physica Scripta* **9** (1974) 133.
- [72] J.J. Yeh, and I. Lindau, *Atomic Data and Nuclear Data Tables* **32** (1985) 1-155.
- [73] I.T. McGovern, *et al.*, *Physica B/C* **99 (B)** (1980) 415-419.
- [74] P. Oelhafen, and J.L. Freeouf, *Journal of Vacuum Science and Technology A* **1** (1983) 96-97.
- [75] J. Schäfer, *et al.*, *Physical Review B* **53** (1996) 7762-7774.
- [76] H. Estrade-Szwarckopf, and B. Rousseau, *Journal of the Physics and Chemistry of Solids* **53** (1992) 419-436.
- [77] P.H. Citrin, G.K. Wertheim, and Y. Baer, *Physical Review B* **16** (1977) 4256-4282.
- [78] Y. Baer, P.H. Citrin, and G.K. Wertheim, *Physical Review Letters* **37** (1976) 49-52.
- [79] M. Cardona, and L. Ley, *Photoemission in Solids I*, in *Photoemission in Solids I*. Springer, Berlin, Heidelberg, New York 1979, p. 210-217.
- [80] J. Krieg, P. Oelhafen, and H.-J. Güntherodt, *Solid State Communications* **42** (1982) 831-833.
- [81] P. Reinke, and P. Oelhafen, *J. Appl. Phys.* **81** (1997) 2396-2399.
- [82] R.F. Willis, B. Fitton, and G.S. Painter, *Physical Review B* **9** (1974) 1926-1937.
- [83] F. Maeda, *et al.*, *Physical Review B* **37** (1988) 4482-4488.
- [84] P. Oelhafen, *et al.*, *Physical Review Letters* **44** (1980) 197-200.



- [85] B.R. Weinberger, *et al.*, *Physical Review Letters* **41** (1978) 1417-1421.
- [86] N.F. Mott, and J. Jones, *Theory of the Properties of Metals and Alloys*, Dover, New York 1958.
- [87] J.F. Moulder, *et al.*, *Handbook of X-ray Photoelectron Spectroscopy*, Perkin-Elmer Corporation, Physical Electronics Division, Eden Prairie (Minnesota, USA) 1992.
- [88] A. Barrie, and F.J. Street, *Journal of Electron Spectroscopy and Related Phenomena* **7** (1975) 1-31.
- [89] J. Fink, *et al.*, *Physical Review B* **30** (1984) 4713-4718.
- [90] G.E. Murch, and A.S.N. (Eds.), *Diffusion in crystalline solids*, Academic Press, Orlando 1984, 482.
- [91] M.V. Koudriachova, N.M. Harrison, and S.W.d. Leeuw, *Physical Review Letters* **86** (2001) 1275-1278.
- [92] R. Schlögl, *Electron spectroscopy of graphite intercalation compounds*, in *Graphite Intercalation Compounds II*, H. Zabel and S.A. Solin, Editors. Springer Verlag, Berlin, Heidelberg 1992, p. 74-89.
- [93] C. Hartwigsen, W. Witschel, and E. Spohr, *Physical Review B* **55** (1997) 4953-4959.
- [94] A. Metrot, *et al.*, *Synthetic Metals* **1** (1979/80) 363-369.
- [95] K. Wandelt, *Surface Science Reports* **2** (1982) 1-121.
- [96] B. Rousseau, M. Vayer-Besançon, and H. Estrade-Szwarckopf, *Solid State Communications* **99** (1996) 143-147.
- [97] J. Hrbek, Y.W. Yang, and J.A. Rodriguez, *Surface Science* **296** (1993) 164-170.
- [98] P.B. Leezenberg, W.H. Johnston, and G.W. Tyndall, *Journal of Applied Physics* **89** (2001) 3498-3507.
- [99] G.K. Wertheim, P.M.T.M.V. Attekum, and S. Basu, *Solid State Communications* **33** (1980) 1127-1130.
- [100] J.P. Contour, *et al.*, *J. Microsc. Spectrosc. Electron.* **4** (1979) 483-491.
- [101] J.-U. Thiele, P. Kania, and P. Oelhafen, *J. Vac. Sci. Technol. A* **15** (1997) 1739-1744.
- [102] S. Spruytte, *et al.*, *Journal of Vacuum Science and Technology A* **19** (2001) 603-608.
- [103] J.-U. Thiele, and P. Oelhafen, *Solid State Communications* **93** (1995) 29-32.

- [104] A. Behr, *Carbon Dioxide Activation by Metal Complexes*, VCH Verlagsges., Weinheim 1988.
- [105] S. Hadenfeldt, *et al.*, *Surface Science* **352-354** (1996) 295-299.
- [106] W.A. Hart, and J. O.F. Beumel, *Lithium and its compounds*, in *Comprehensive Inorganic Chemistry*, J.C. Bailar, *et al.*, Editors. Pergamon Press, Oxford 1973.
- [107] J. Schäfer, J. Ristein, and L. Ley, *Diamond and Related Materials* **3** (1994) 861-864.
- [108] H. Raether, in *Excitation of Plasmons and Interband Transitions by Electrons*. Springer, Berlin, Heidelberg, New York 1980, p. 46-49.
- [109] K. Siegbahn, *Journal of Electron Spectroscopy and Related Phenomena* **5** (1974) 3-97.
- [110] N.A.W. Holzwarth, S. Rabii, and L.A. Girifalco, *Physical Review B* **18** (1978) 5190-5205.
- [111] G. Institut, *Lithium Ergänzungsband*. 8. ed. Gmelins Handbuch der Anorganischen Chemie, Verlag Chemie, Weinheim 1960.
- [112] E.U. Condon, and H.O. (Eds.), *Handbook of Physics*. 2. ed, McGraw-Hill, New York 1967.
- [113] C. Jardin, and D. Robert, *Applied Surface Science* **35** (1988) 495-506.
- [114] C. Jardin, P. Durupt, and J. Davenas, *Radiation Effects and Defects in Solids* **137** (1995) 29-34.
- [115] G. Indlekofer, and P. Oelhafen, *Journal of Non-Crystalline Solids* **117/118** (1990) 340-343.
- [116] F. Beuneu, *et al.*, *Physical Review B* **55** (1997) 11263-11269.
- [117] F. Beuneu, P. Vajda, and O.J. Zogal, *Physical Review Letters* **83** (1999) 761-763.
- [118] H. Gnaser, *Low-Energy Ion Irradiation of Solid Surfaces*. Springer Tracts in Modern Physics, ed. G. Höhler, *et al.*, Springer, Berlin, Heidelberg, New York 1999.
- [119] P. Reinke, *et al.*, *Physical Review B* **54** (1996) 7067-7073.
- [120] A. Refke, V. Philipps, and E. Vietzke, *Journal of Nuclear Materials* **250** (1997) 13-22.
- [121] J. Hölzl, and F.K. Schulte, *Work Function of Metals*, in *Solid Surface Physics*, G. Höhler, Editor. Springer, Berlin, Heidelberg, New York 1979.
- [122] H.P. Bonzel, A.M. Bradshaw, and G. Ertl, eds. *Physics and Chemistry of Alkali Metal Adsorption*. Elsevier, Amsterdam, Bad Honnef, Germany. 1989.
- [123] A.F. Bobkov, *et al.*, *Journal of Vacuum Science and Technology B* **19** (2001) 32-38.

- 
- [124] F. Hofmann, *et al.*, *Plasma Physics and Controlled Fusion* **36** (1994) B277-B287.
- [125] R.A. Pitts, R. Chavan, and J.-M. Moret, *Nuclear Fusion* **39** (1999) 1433-1449.



## 13 Danksagung

Eine Doktorarbeit besteht nicht nur aus dem vorgelegten Büchlein, sie umfasst wichtige Jahre in einem Leben, die geprägt sind von den Menschen, mit denen man zusammenkommt. Für die zurückliegende Zeit möchte ich darum einigen Personen danken:

- Herrn Professor Peter Oelhafen für die vertrauensvolle Zusammenarbeit und für die Möglichkeit, diese Arbeit durchzuführen.
- Herrn Professor Ernst Meyer für die Übernahme des Korreferats der Arbeit.
- Herrn Roland Steiner für seinen dauernden Einsatz und für die Plünderung seines technischen Erfahrungsschatzes.
- Einer ganzen Reihe von Kolleginnen und Kollegen für Rat und Tat und für die Atmosphäre, in der ich mich schnell und in wechselnder Besetzung wohlfühlen konnte. Es sind dies in der Reihenfolge ihres Auftretens in der Anstalt: Yvette Kuster, Roland Kilper, Holger Stupp, Jürgen Geng, Alain Gremaud, Andreas Schüler, Thormen Wrase, Ralf Wahrenberg, Ivan Videnovic, Teresa de los Arcos, Gunnar Garnier, Shui Ching Ho, Georges Reber, Michael Büttner, Jamila Boudaden, Marc Ley sowie Stefan Albietz.
- Für technischen Beistand Frau Verena Thommen und den Herren Peter Reimann, Michael Steinacher, Werner Erni und Hans-Jörg Dingnis. Herrn Werner Roth danke ich besonders herzlich für Hektoliter flüssigen Stickstoffs!
- Den Damen Astrid Kalt, Barbara Kammermann, Elisabeth Holdermann sowie Herrn François Erkadoo für ihre Hilfsbereitschaft und für die Zusammenarbeit in Sachen Institutsbibliothek.
- Den Vertretern des Bundesamtes für Bildung und Wissenschaft, Herrn Dr. Berthet und Herrn Dr. Conscience für ihr grosses Interesse und ihre Unterstützung.
- Herrn Dr. Richard Pitts für Zusammenarbeit und spannende Einblicke.

Nun endlich kommt ein ganz spezieller Dank, der mir besonders am Herzen liegt und den ich mir für den Schluss aufgehoben habe: Ich möchte mich sehr herzlich bei Frau PD Dr. Petra Reinke dafür bedanken, dass sie mich nach Basel geholt und gelegentlich ins kalte Wasser geworfen hat – aber nie ohne Rettungsring. Fachlich wäre die Arbeit ohne sie nur schwer möglich gewesen und menschlich hätte ich sie mir ohne Petra Reinke nicht vorstellen können und wollen. Danke für alles und bis bald! Pass auf Dich auf.

Den Menschen, die vor allem Anteil am Leben ausserhalb des Instituts hatten und haben, danke ich für Freundschaft, Wärme, Geduld und für den ganzen Rest.

Liebe Eltern, lieber Michael, ich bin weit weg, das stimmt - aber es tut gut zu wissen, dass Ihr da seid. Es gibt Dinge im Leben, für die wir uns zu selten wenigstens zu bedanken *versuchen* - und vielleicht gibt es auch Dinge, bei denen es uns nie gelingt. Diesmal versuche ich es:

Ich danke Euch.



## 14 Curriculum vitae

### Persönliche Daten

**Name:** Matthias Töwe  
**Eltern:** Werner und Hannelore Töwe, geb. Heese  
**geboren:** 19. Juli 1970 in Hamburg  
**Nationalität:** deutsch

### Bildungsgang

**August 1976 bis Juli 1980:** Besuch der Grundschule in Hamburg.

**August 1980 bis Mai 1989:** Besuch des Matthias-Claudius-Gymnasiums in Hamburg bis zum Abitur.

**Juni 1989 bis August 1990:** Ableistung des Wehrdienstes.

**Oktober 1990:** Beginn des Studiums der Chemie an der Universität Hamburg.

**April 1991:** Aufnahme in die überparteiliche Studienstiftung des Deutschen Volkes.

**Oktober 1997:** Diplom in Chemie. Diplomarbeit: "Plasmaaktivierte Gasphasenabscheidung (PA-MOCVD) von titanoxidhaltigen Kohlenstoffschichten aus Titan(IV)-isopropylat".

**Nov. 1997 bis April 2001:** Doktorarbeit in Experimentalphysik bei Prof. Dr. P. Oelhafen im Institut für Physik der Universität Basel.  
Öffentliche Doktorprüfung am 18. Oktober 2001.

An meiner Ausbildung waren neben weiteren die folgenden Dozentinnen und Dozenten beteiligt:

In Basel Frau PD P. Reinke und Herr Prof. P. Oelhafen.

In Hamburg Frau Prof. E. Thorn und die Herren Professoren und Dozenten C. Benndorf, R.D. Fischer, W. Francke, J. Heck, B. Kastening, W. Kirstein, J. Kittsteiner, G. Klar, W.A. König, R. Kramolowsky, A. Krebs, H.R. Kricheldorf, H. Kropf, H. Lechert, P. Margaretha, K. Nagorny, A. Reller, H. Sinn, J. Thiem, F. Thieme, J. Voss, H.G. Zachmann.